

ΠΟΛΥΤΕΧΝΕΙΟ ΚΡΗΤΗΣ  
ΤΜΗΜΑ ΜΗΧΑΝΙΚΩΝ ΟΡΥΚΤΩΝ ΠΟΡΩΝ  
ΕΡΓΑΣΤΗΡΙΟ ΕΦΑΡΜΟΣΜΕΝΗΣ ΓΕΩΦΥΣΙΚΗΣ

Migration velocity analysis on synthetic seismic data from South Crete

Μεταπτυχιακή διατριβή

Αλέξανδρος Τσιώλης

Εξεταστική Επιτροπή

Αντώνιος Βαφείδης, Καθηγητής (επιβλέπων)

Εμμανουήλ Μανούτσογλου, Καθηγητής

Σπυρίδων Μπέλλας, Ερευνητής ΙΤΕ

Χανιά

Δεκέμβριος, 2021

## ΠΕΡΙΛΗΨΗ

Στην παρούσα μεταπτυχιακή εργασία εφαρμόστηκε η μέθοδος της ανάλυσης ταχυτήτων χωροθέτησης (MVA) σε συνθετικά δεδομένα νότια της Κρήτης. Τα συνθετικά δεδομένα αποκτήθηκαν από προηγούμενη διπλωματική εργασία που διεξήχθη στο Εργαστήριο Εφαρμοσμένης Γεωφυσικής του Πολυτεχνείου Κρήτης.

Αρχικά, κατασκευάστηκε ένα αρχικό μοντέλο μέσω των τετραγωνικών ταχυτήτων που προέκυψαν από τις τμηματικές ταχύτητες που χρησιμοποιήθηκαν για τη δημιουργία των συνθετικών δεδομένων. Έπειτα, πραγματοποιήθηκε χωροθέτηση Kirchhoff πριν την υπέρθεση σε όλα τα δεδομένα κοινής πηγής, ενώ κατασκευάστηκε και η χωροθετημένη τομή για τον έλεγχο της διαδικασίας της χωροθέτησης. Πρέπει να σημειωθεί ότι ο αριθμός των πηγών ήταν περιορισμένος, οπότε συνιστάται η αύξηση του αριθμού των πηγών. Επίσης, συνιστάται η δοκιμή άλλων μεθόδων χωροθέτησης, οι οποίες ίσως αποδίδουν καλύτερα σε περιοχές με κεκλιμένους ανακλαστήρες.

Στη συνέχεια, δημιουργήθηκαν τα δεδομένα κοινού σημείου απεικόνισης (CIGs) με τη χρήση του αλγορίθμου CMP\_Synthetics. Τα CIG Supergathers συνεισφέρουν στην αύξηση του αριθμού των ίχνων για την ανάλυση ταχυτήτων, αλλά η επιθυμητή ανάλυση δεν επιτεύχθηκε λόγω της μεγάλης απόστασης μεταξύ των CIGs. Ακόμα, εφαρμόστηκε αντίστροφη δυναμική διόρθωση στα CIGs και δημιουργήθηκαν τρία CIG Supergathers. Επιπροσθέτως, πραγματοποιήθηκε ανάλυση ταχυτήτων για κάθε CIG Supergather και υπολογίστηκαν οι τμηματικές ταχύτητες.

Εφαρμόστηκαν δύο μέθοδοι επιλογής ταχυτήτων. Η πρώτη μέθοδος βασίστηκε στα δεδομένα της ανάλυσης ταχυτήτων χωροθέτησης και η δεύτερη στα αρχικά δεδομένα, ενώ πραγματοποιήθηκε και σύγκριση των αποτελεσμάτων τους. Για μεγάλες αποστάσεις μεταξύ πηγής και δέκτη, η χρονική απόκλιση είναι πιθανό να είναι μεγάλη, οπότε οι ανακλάσεις σε μακρινά ίχνη δεν είναι ορατές. Η χρονική απόκλιση σε μακρινά ίχνη θα μπορούσε να είναι ορατή αν ο διπλός χρόνος διαδρομής δε μειωνόταν στα 5,5 s και αυτό ίσως αποτελεί την πηγή των επιπλοκών της διαδικασίας της ανάλυσης ταχυτήτων. Η ανάλυση ταχυτήτων χωροθέτησης αποδίδει καλύτερα για τον πρώτο ανακλαστήρα στα 3,5 s και τον τρίτο στα 4,5 s διότι είναι επίπεδοι, αντιθέτως με τους υπόλοιπους. Οι ανακλαστήρες πρέπει να είναι επίπεδοι για τα CIG Supergathers στην θέση των CIGs. Συνιστάται η μείωση της απόστασης μεταξύ των CIGs που χρησιμοποιούνται για τη δημιουργία των τριών CIG Supergathers, η οποία μπορεί να επιτευχθεί αυξάνοντας την υπεδαφική κάλυψη στα αρχικά δεδομένα. Συνεπώς, η διαδικασία μπορεί να είναι επιτυχής χρησιμοποιώντας αυτά τα CIG Supergathers.

## ABSTRACT

In the present thesis, migration velocity analysis (MVA) method was applied on synthetic seismic data from South Crete. The synthetic data were obtained from a previous thesis conducted in the Applied Geophysics laboratory of Technical University of Crete.

At first, the initial model of RMS velocities, resulting from the interval velocities used for the synthetic data creation, was produced. Secondly, prestack Kirchhoff migration was conducted for each and every common shot gather and the migrated section was produced in order to examine Kirchhoff migration. It should be mentioned that the number of sources is limited, so it is recommended to increase this number. The examination of other prestack migration methods is recommended, which may perform better at areas with dipping reflectors.

Eventually, common image gathers (CIGs), were created using the CMP\_Synthetics algorithm. CIG Supergathers contribute to increasing the number of traces for the velocity analysis, but the required analysis was not achieved because of the large distance between the CIGs. Furthermore, inverse NMO correction was applied on the CIGs and three inverse NMO-corrected CIG Supergathers were created. Subsequently, velocity analysis was conducted for each and every inverse NMO-corrected CIG Supergather and interval velocities were calculated.

Two different picking methods were conducted. The first picking was based on the MVA data and the second was based on the initial data with their results being compared with each other. For large offsets, move-out is possible to be large and as a consequence, reflections at distant traces are not visible. Move-out at distant traces could be visible if the records were not cut at two-way traveltimes 5,5 s. This might be the source of the migration velocity analysis complications. The migration velocity analysis seems to perform better for the first reflector at 3,5 s and the third at 4,5 s because they are flat in contrast to the rest. For the CIG Supergathers, the reflectors should be flat at the involved image point locations. It is recommended to reduce the spacing between the CIGs used for the creation of the three CIG Supergathers, which could be achieved by increasing the fold of the initial data. Hence, the process could be more successful utilizing these CIG Supergathers.

## ΠΡΟΛΟΓΟΣ

Η συγκεκριμένη μεταπτυχιακή εργασία πραγματοποιήθηκε στη σχολή Μηχανικών Ορυκτών Πόρων του Πολυτεχνείου Κρήτης στα πλαίσια του μεταπτυχιακού προγράμματος 'Γεωτεχνολογία και Περιβάλλον'. Το ενδιαφέρον που μου προκάλεσαν τα μαθήματα του κλάδου της Γεωφυσικής κατά τη φοίτησή μου στο Πολυτεχνείο ως προπτυχιακός και μεταπτυχιακός φοιτητής αποτέλεσε το λόγο της επιλογής του συγκεκριμένου θέματος.

Στο σημείο αυτό θα ήθελα να ευχαριστήσω τον επιβλέποντα καθηγητή κύριο Βαφείδη Αντώνιο για την ανάθεση της μεταπτυχιακής εργασίας και την καθοδήγησή του, τον κύριο Ανδρονικίδη Νικόλαο και τον κύριο Κρητικάκη Γεώργιο από το διδακτικό προσωπικό του εργαστηρίου Εφαρμοσμένης Γεωφυσικής για τη σημαντική συνεισφορά τους κατά την επεξεργασία των μετρήσεων, την οικογένειά μου και τα κοντινά μου πρόσωπα.

# TABLE OF CONTENTS

ΠΕΡΙΛΗΨΗ.....	ii
ABSTRACT.....	iii
ΠΡΟΛΟΓΟΣ.....	iv
TABLE OF CONTENTS.....	v
CHAPTER 1: SEISMIC REFLECTION.....	1
1.1 Introduction.....	1
1.2 Seismic waves.....	1
1.3 Principles of seismic waves propagation.....	2
1.4. Diffraction.....	3
1.5 Seismic reflection at sea.....	3
1.6 Conventional seismic data processing.....	4
1.6.1 Preprocessing.....	4
1.6.2 Deconvolution and trace balancing.....	5
1.6.3 CMP sorting.....	6
1.6.4 Velocity analysis.....	7
1.6.5 NMO correction and stacking.....	8
1.6.6 Residual statics corrections.....	9
1.6.7 Time variant band-pass filtering – Gain.....	9
1.6.8 Migration.....	9
1.6.9 Gain.....	10
CHAPTER 2: VELOCITY MODEL BUILDING.....	11
2.1 Introduction.....	11
2.2 Representation and picking.....	11
2.3 Inversion.....	12
2.4 Velocity model building techniques.....	15
2.5 Common image gathers.....	16
2.6 Migration velocity analysis.....	17
CHAPTER 3: SYNTHETIC DATA CREATION.....	19
CHAPTER 4: DATA PROCESSING.....	23
4.1 Prestack migration.....	23
4.2 Common image gathers.....	27
4.3 Inverse NMO correction.....	34

4.4 Velocity analysis .....	40
4.4.1 Picking based on MVA data .....	40
4.4.2 Picking based on initial data .....	42
4.4.3 Results comparison .....	46
CHAPTER 5: CONCLUSIONS AND RECOMMENDATIONS .....	48
REFERENCES .....	49
ANNEX .....	51

## CHAPTER 1: SEISMIC REFLECTION

### 1.1 Introduction

The most well-known and extensively used geophysical technique is seismic reflection surveying. The hydrocarbon industry's massive investment in its development, combined with the evolution of computing and electronic technology, has resulted in the technique's current level of sophistication. Seismic sections can be constructed in order to display features of geological formations on scales ranging from the top tens of meters of the drift to the entire lithosphere. The seismic data process generates a seismic section, which is an image of the subsurface structure, contributing to the method's success. The seismic section is similar to, but essentially different from, a depth section of the geology. Geologists can make accurate interpretations only by understanding how the seismic reflection is conducted and the seismic sections are produced (Kearey, Brooks and Hill, 2002).

### 1.2 Seismic waves

The two major categories of seismic waves are body and surface waves. Body waves travel through the bulk of a medium and surface waves are confined to the interfaces between media with contrasting elastic properties, particularly the surface of the ground. The two types of body waves that can pass through an elastic medium are the P-waves and the S-waves. P-waves, also called primary waves, are the most significant in seismic surveys (Reynolds, 2011). Their velocity, which is independent from frequency, is greater than the other types of waves and they are characterized by the same particle oscillation and traveling direction. S-waves velocity, which is also independent from frequency, is less than the P-waves but greater than the surface waves velocity and their particle oscillation direction is vertical to traveling direction. (Veeken and van Moerkerken, 2013).

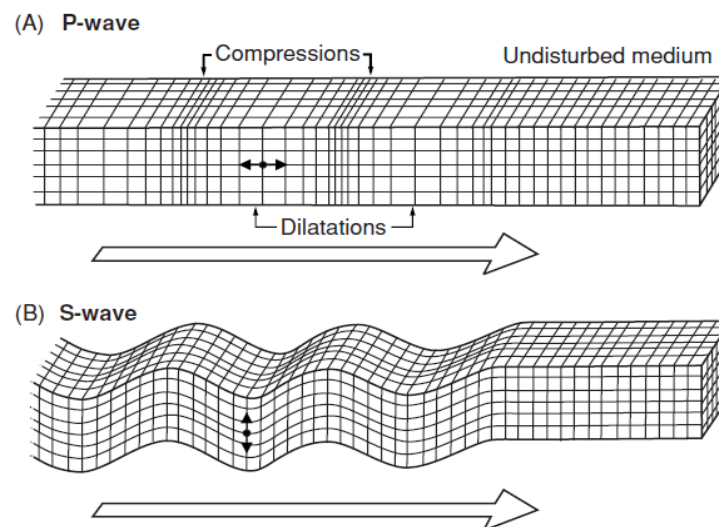


Figure 1.1: Elastic deformations and ground particle motions associated with the passage of body waves. (A) P-Wave and (B) S-Wave (Bolt, 1982).

Furthermore, the two types of surface waves are the Rayleigh and Love waves. Rayleigh waves are characterized by elliptical particle oscillation on a plane which is vertical to the traveling direction, large amplitudes, attenuation as the depth increases and velocity that is dependent on the frequency. Love waves particle oscillation direction is parallel to the horizontal plane and vertical to the traveling direction and their velocity is also dependent on frequency (Veeken and van Moerkerken, 2013).

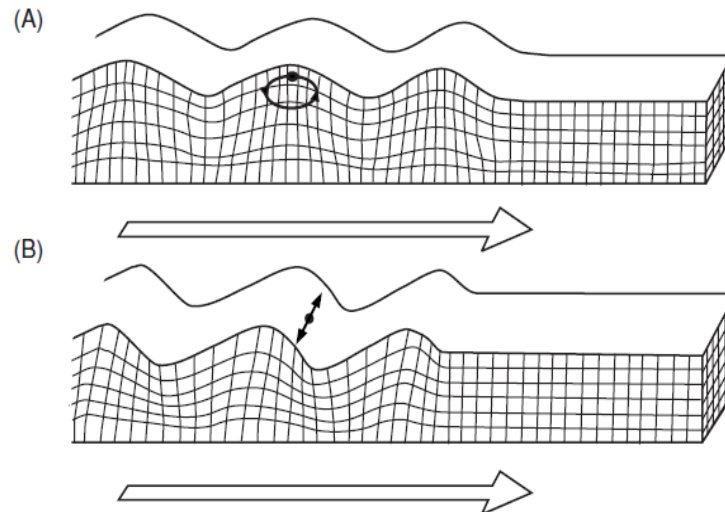


Figure 1.2: Elastic deformations and ground particle motions with the passage of surface waves. (A) A Rayleigh wave and (B) a Love wave (Bolt, 1982).

### 1.3 Principles of seismic waves propagation

Seismic waves velocity is determined by the physical properties of the surrounding rocks. When seismic pulses travel through homogeneous rocks, they travel in every direction with the same velocity away from the seismic source so that the wavefront is a sphere at any subsequent time (Kearey, Brooks and Hill, 2002). Wavefronts are defined as points on the wave with the same amplitude at the same time and raypaths are lines that represent the direction of the seismic waves propagation (Veeken and van Moerkerken, 2013).

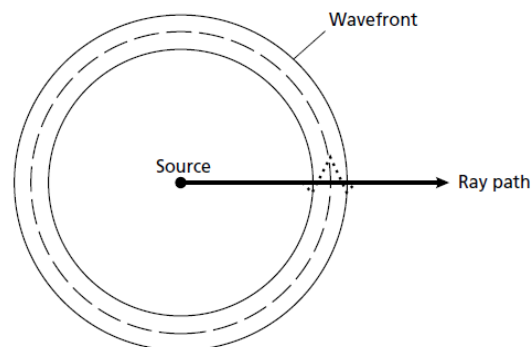


Figure 1.3: The relationship between a raypath to the associated wavefront (Kearey, Brooks and Hill, 2002).

## 1.4. Diffraction

The radial scattering phenomenon of incident seismic energy occurs in the case of precipitous discontinuities in interfaces or structures characterized by smaller radius of curvature than the wavelength of incident waves. This phenomenon is known as diffraction. Edges of faulted layers and small isolated objects in a homogeneous layer are the most frequent diffraction sources in the ground (Kearey, Brooks and Hill, 2002).

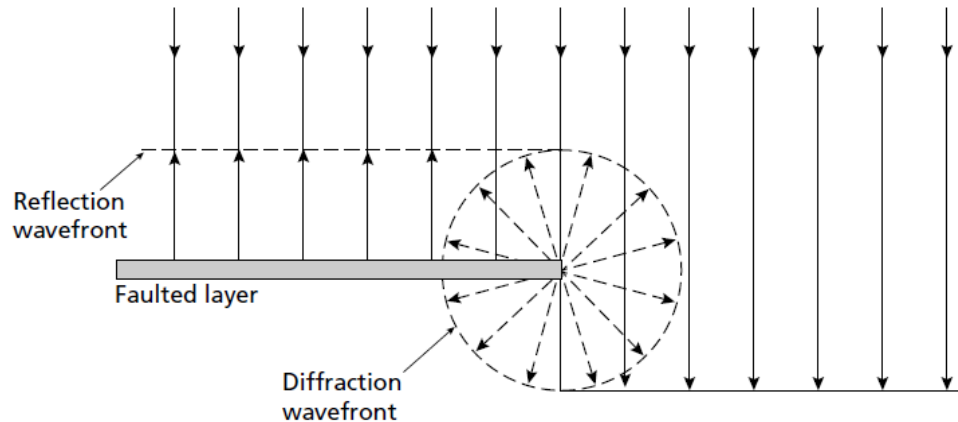


Figure 1.4: Diffraction due to the truncated end of a faulted layer. (Kearey, Brooks and Hill, 2002).

## 1.5 Seismic reflection at sea

In seismic surveys, a source produces seismic waves that are transmitted to the subsurface. Several waves return to the surface after being reflected or refracted at geological boundaries of the subsurface. The ground motion of the returning waves is being detected by instruments along the surface that measure the arrival times of the waves at different ranges from the source. The interfaces of the subsurface can be mapped by converting these travel times into depth values (Kearey, Brooks and Hill, 2002).

In marine operation, large vessels equipped with sources and receivers dragged by the boat, are continuously moving from one shot to another. The fact that no time is spent moving the receivers, makes marine acquisitions more economical and fast than land acquisitions. Usually, a pressure differential induced into the water column is used as source since transmitting energy directly into the subsurface, as in land surveys, is not possible. The pressure difference passes through the water column and into the subsurface and is reflected to the surface. Airguns are the most popular seismic sources and hydrophones are the typical receivers in marine surveys (<https://wiki.seg.org/wiki/Acquisition>).

Each receiver records a trace, which represents the seismic signal amplitude and noise. When the source is triggered, multiple receivers are active, resulting in multiple traces. The collection of traces recorded from a single source point is known as seismic record. A record is a section or cube of data containing an horizontal axis for distance or geographic position and a vertical axis for recording time. Each trace is plotted at its receiver position, with positive and negative deviations from zero representing

changes in amplitude. The vertical axis is commonly used to represent time rather than depth. The signal must travel from the surface to the reflector and back to the receiver on the surface, thus the recording time is two-way traveltime (TWT) (Nolen-Hoeksema, 2014).

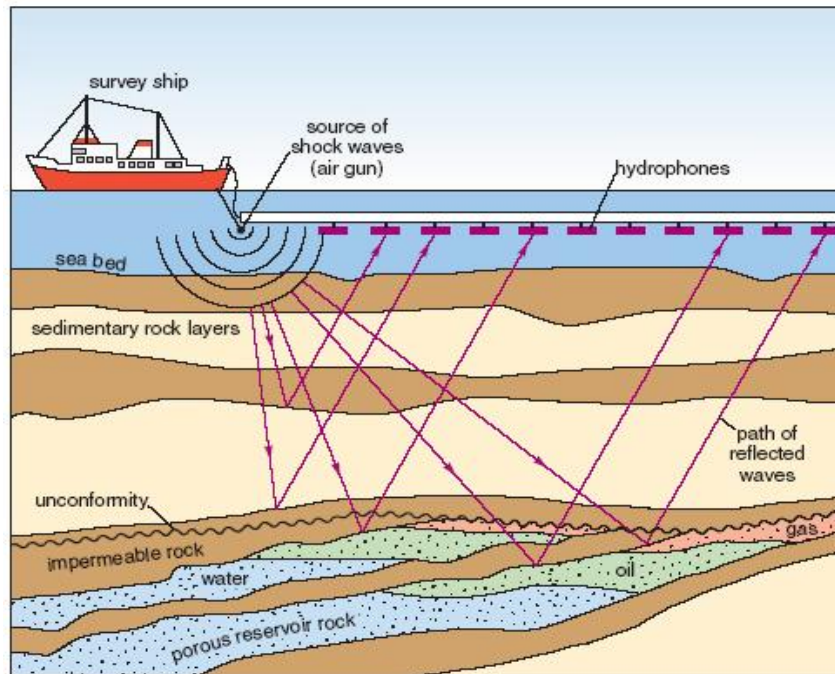


Figure 1.5: Marine acquisition layout ([https://archive.epa.gov/esd/archive-geophysics/web/html/marine\\_seismic\\_methods.html](https://archive.epa.gov/esd/archive-geophysics/web/html/marine_seismic_methods.html)).

## 1.6 Conventional seismic data processing

### 1.6.1 Preprocessing

Field data are recorded in a multiplexed mode using a specific format. Firstly, the data are demultiplexed by being converted into a usable format. The preprocessing stage also includes trace editing, where polarity reversals are corrected and noisy traces, traces with transient glitches or monofrequency signals are erased. In order to adjust the amplitude effect of waveform divergence, a gain recovery function is applied on the data. This entails utilizing a geometric spreading function that is traveltime dependent, as well as an average primary velocity function associated with primary reflections. Moreover, an exponential gain function is applied in order to achieve attenuation losses compensation. Furthermore, there is the optional usage of the wide band-pass filter before the deconvolution stage. Finally, the geometry of the field is incorporated with the data, which may occur before the offset dependent gain corrections. It must be mentioned that erroneous field geometry set ups cause various complications in data processing (Yilmaz, 1987).

### 1.6.2 Deconvolution and trace balancing

The purpose of prestack deconvolution is improving temporal resolution by compressing the effective source wavelet incorporated into the seismic trace to a spike. Also, predictive deconvolution function is frequently applied. Conventional processing deconvolution techniques are based on optimum Wiener filtering (Yilmaz, 1987).

Deconvolution is a process that rectifies a previous convolution action. The operation of the convolution is given below (Kearey, Brooks and Hill, 2002):

$$\gamma(t) = g(t) * f(t) \quad (1.1)$$

where  $g(t)$ : the input waveform

$f(t)$ : the filter of impulse response

$\gamma(t)$ : the filtered output

Knowing  $f(t)$  and  $\gamma(t)$ , the recovery of  $g(t)$  represents a deconvolution operation. Suppose that  $f'(t)$  is the function that must be convolved with  $\gamma(t)$  in order to recover  $g(t)$  (Kearey, Brooks and Hill, 2002):

$$g(t) = \gamma(t) * f'(t) \quad (1.2)$$

Substituting for  $\gamma(t)$  as given by the equation (1.1) (Kearey, Brooks and Hill, 2002):

$$g(t) = g(t) * f(t) * f'(t) \quad (1.3)$$

Moreover (Kearey, Brooks and Hill, 2002):

$$g(t) = g(t) * \delta(t) \quad (1.4)$$

where  $\delta(t)$ : a spike function which is a time function  $g(t)$  convolved with a spike function, producing an unchanged convolution output function  $g(t)$ .

From the equations (1.3) and (1.4) (Kearey, Brooks and Hill, 2002):

$$f(t) * f'(t) = \delta(t) \quad (1.5)$$

As long as the impulse response  $f(t)$  is known,  $f'(t)$  can be used in equation 1.3 in order to recover the input signal  $g(t)$ . The deconvolution operator is represented by the  $f'(t)$  function (Kearey, Brooks and Hill, 2002). After deconvolution, trace balancing is applied in order to bring the data to a common root-mean-squared (RMS) level (Yilmaz, 1987).

### 1.6.3 CMP sorting

Usually, the reflected seismic energy is not sufficient, so it is essential to increase the signal to noise (S/N) ratio of most data (Kearey, Brooks and Hill, 2002). In the stage of CMP (Common Midpoint) sorting, a transformation from shot-receiver to midpoint-offset coordinates is applied on the seismic data. Also, CMP sorting requires information about the field geometry. Although seismic data are acquired in shot-receiver coordinates, most processing is usually performed in midpoint-offset coordinates. This coordinate transformation is accomplished by sorting the data into CMP gathers. Every single trace is assigned to the midpoint between the associated shot and receiver positions. A CMP gather is produced by grouping together the traces with the same midpoint locations. It should be noted that the term CDP (Common Depth Point) is regularly used instead of CMP. When the depth point is on a horizontally flat reflector and the medium above is layered horizontally, CMP and CDP gathers are equivalent (Yilmaz, 1987).

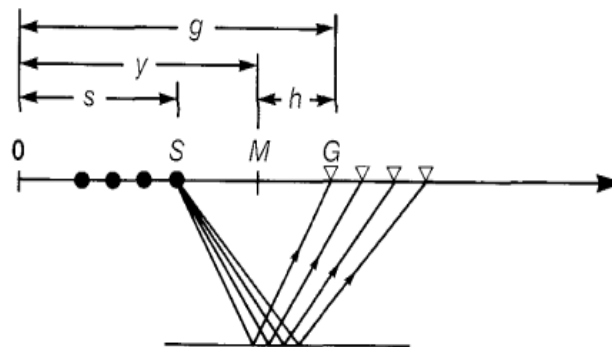


Figure 1.6: Acquisition of seismic data in shot-receiver coordinates (Yilmaz, 1987).

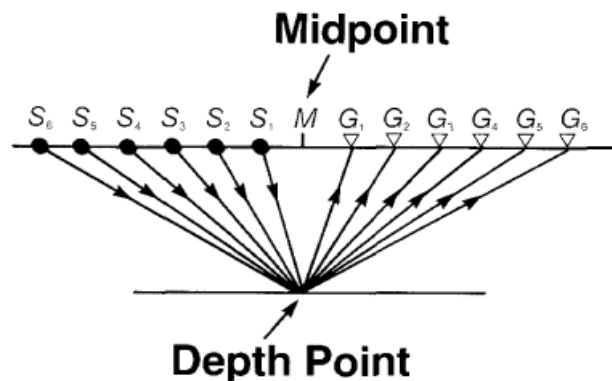


Figure 1.7: Processing of seismic data in midpoint-offset coordinates (Yilmaz, 1987).

### 1.6.4 Velocity analysis

The purpose of the velocity analysis is to improve the reflection signal of the seismic stack data and it is one of the most essential steps in seismic data processing. Usually, the procedure is based on an approach of trial and error. In order to NMO-correct the traces of a CMP gather, a set of trial velocity functions is utilized. The signal to noise ratio is the criterion to determine the correct velocity of the stacked NMO-corrected signal of reflection. The output of the velocity analysis process is a stacking velocity for each event of reflection, plotted as function of reflection two-way zero-offset time called velocity spectrum (Alsadi, 2017).

In Figure 1.8, several seismic events are traced in red. Due to the different curvature of the hyperbola, different velocities result in different energy summation on the different gather traces. With increasing time, the dip and curvature of the seismic reflections decrease. In other words, velocity increases with depth because when sediments are buried deeper, they become compacted and cemented. Generally, older rocks have higher interval velocities and as cementation increases, rocks get more dense and their permeability and porosity decreases (Veeken and van Moerkerken, 2013).

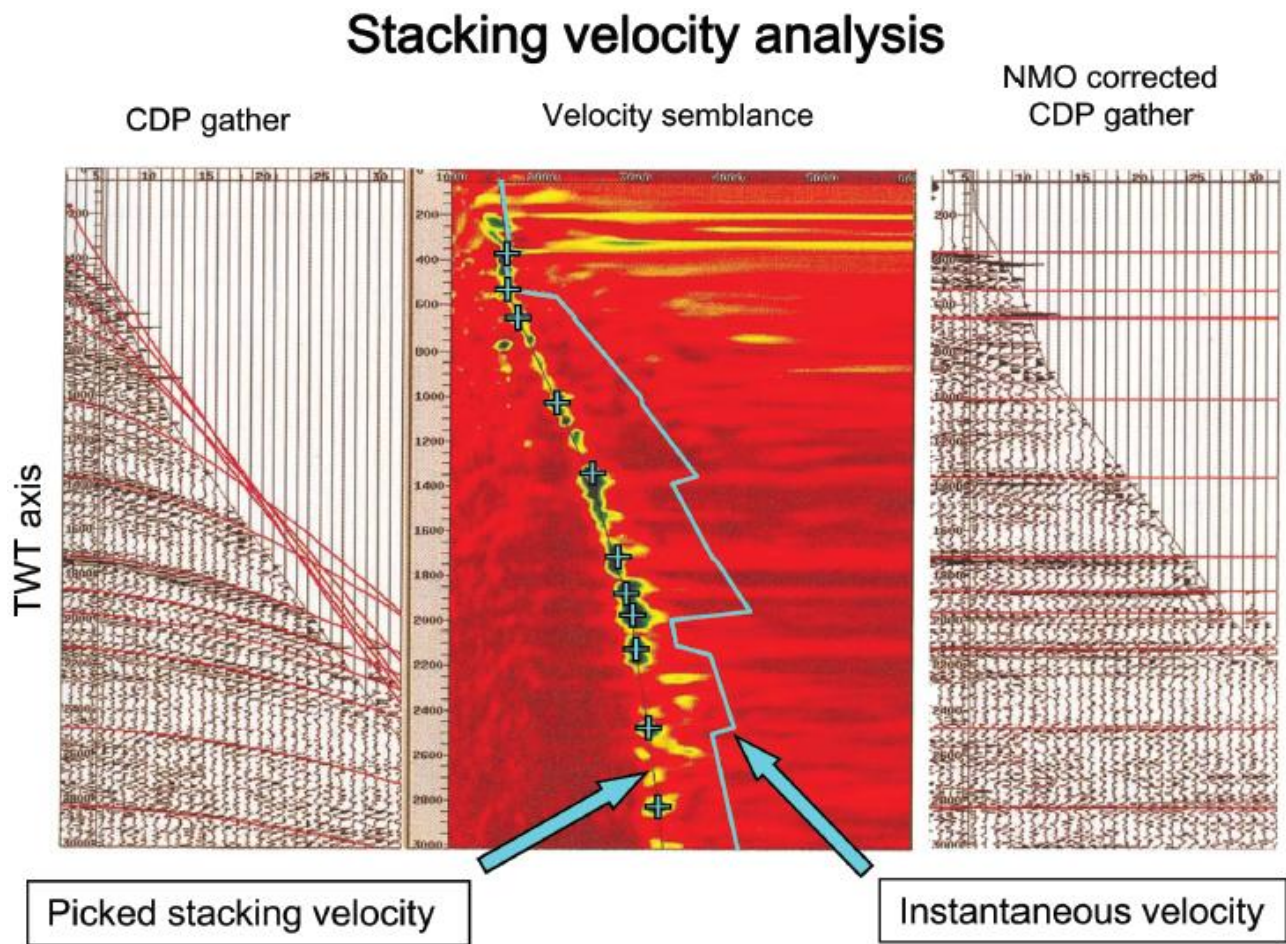


Figure 1.8: Stacking velocity analysis (Veeken and van Moerkerken, 2013).

The velocity spectrum shown in the middle of Figure 1.8 has an horizontal scale of velocity. At each time sample and for each velocity, the total amount of stacked energy on the CDP traces is being computed. After the NMO correction, it is colour coded and the results are displayed in a semblance plot in the center of the velocity panel. The semblance plot is aiming to simplify the velocity picking. It is essential to link the correct energy patches on the semblance plot in order to pick the right stacking velocity profile. Sometimes, the picking procedure can be complex when the data are noisy. In the plot, the light and bluish colours imply the presence of increased seismic energy and the crosses represent the subsequent velocity picks selected for the determination of the optimal NMO correction. On the right side, the solid blue line is the corresponding interval velocity based on the picked velocity function and extremely right, the NMO-corrected CDP gather is displayed. Now the red lines became straight horizontal lines, which indicates that the velocity field chosen for the NMO correction is satisfying and it will result in the best stacked zero-offset seismic trace. The interval velocities can be measured from the reflection times, but the dataset quality affects their reliability (Veeken and van Moerkerken, 2013).

Semblance is a measure of multichannel coherence which can be calculated by the equation below (Sheriff, 2002):

$$S_c(k) = \frac{\sum_{j=k-N/2}^{k+N/2} [\sum_{i=1}^M f_{ij}]^2}{M \times \sum_{j=k-N/2}^{k+N/2} \sum_{i=1}^M (f_{ij})^2} \quad (1.6)$$

where  $S_c(k)$ : the semblance coefficient

$f_{ij}$ : the  $j^{th}$  sample of the  $i^{th}$  trace

$M$ : the number of channels summed

$N$ : the window of width centered on the  $k^{th}$  sample

### 1.6.5 NMO correction and stacking

Applying NMO (Normal Moveout) correction to CMP data, leads to summing the energy of the numerous traces as they will all line-up in a horizontal sense at a given time  $T_0$ .  $T_0$  corresponds to the travel time of the shortest raypath, straight down to the reflector and up again to the receiver. Theoretically,  $T_0$  is the travel time to the reflector at a zero-offset position, so the shot and the receiver are supposed to be in the same position, which is not physically possible, but it is computed using interpolation from the T-X plot of other measured data. The NMO-corrected traces summing is performed in the stacking process. The total amplitude is subdivided by the traces number in the procedure of stacking. Thus, single-raypath sections and multi-raypath stacks can be compared in amplitude (Veeken and van Moerkerken, 2013).

### 1.6.6 Residual statics corrections

Before stacking, an additional step is required for the majority of the data because the moveout in CMP gathers does not always fit perfectly to a hyperbolic trajectory. This occurs because of the velocity irregularities near to the surface that cause static or dynamic distortion complications. Residual statics corrections are applied on the NMO-corrected CMP gathers in order to increase the quality of stacking. The estimated residual corrections are performed on the initial CMP gathers that are not NMO-corrected. Therefore, in order to improve the velocity picks, repeated velocity analyses are conducted. The CMP gathers are NMO-corrected and eventually stacked with this upgraded field of velocity. (Yilmaz, 1987).

### 1.6.7 Time variant band-pass filtering – Gain

Sometimes, predictive deconvolution is efficient in suppressing reverberations or multiples and in additional spectrum whitening. Time variant band-pass filtering is applied to suppress noisy bands of frequencies. Consequently, some type of gain is applied to enhance weak reflections (Yilmaz, 1987).

### 1.6.8 Migration

If the position of the recorded trace at the midpoint between the shot and the receiver are plotted, the event of the reflection will not appear at its actual location. Migration is the procedure of creating an image from the recorded seismic data, by repositioning the reflection events into their correct subsurface locations. The two major categories of migration are time migration and depth migration. Both of them can be performed either before (prestack migration) or after (poststack migration) stack (Jones, 2010).

Prestack migration provides better accuracy for dipping events and higher S/N ratio. For dipping events and non-zero offset traces, prestack migration focuses energy at the right position. Prestack migration distributes non-focal energy more evenly, resulting in less background noise. Even for flat data, both of these effects would enhance the S/N ratio of the image. Although, the prestack migrated images are possible to be noisier than the poststack migrated images in shallow layers, but this can be acceptable. Testing by different techniques and parameters is frequently used in order to find the ideal image and ensure that the results are reliable. However, because of the fact that prestack migration is more accurate in principle, the best image is usually found with the use of prestack migration (Wu, 2001).

In time migration, time is the vertical dimension in the migrated seismic sections and in the case of depth migration, the migrated reflection times are converted into reflector depths (Kearey, Brooks and Hill, 2002). Time migration is characterized by the assumption that the velocity is laterally invariant. Depth migration offers more accurate results and is classified into wavefield extrapolation based and ray based methods. The wavefield extrapolation based depth migration method provides direct wave equation solution and the ability of handling more complex cases. The ray based depth migration methods have the advantage of being computationally efficient, but their disadvantage is the limited fidelity of complex structures. As the depth migration process becomes more challenging, the velocity model needs to be more precise in order to build an accurate image (Jones, 2010).

### 1.6.9 Gain

Usually, gain is applied on seismic data for displaying or spherical spreading correction. A gain function, based on a predefined criterion, is generated from the data and multiplied with the trace amplitudes at each time sample. An undesirable aspect of gain application is the fact that, along with the strengthening of the reflections, the data noise components are also increased (Yilmaz, 1987).

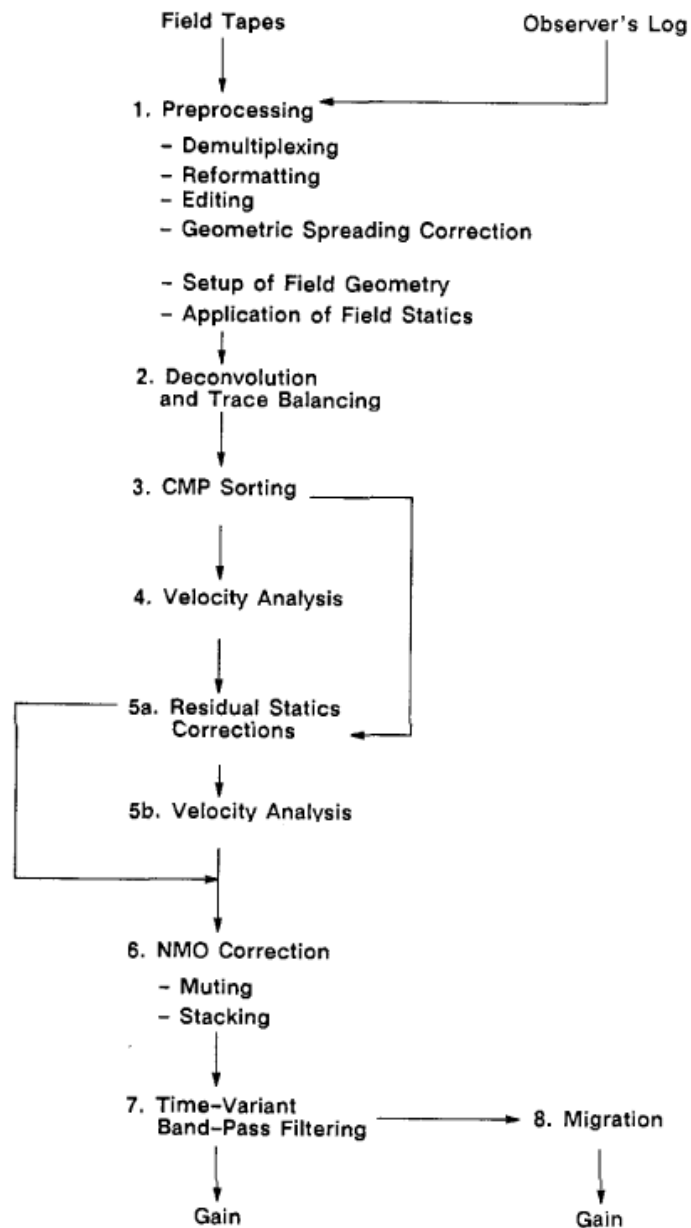


Figure 1.9: Conventional flowchart of seismic data processing (Yilmaz, 1987).

## CHAPTER 2: VELOCITY MODEL BUILDING

### 2.1 Introduction

The estimation of the subsurface velocity is necessary in order to perform migration to the seismic data. Estimating velocity from seismic data is an ill-posed inverse problem, because the data do not contain all of the information required to create a velocity function which varies arbitrarily with depth and along horizontal directions. Although, in many practical situations there is a priori knowledge of the velocity function's behavior which supplements the seismic data information. Usually, this priori knowledge and the information contained in the data are enough to constrain the problem (Biondi, 2006).

In seismic imaging, velocity has two functions. Firstly, it affects data focusing and secondly, it determines the position of imaged reflectors in physical space. As a result, the velocity component that affects the focusing of the data is called focusing velocity and the velocity component that affects the reflectors mapping is called mapping velocity. A common example of focusing velocity function is the RMS velocity function, which is used by Kirchhoff time migration. An example of mapping velocity function is the interval velocity utilized to conduct map migration of time-migrated images. Mapping and focusing velocities are obviously interconnected, and in some circumstances, they are defined by a single velocity function and they are simultaneously computed. Therefore, it is crucial to separate these two types of velocity components due to the fact that their estimates differ in terms of attributes. Additionally, they often are sequentially estimated, with the focusing velocity preceding the mapping velocity estimation (Biondi, 2006).

The majority of velocity estimation methods is based on data of the reflections kinematics. An essential difference among the most of such methods is whether the kinematics are measured from the migration results in the image domain or are measured directly from the data in the time domain. In case of simple geological structures and smooth variations of the lateral velocity, the data domain techniques usually offer accurate estimates of focusing and mapping velocities. Nevertheless, data domain methods tend to fail when geological structures or the velocity function are complex. The capabilities of migration could be utilized in order to focus and simplify the data, enabling the reliable measuring of reflections kinematics and the accurate velocity estimates (Biondi, 2006).

### 2.2 Representation and picking

Generally, velocity model building techniques include the phases of picking and inverting. Each phase has its own errors and assumptions. The phase of picking can occur before or after migration and it can be conducted on a single offset for many horizons or for series of offsets. In case of complex formations, tracing and discriminating the various arrivals branches of diffraction heberboloids is very difficult, so picking before migration implies large error (Jones, 2003).

The representation of the velocity model can advance or restrain the potential of updating the velocity field in a flexible way and it is interconnected with the velocity error picking. When sparse picking is applied and an inaccurate pick is encountered, which is later rejected, then an inconsistency that can be unacceptable large, will remain in the picking grid. Consequently, sparse velocity picking is

possible to cause aliasing in the velocity representation. The main types of velocity models are the layer based and the gridded. In the occasion of the layer based models, picking is simple when constant reflectors are visible as the picking of the update information can be conducted along the boundaries of the reflector. However, when the velocity field does not follow visible reflectors, an a-priori assumption about the velocity behavior is required. In the occasion of the gridded models, a scatter of picks is made, and the resulting ‘cloud’ of values input to the inversion scheme. Furthermore, a hybrid representation that combines the benefits of both types of models can be utilized (Jones, 2010).

### 2.3 Inversion

In practice, applications of inversion methods can be divided into two categories. The first category is data modeling and the second is earth modeling. Deconvolution and residual statics corrections are examples of seismic inversion for data modeling. In data and earth modeling, there is a difference between processing and inversion. The fundamental purpose of processing is to create an earth model in time with an accompanying earth image in time. This earth image could be a time-migrated section or volume of data. The most common type of an earth model representation in time is in the form of a velocity field, which must be characterized by smooth variations in both time and space. Contrastingly, inversion is aiming to create an earth model in depth with an accompanying earth image in depth. This earth image could be a depth-migrated section or volume of data. A detailed velocity depth model, which includes layer boundaries with velocity contrast, is commonly used to represent an earth model in depth. Dix conversion and inversion of stacking velocities, coherency inversion, and analysis of image gathers from prestack depth migration are practical methods of layer velocity estimation (Yilmaz, 2001).

Dix (1955) inversion process in order to estimate interval velocities from picked RMS, or stacking, velocities and corresponding traveltimes is described by the equation below (Koren and Ravve, 2006). Assuming a stack of  $m$  horizontal layers, with layer thickness  $\Delta Z_j$ , interval velocities  $U_j$ ,  $j=1, m$ , and near-vertical raypaths, Dix demonstrated that (Nowroozi, 1989):

$$U_j^2 = \frac{T_{j+1} \times V_{j+1}^2 - T_j \times V_j^2}{T_{j+1} - T_j} \quad (2.1)$$

where  $T_j, T_{j+1}$ : the two-way vertical traveltimes to interfaces  $j$  and  $j+1$ , respectively

$V_j, V_{j+1}$ : the RMS velocities to interfaces  $j$  and  $j+1$ , respectively

Also, (Nowroozi, 1989):

$$U_j^2 = \frac{X_{j+1} - X_j}{T_{j+1} - T_j} \times \frac{dx}{dt} \quad (2.2)$$

where  $dx/dt$ : the inverse ray parameter  $P_i$

$(X_j, T_j)$  and  $(X_{j+1}, T_{j+1})$ : the coordinates of two points with the same slope ( $dx/dt$ ), on the reflections associated with the interfaces  $j$  and  $j + 1$ , respectively.

Moreover, the thickness  $\Delta Z_j$  of the layer  $j$  is calculated by (Nowroozi, 1989):

$$\Delta Z_j^2 = \frac{U_j^2 \times (T_{j+1} - T_j)^2 - (X_{j+1} - X_j)^2}{4} \quad (2.3)$$

During the model estimation, every tomographic inversion technique takes into consideration the error factor and constructs the model in order to minimize it. The key ingredient of an inversion scheme is the relationship between accuracy and speed. An aspect of the process is being represented using some assumptions which are made about the physical process in conjunction with some equations that permit the association of some measurements with the velocity model. The reduction of the dissimilarities between the observed and computed data is conducted relatively with the present interpretation of the velocity model. The first stage of tomographic inversion is to forward the model and calculate the differences between the observed and calculated data and the second stage includes the perturbation of the model in order to diminish these differences to a satisfying level (Jones, 2003).

For some schemes, such as a simple vertical Dix inversion of the picked errors, the update is not tomographic. In these circumstances, the updated data are not being attributed to their correct spatial locations. The general workflow of the most velocity model building methods is depicted in Figure 2.1. A starting depth model is generated using initial information such as stack times  $T_s$  and RMS velocity. This feeds into an iterative loop for velocity updates, resulting in a migration run of high fidelity. Tomographic schemes are described in Figure 2.2, where the velocity model is iteratively perturbed in an effort to reduce the inequalities between the observed and modelled data (Jones, 2003).

Tomographic inversion encloses a group of techniques that can theoretically produce a velocity model with the appropriate level of complexity for migration. Ideally, the tomography's basis should be combined with an appropriate migration scheme. The data fed to the tomography must be accurate in order to obtain a precise output. Furthermore, the data should be sufficiently sampled in order to resolve the level of detail required in the model and migrate it accordingly (Jones, 2010).

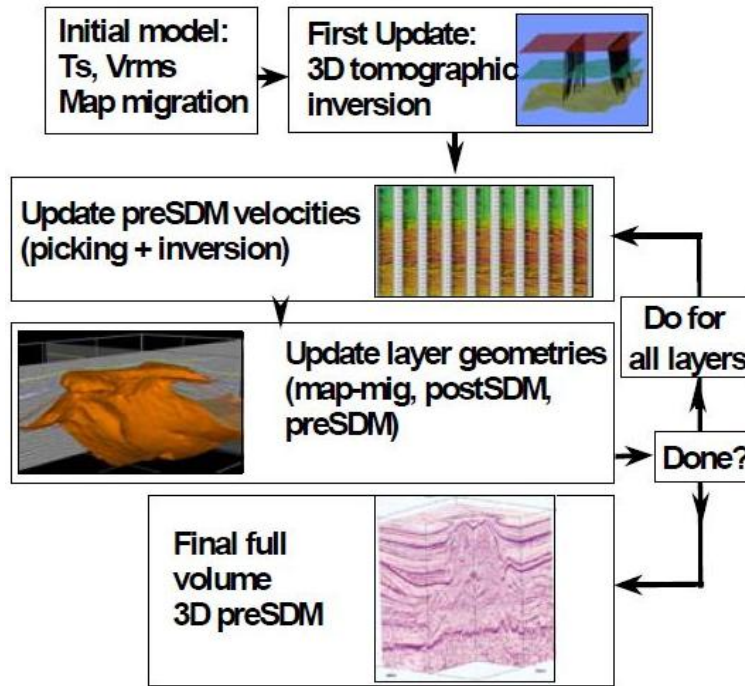


Figure 2.1: General velocity update scheme (Jones, 2003).

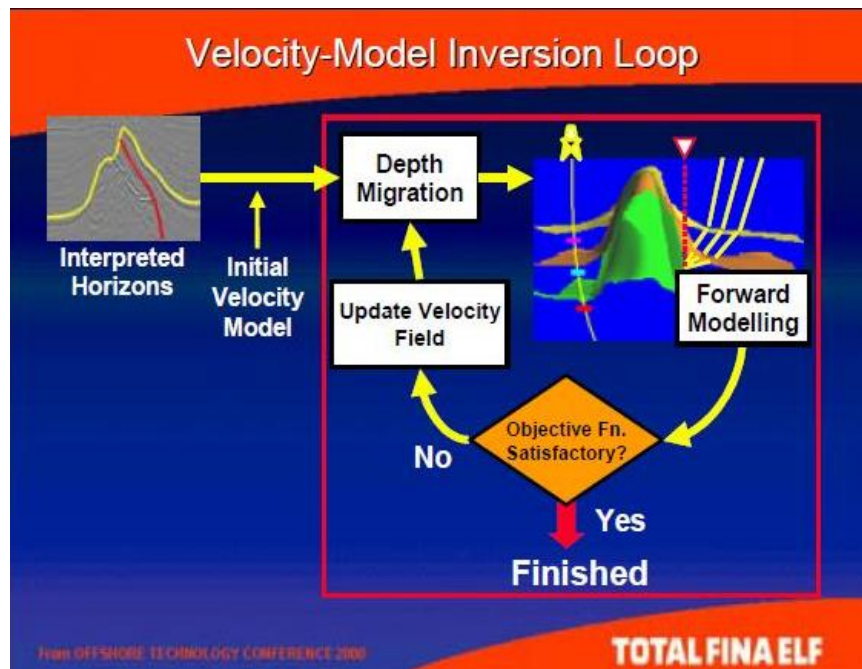


Figure 2.2: General tomography and model update workflow (Jones, 2003).

## 2.4 Velocity model building techniques

In the present thesis, the examined velocity model building technique is migration velocity analysis (MVA). Some of the rest main velocity model building techniques are described below:

- Manual tomography
- Stereotomography, which uses picked travel times and slopes from the shot and receiver gathers and builds a ray-based tomographic system to generate the velocity model update (Zhao, 2020).
- Inversion of the dip information yields model update (Jones, 2003).
- Deregowski loop, which is the most basic technique for simple post-migration model update. This technique's disadvantages are the facts that the events are picked at wrong spatial location and the RMS error picked is then inverted vertically. In order to succeed a correct model update, the velocity error should be picked in its correct location. Then, the velocity model should be updated by inverting along the normal to the reflector that is being updated (Jones, 2003).
- CRP-scan, where a unique migration is conducted for every suite of models and the generated scan of CRP gathers is built to select the flattest. As a result, the error is picked in its correct spatial location (Jones, 2003).
- 3D tomographic inversion of picked zero-offset stack times and stacking velocities, where a 3D model is perturbed globally, and for each perturbation, the multi-offset ray traced CMP arrival times are fitted with a hyperbola that is utilized to determine a stack time and stacking velocity related with the current perturbation of the model. The model is perturbed iteratively in order to reduce the contrast between observed and calculated stack times and stacking velocities. This technique is characterized by restrictions in providing an initial model (Jones, 2003).
- Tomographic inversion of picked zero-offset time-migrated times and DMO (Dip Moveout) velocities, which is similar to the previous method but with the benefit of using observables picked from migrated data. As a result, the input data are more accurate for complex geometries, but there are limitations when the scheme demands demigration of the picks and backing-out DMO effects from the velocities (Jones, 2003).
- CFP (Common Focal Point) analysis, which is based on the theory that the subsurface parametrization must be delayed as much as possible in the seismic processing in order to avoid bias. The wavefield operators from seismic data are estimated first and the velocity model is not in the iteration loop (Jones, 2003).
- Tomographic inversion of prestack multi-offset arrival times, which can create a starting model very quickly, but the picking is very difficult in complex areas (Jones, 2003).
- Tomographic inversion of prestack time migrated multi-offset arrival times, where the complications of picking on unmigrated data in order to obtain the prestack multi-offset input for the scheme of the tomographic inversion are avoided (Jones, 2003).
- Tomographic inversion of prestack depth migrated multi-offset arrival depths, where the drawback of picking on unmigrated data is also avoided. Picks of residual depth error that are conducted for each and every offset on an event are fed to the scheme of the inversion in order to decrease the residual errors. In addition, this technique can be combined with the CRP-scanning. In this case, the inversion input can be picked from the most flat gathers coming from a preSDM with a set of perturbed models of velocity. Some techniques are aiming to solve the inverse problem globally for all residuals and some others use layer stripping and work iteratively (Jones, 2003).

- Wavefield extrapolation (non-Kirchhoff) techniques, which provide a more complete solution for multi-pathing problems than single arrival Kirchhoff. However, the availability of gathers after migration is barrier in wavefield extrapolation migration. Common shot migration does not generate prestack data by default because during imaging, the offsets are converted to zero-offset. (Jones, 2003).
- Deep learning-driven velocity model building techniques, which produce velocity models using as input raw seismic data and analog velocity models, which are created by a generative adversarial network (GAN). It is proven that the GANs are dominant category of generative models. The DL workflow includes the unsupervised label generation using the GAN, the equivalent data generation and the convolutional network training, where predicted models are constructed using the generated data. During the stage of the convolutional network training, which is happening once, the optimum parameters of the neuronal network are found in order to match the predicted and the generated data. After the training stage, the tomography operator can predict velocity models for real input data. In other words, the tomography operator is trained for many representative cases and it produces cases using real data. In conclusion, the DL-based tomography workflow can be conducted using the GANs advantages to train a tomography operator reaching to spectacular results (Araya-Polo, Farris and Florez, 2019).

## 2.5 Common image gathers

When Kirchhoff migration is conducted, the data are displayed as a function of their offset by subdividing the integration domain during the summation. The migrated cubes created by this subdivision, known as partial images, use only a data subset and the entire image is a hypercube produced by the ensemble of all these partial images (Biondi, 2006).

The evaluation of the variations between the partial images at a fixed image point is very beneficial for the velocity analysis. In order to execute this analysis, the subsets of the entire image with fixed surface locations, known as common image gathers (CIGs), are frequently displayed. When the partial images are functions of the data offset, they are called offset-domain image gathers (ODCIGs) and when they are functions of the reflection angles, they are called angle-domain common image gathers (ADCIGs). ODCIGs the simplest category of CIGs that can be constructed by Kirchhoff migration, but large variations of lateral velocity could reduce their efficiency. On the contrary, ADCIGs are more reliable in these situations (Biondi, 2006).

In the case of a correct velocity model, the reflections in the common image gathers should be horizontal. Also, they should reinforce each other when they are stacked. If the reflections have upward or downward curvature as a function of offset in the CIGs, and the velocity model update is based on this behaviour as a function of offset, then the velocity model is erroneous (Deregowski, 1990, Liu and Bleistein, 1995).

## 2.6 Migration velocity analysis

In general, CMP stacking, velocity estimation and migration are considered to be separate procedures. Therefore, they share a common theoretical base, which is the scalar wave equation. Migration and CMP stacking demand information about velocity in order to evaluate it. If the subsurface medium is horizontally layered, there is not a recognizable difference between migration and stacking velocities, but in case of dipping reflectors there can be contrast. Migration velocity does not depend on dip, whereas stacking velocity is sensitive to the dip of the reflection interface. As a result, it is necessary to use a velocity field which is corrected for dips that exist in the data. Thus, every process that obtains acceptable velocities for migration should rely on data from several neighboring CMP gathers (Yilmaz, 2001).

Migration velocity analysis can be conducted similarly to stacking velocity analysis. Generally, in order to estimate stacking velocities, moveout correction is applied on a CMP gather and the traces are stacked in the gather with the use of a range of constant velocities. The results can be used to determine velocity, either as a set of CVS (constant-velocity-stack) panels or as a set of velocity spectra at certain locations along the line. Theoretically, the estimation of migration velocities requires prestack migration, using a range of constant velocities, and producing selected gathers in their migrated positions. The major difference between migration and stacking velocity estimation is that migration velocity requires the whole prestack data set and the stacking velocity only requires individual CMP gathers (Yilmaz, 2001).

The extraction of velocity information in the data space is both imprecise and time-consuming in the presence of complex structures and large lateral velocity changes. In these circumstances, the image space is a preferred domain for collecting kinematic data since the migration focuses and simplifies the events. MVA methods are methods of velocity estimation that utilize migration's focusing capabilities to retrieve kinematic information more accurately. Migration velocity analysis is an iterative method with two steps. Firstly, prestack migration is used to image the data (Biondi, 2006). The flexibility of prestack Kirchhoff migration allows to output selected CMP gathers at their migrated locations. As a result, this method provides the capability of generating a migration velocity field by picking RMS velocity functions from the selected output gathers (Yilmaz, 2001). Secondly, the velocity function is updated on the basis of the migration results. The global convergence of this procedure is a primary concern and in order to ensure it, the initial velocity model must be characterized by high quality (Biondi, 2006).

The extraction of kinematic information from the migrated image cube is MVA's first challenge. The accuracy of the velocity function in the data domain is determined by assessing the coherency of the data in CMP gathers along the offset axes after NMO correction. In the image domain, the velocity function precision is determined by measuring the reflections focusing in the migrated image. The most frequent criterion to examine the focusing is the image coherence in CIGs after migration. Coherency is measured along the offset axes when offset-domain CIGs are formed. It is noteworthy that in the CIGs, the departure from flatness of the events is called residual moveout (RMO). Usually, it is more robust in the migrated domain to assess the RMO as a function of one or a few factors rather than calculating the depth errors for each offset or angle, as it is in the data domain. For reliable measurements, the residual moveout parameterization must be chosen carefully (Biondi, 2006).

Another advantage of extracting kinematic information in the migrated domain instead of the data domain is that in the migrated domain, the reflections focusing and the RMO can be both measured. By

using residual prestack migration and constructing velocity spectra similar to the RMO spectra, the residual focusing necessary for optimal data imaging may be evaluated. If the purpose of migration velocity analysis is a simple estimation of an accurate RMS velocity function for prestack time migration, the measurements of RMO parameters are being used to update the RMS velocity function directly. However, if migration velocity analysis aims to perform depth migration with an interval velocity function, the kinematics errors measured from migrated gathers should be translated into interval velocity updates (Biondi, 2006).

A straightforward procedure is followed in order to update the velocity function with the use of CIGs. Firstly, inverse NMO correction is applied on the CIG gathers, according to the RMS velocity used for the data migration. Secondly, the conventional velocity spectra is constructed for the CIGs. Thirdly, a new RMS velocity function is created using the stacking velocities derived from the velocity spectra. The new function is used in order to migrate the data again. The process can be repeated, if necessary, to improve the velocity even more (Biondi, 2006).

MVA is widely known in the industry due to its simplicity. Although, this method has the drawback that it assumes an horizontally layered model with no lateral velocity variations. In case of dipping reflectors or lateral velocity variations, MVA is erroneous in estimating the optimal time migration velocity. Furthermore, MVA requires manual NMO velocity picking in each iteration, and as the density of MVA increases, the cost increases significantly (Zhao, 2020).

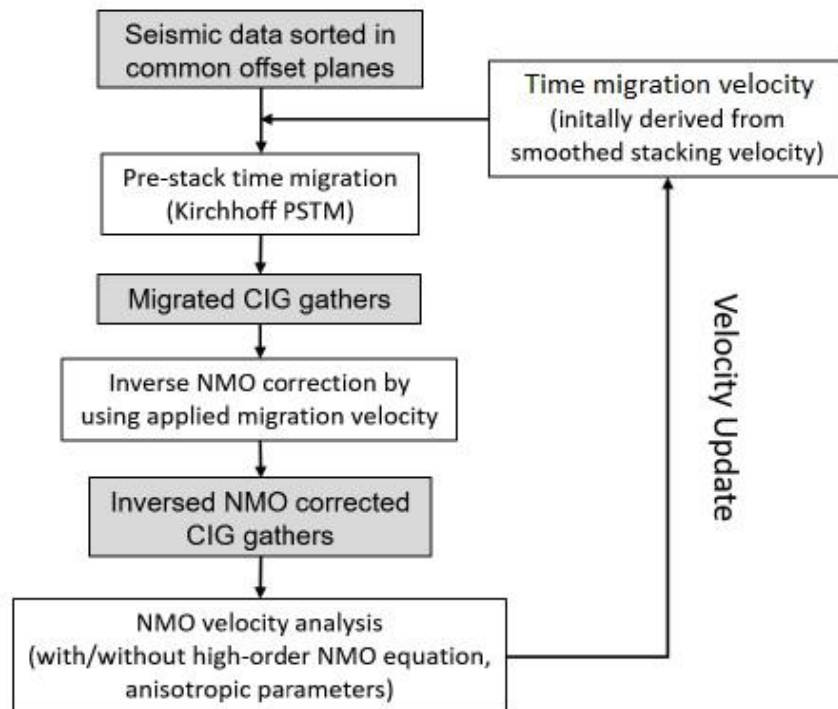


Figure 2.2: Conventional workflow of MVA (Zhao, 2020).

## CHAPTER 3: SYNTHETIC DATA CREATION

The synthetic data used in the present thesis are obtained from a previous thesis that took place in the Applied Geophysics laboratory of Technical University of Crete. The geological model used as input for the creation of the synthetic data was generated by seismic reflection data from South Crete. Therefore, it is not possible to display the area of study on the map. The synthetic seismic reflection data were generated by algorithms created in Matlab, which are based on the finite difference method and simulate the seismic waves propagation in two dimensions. It should be mentioned that this particular survey is a sea survey and the upper surface of model is free boundary. The initial model parameters are mentioned below:

- Horizontal extend of model: 8345 m
- Vertical extend of model: 6000 m
- Minimum S-wave velocity: 900 m/s
- Dominant frequency of the source: 10 Hz
- Receiver increment: 5 m

Then, the seismic layers which indicate the coordinates of each layer boundaries are inserted. Afterwards, the velocities of P-waves and S-waves and the density are inserted.

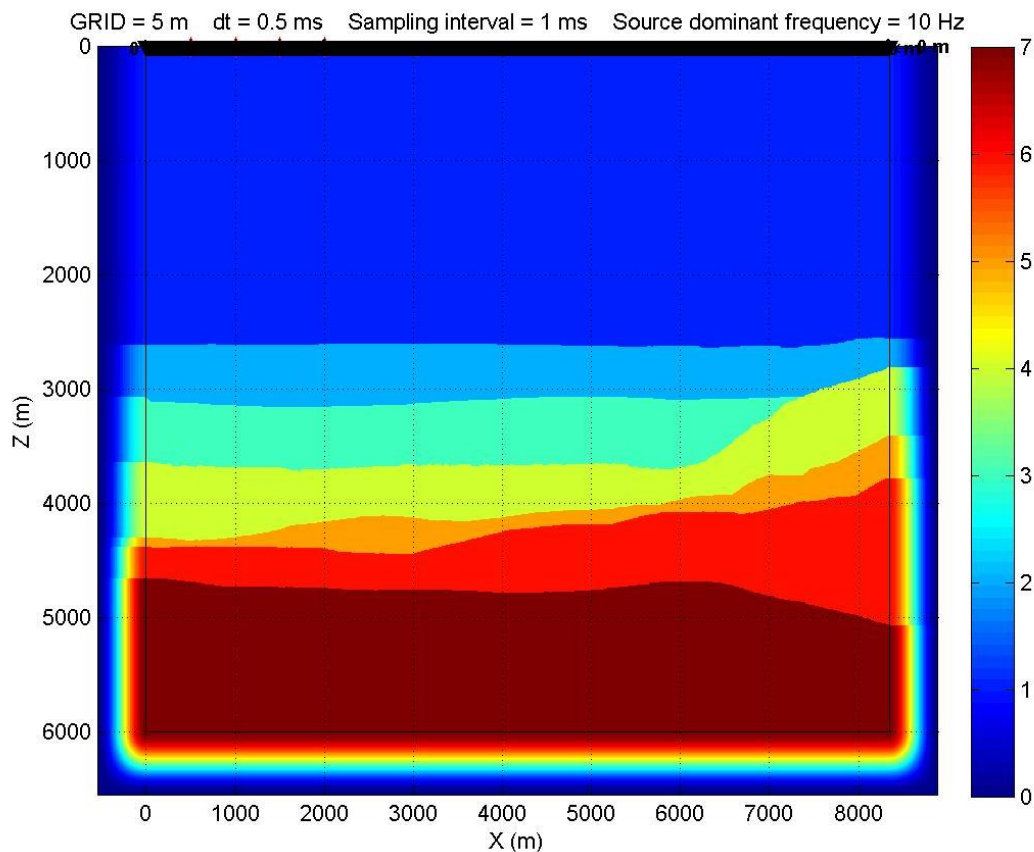


Figure 3.1: Synthetic model of seismic layers.

The parameters entered in PSV SYNTHETICS software for each seismic layer are presented in Table 3.1.  $V_p$  is the P-waves velocity,  $V_s$  is the S-waves velocity and  $\rho$  is the density. S-waves do not propagate in liquids, so their velocity in water is equal to zero. However, in order to avoid computation issues of PSV SYNTHETICS it was set equal to 0,01 m/s.

Table 3.1: Table of velocities and density for each seismic layer.

A/A	$V_p$ (m/s)	$V_s$ (m/s)	$\rho$ (gr/cc)
1 <sup>st</sup> Layer (water)	1500	-	1,023
2 <sup>st</sup> Layer (bottom)	1800	900	1,8
3 <sup>st</sup> Layer	2200	1100	1,9
4 <sup>st</sup> Layer	2500	1250	2
5 <sup>st</sup> Layer	3000	1500	2,2
6 <sup>st</sup> Layer	3800	1900	2,4
7 <sup>st</sup> Layer	5500	2750	2,65

After the synthetic model of seismic layers creation, the parameters of the geometry of the seismic reflection survey were entered and they are mentioned below:

- Source dominant frequency: 10 Hz
- Number of shots: 16
- Shot increment: 500 m
- Z coordinate of source: 10 m
- X coordinate of first source: 500 m
- Receiver array increment: 5 m
- Number of receivers: 1670
- Z coordinate of receivers: 0 m
- X coordinate of first receiver: 0 m

In order to simulate the survey, through PSV SYNTHETICS, this procedure was repeated 16 times for each source position. The source was placed 10 m under the sea surface along the Y axis from 500 m to 8000 m with 500 m step. The hydrophones were placed along the entire length of the model (0-8345 m) with 5 m increment and remained stable without moving for each repetition. After entering the seismic reflection survey parameters of the model, the \*.SMP, \*.SRC and \*.RCV Matlab files were created and they were utilized in data processing. The \*.SMP file contains the model parameters, the \*.SRC file contains the sources parameters and \*.RCV file contains the receivers parameters (Χρηστίδη, 2019).

Common shot gathers for source positions 500, 2500, 4500 and 6500 m are displayed in Figures 3.2, 3.3, 3.4 and 3.5. X-axis corresponds to the distance and the Y-axis to the two-way travel time. For each figure, the first arrival corresponds to direct waves. The other six, from 3,5 to 5,9 s, are attributed to reflected waves that correspond to the reflectors. The last arrival, which appears at the double time in every figure, corresponds to the multiple of the first reflection.

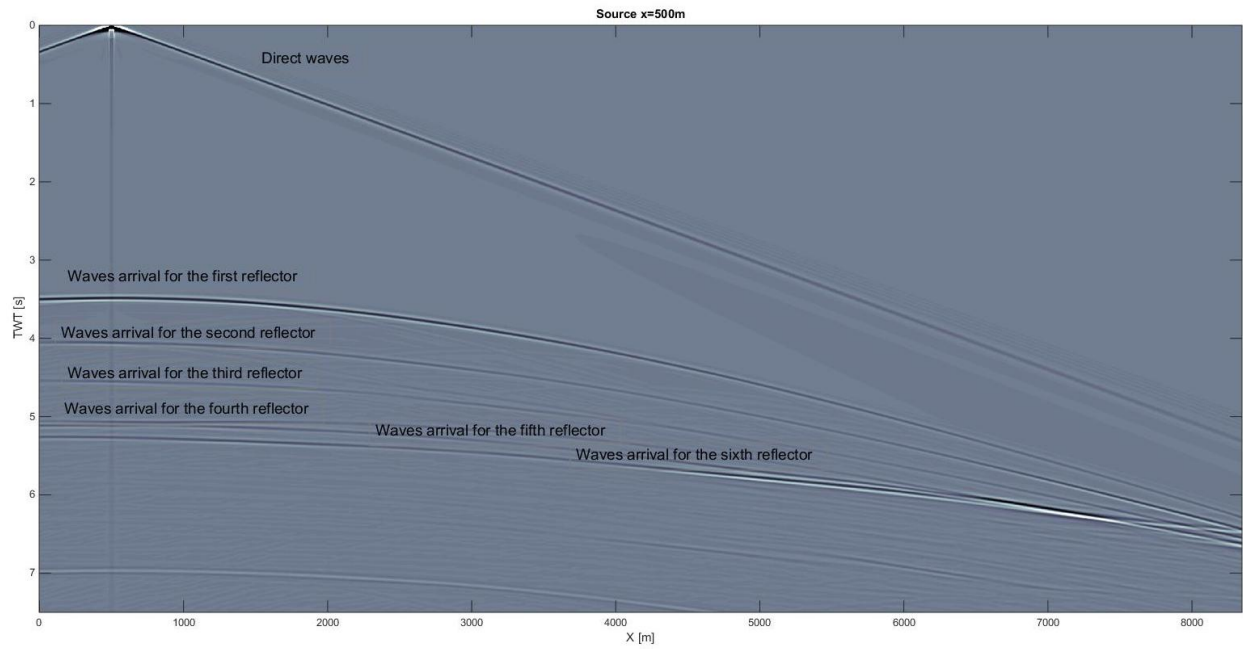


Figure 3.2: Common shot gather. The source is in the position 500 m.

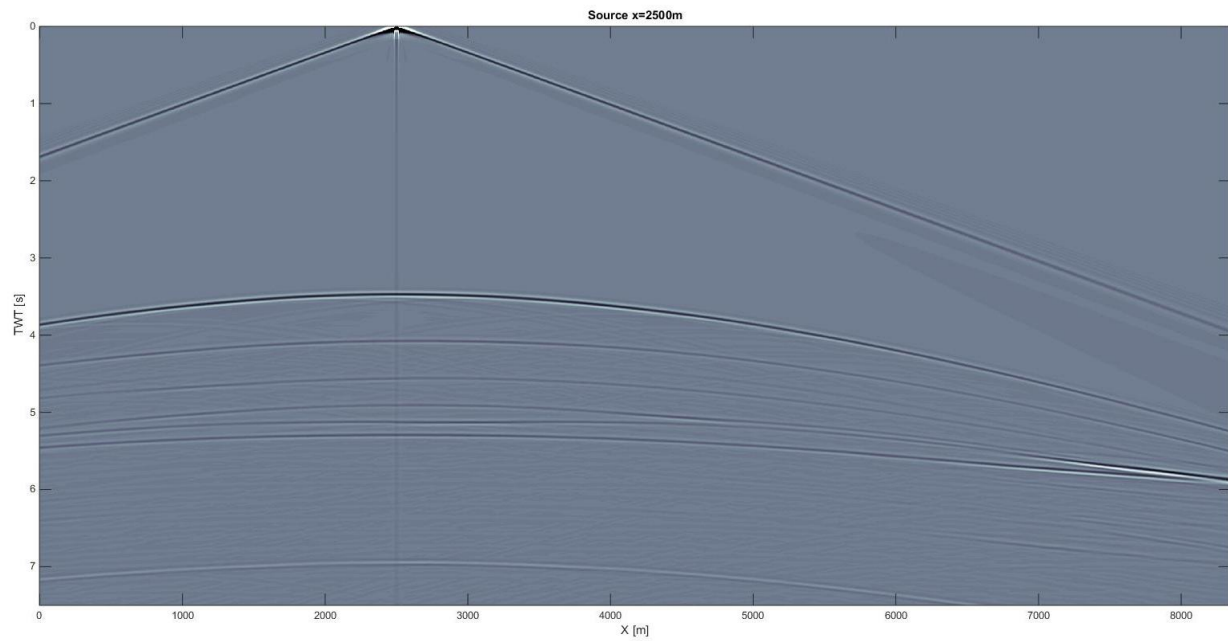


Figure 3.3: Common shot gather. The source is in the position 2500 m.

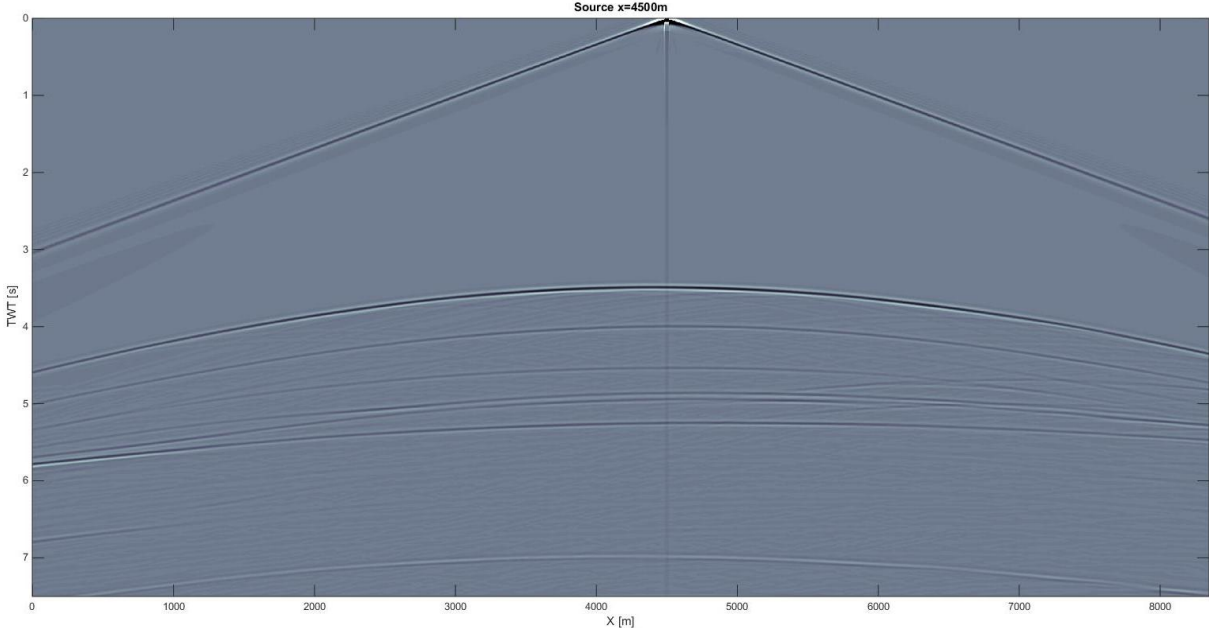


Figure 3.4: Common shot gather. The source is in the position 4500 m.

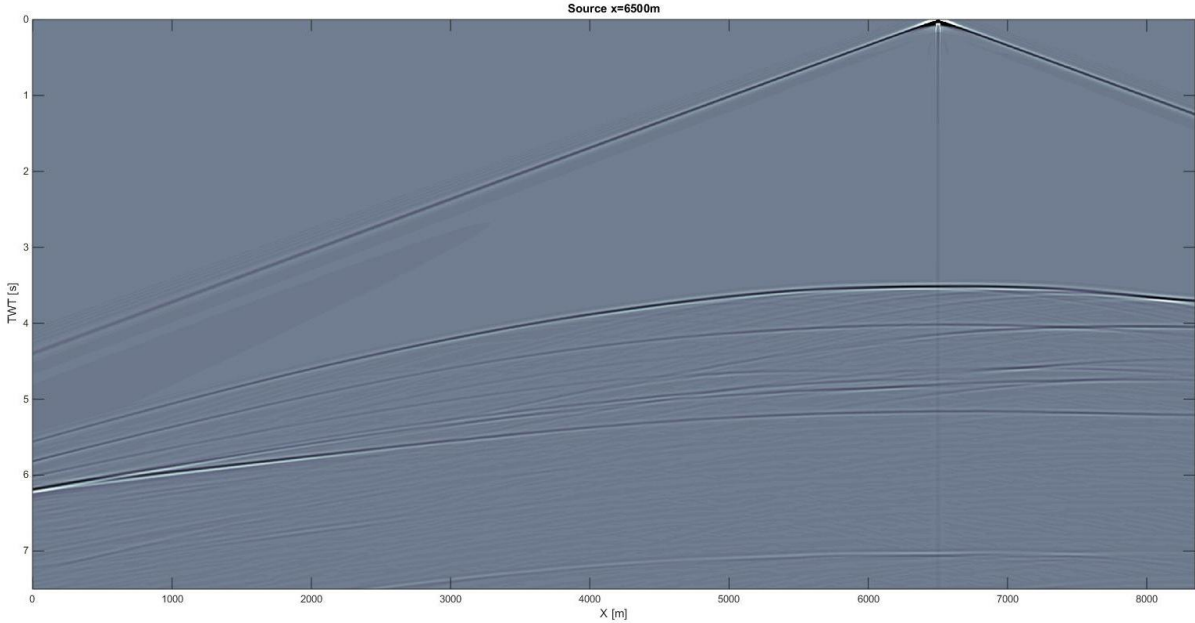


Figure 3.5: Common shot gather. The source is in the position 6500 m.

## CHAPTER 4: DATA PROCESSING

### 4.1 Prestack migration

The data processing was achieved with the use of Matlab and Crewes library. Firstly, prestack Kirchhoff migration was applied on each and every common shot gather. The RMS velocity model used for the migration is displayed in Figure 4.1. The migration output is displayed in Figures 4.2, 4.3, 4.4 and 4.5 for the source positions 500, 2500, 4500 and 6500 m, respectively. Also, the migrated section resulting from the summation of the migrated common shot gathers is displayed in Figure 4.6 and the interval velocity model is displayed in Figure 4.7. The field of interest is from zero to 5,5 s, hence the prestack migration was conducted from zero to 5,5 s in order to reduce the amount of time spent on the procedure. Furthermore, the migration aperture was set 8345 m and the maximum scattering angle limit was set 90°.

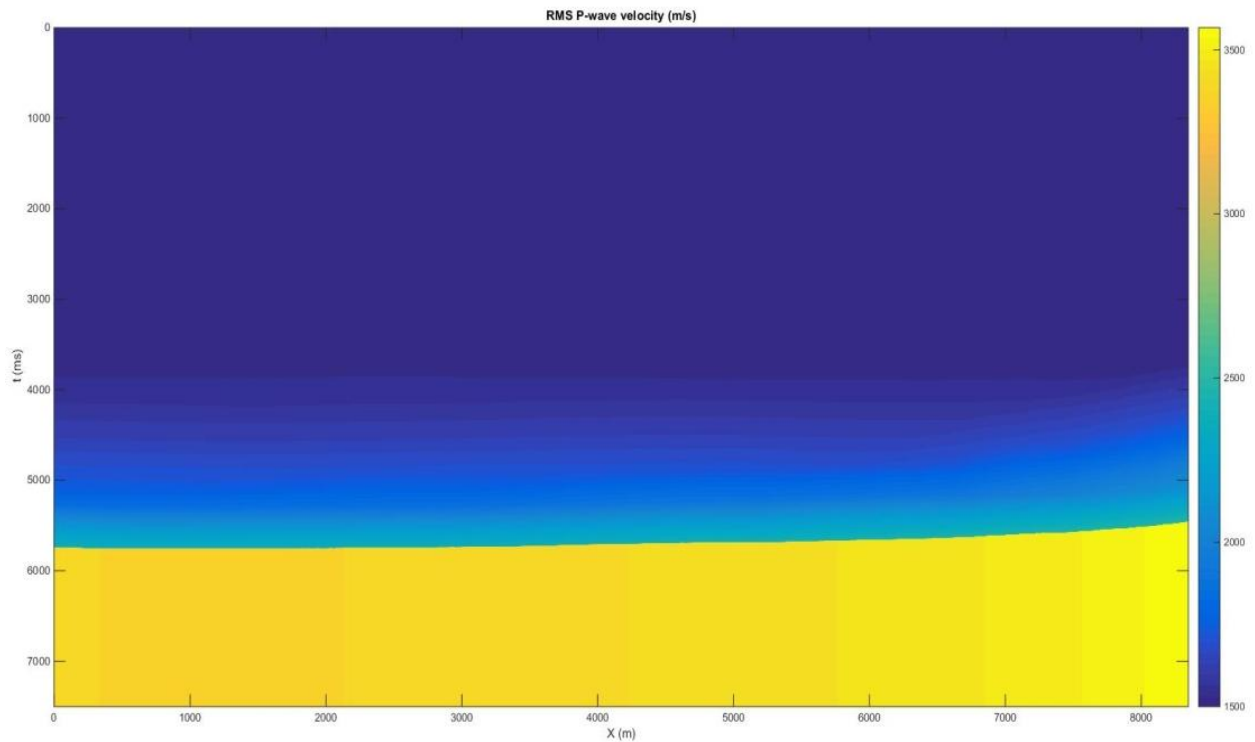


Figure 4.1: RMS P-wave velocity.

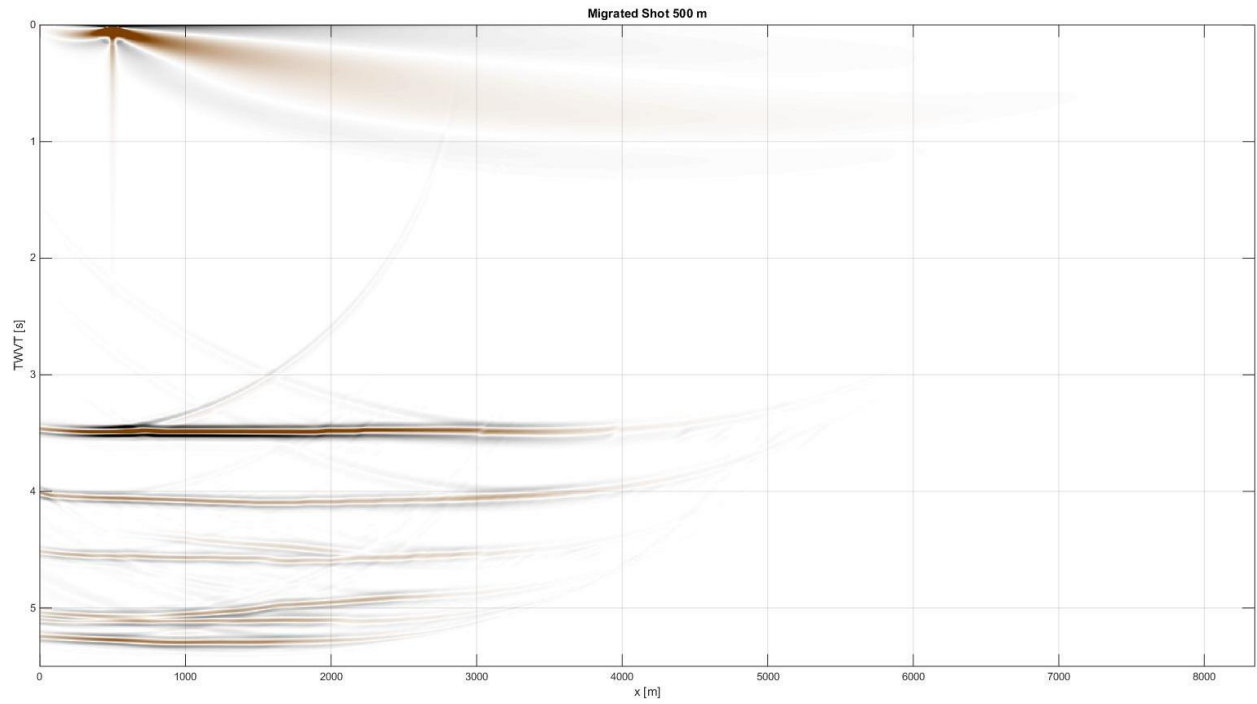


Figure 4.2: Migrated common shot gather. The source is in the position 500 m.

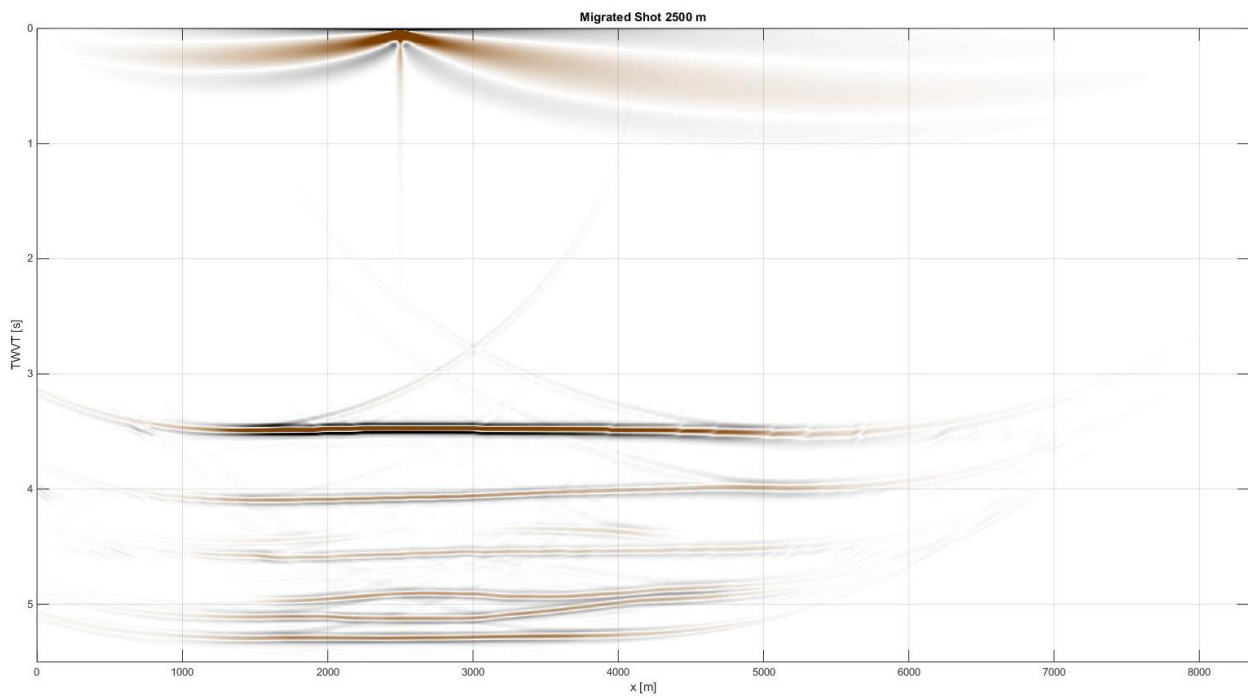


Figure 4.3: Migrated common shot gather. The source is in the position 2500 m.

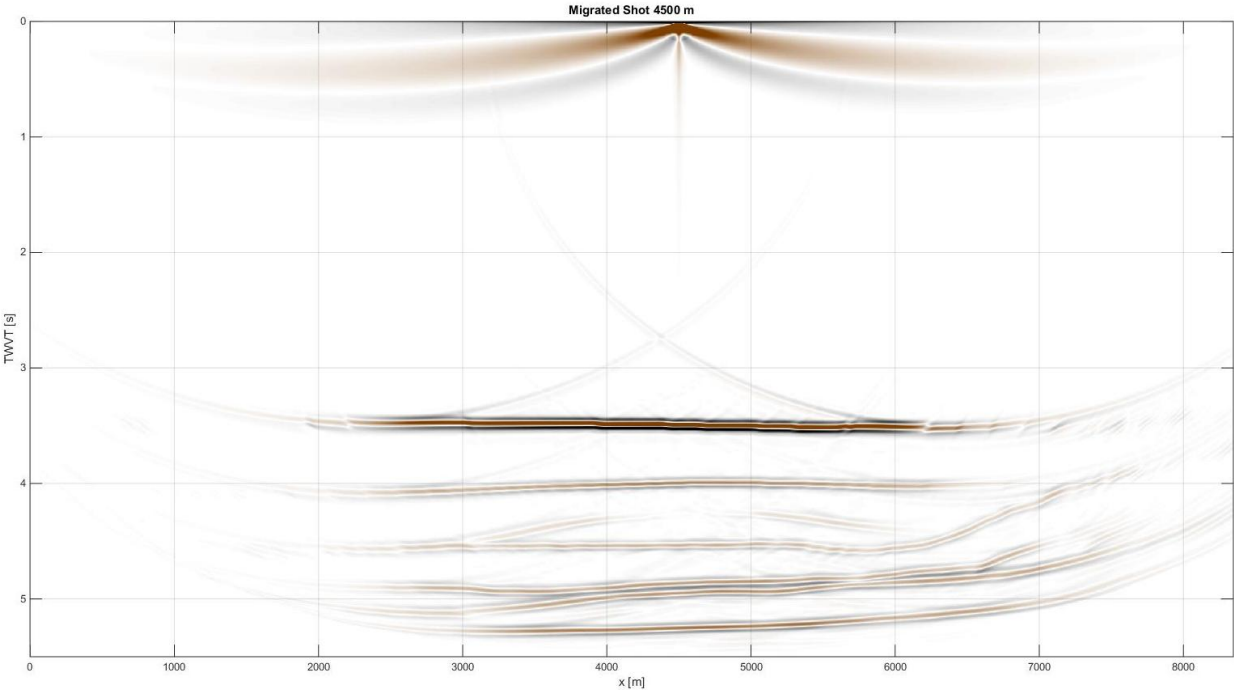


Figure 4.4: Migrated common shot gather. The source is in the position 4500 m.

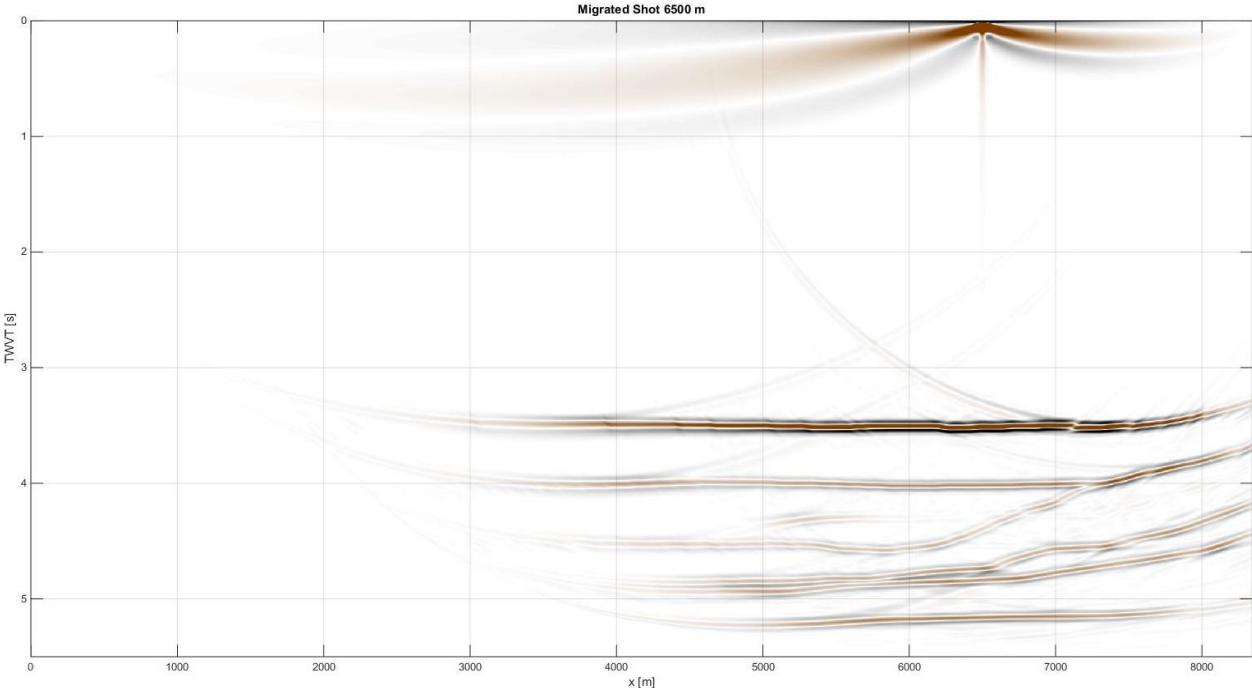


Figure 4.5: Migrated common shot gather. The source is in the position 6500 m.

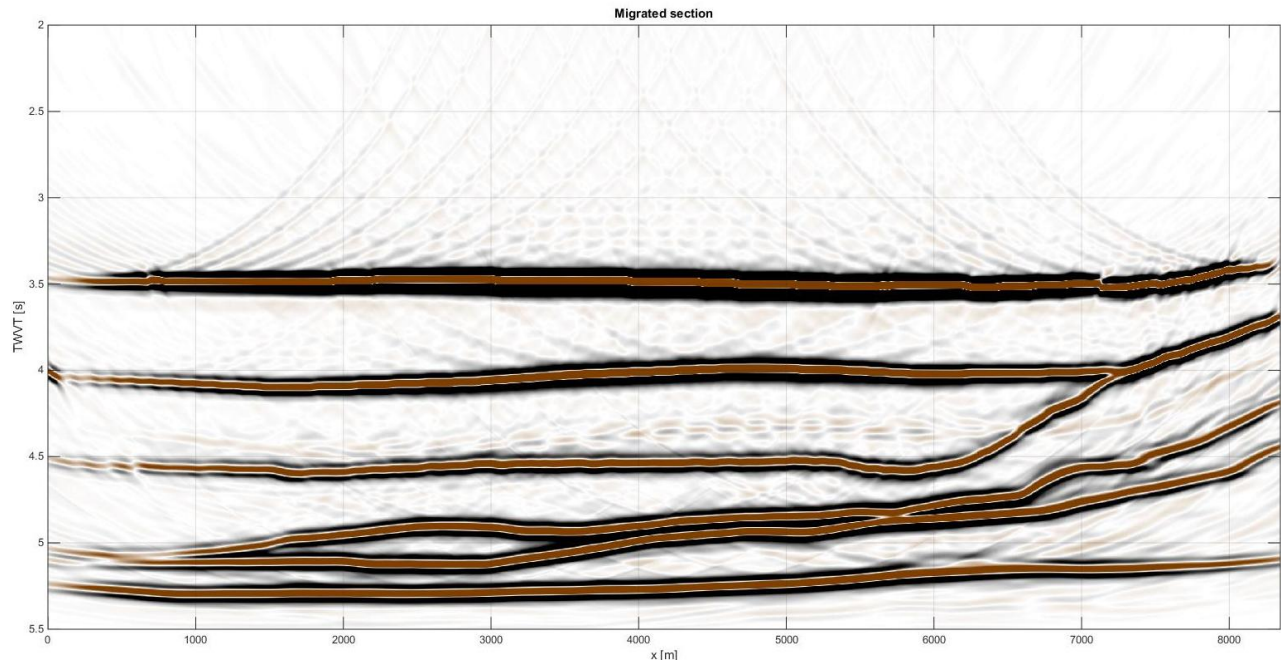


Figure 4.6: Migrated section.

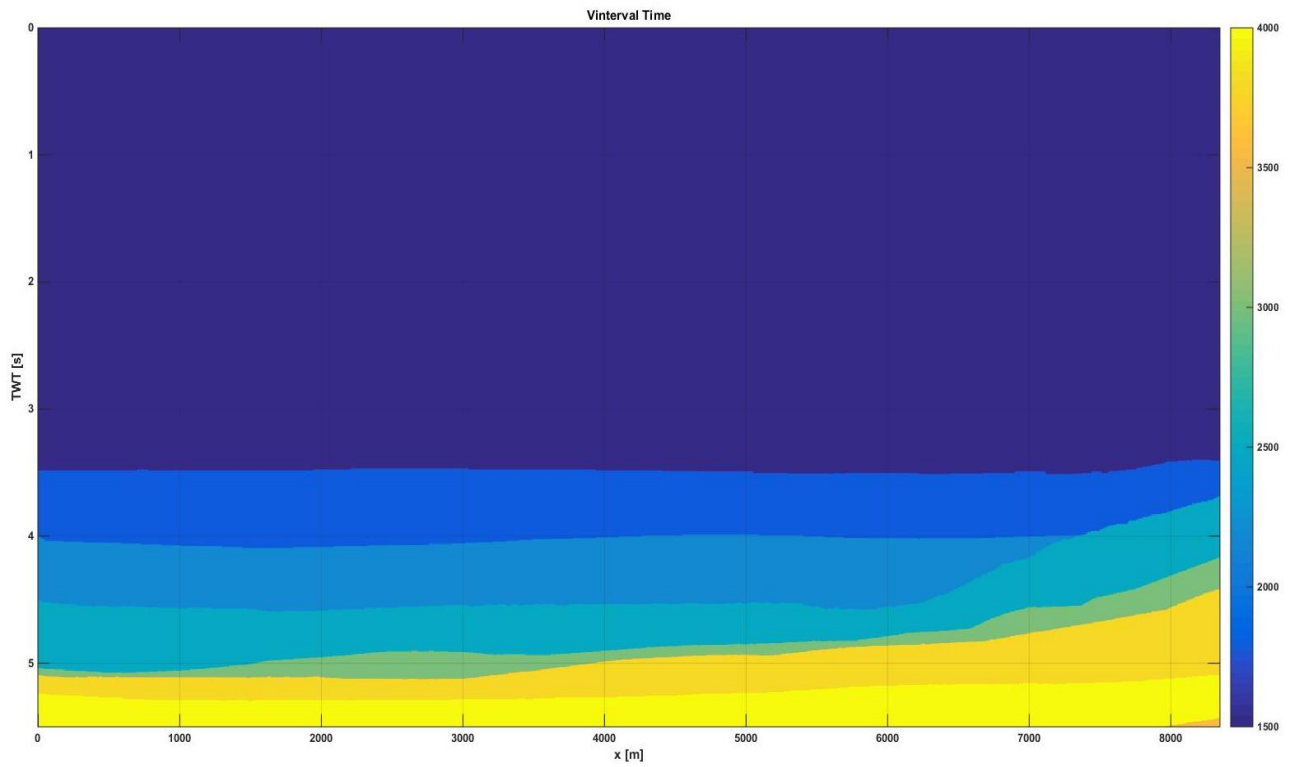


Figure 4.7: Interval velocity.

## 4.2 Common image gathers

Offset-domain common image gathers were created with the use of CMP\_Synthetics algorithm, which also produced the distribution diagram shown in Figure 4.8. It should be noted that the prestack Kirchhoff migration applied interpolation to the data and created 3339 traces. Hence, oversampling was required. The total number of the CIGs is 3170 and the CIGs increment is 2,5 m.

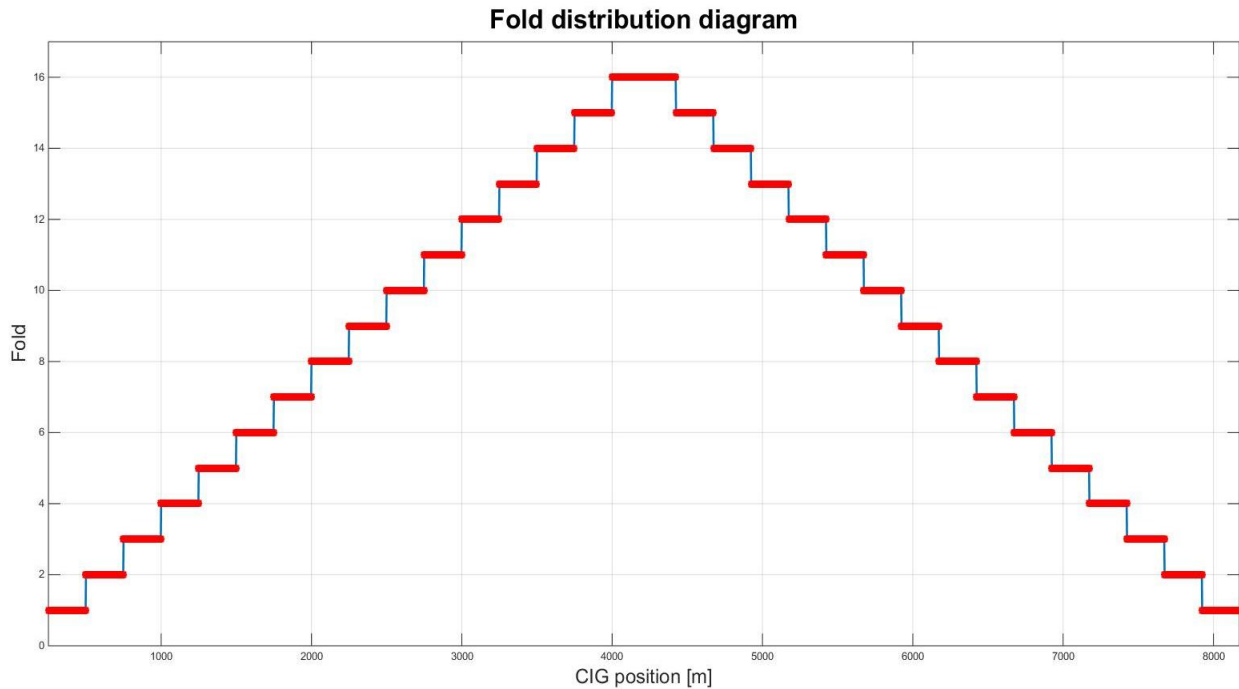


Figure 4.8: Fold distribution diagram.

It should be mentioned that fold is restricted due to the restricted number of sources, so it is necessary to integrate CIGs and produce CIG Supergathers. The fold of each and every integrated CIG was 16. Utilizing three CIGs resulted in increasing fold to 48. Also, the direct waves from zero to 3000 ms were cut. The first CIG Supergather, shown in Figure 4.12, was generated by the integration of the CIGs No. 1501, 1551 and 1601, which are displayed in Figures 4.9, 4.10 and 4.11. In Figures 4.8 to 4.20, the horizontal axis corresponds to offset and the vertical axis corresponds to the two-way vertical traveltme (TWVT), since the data are NMO-corrected.

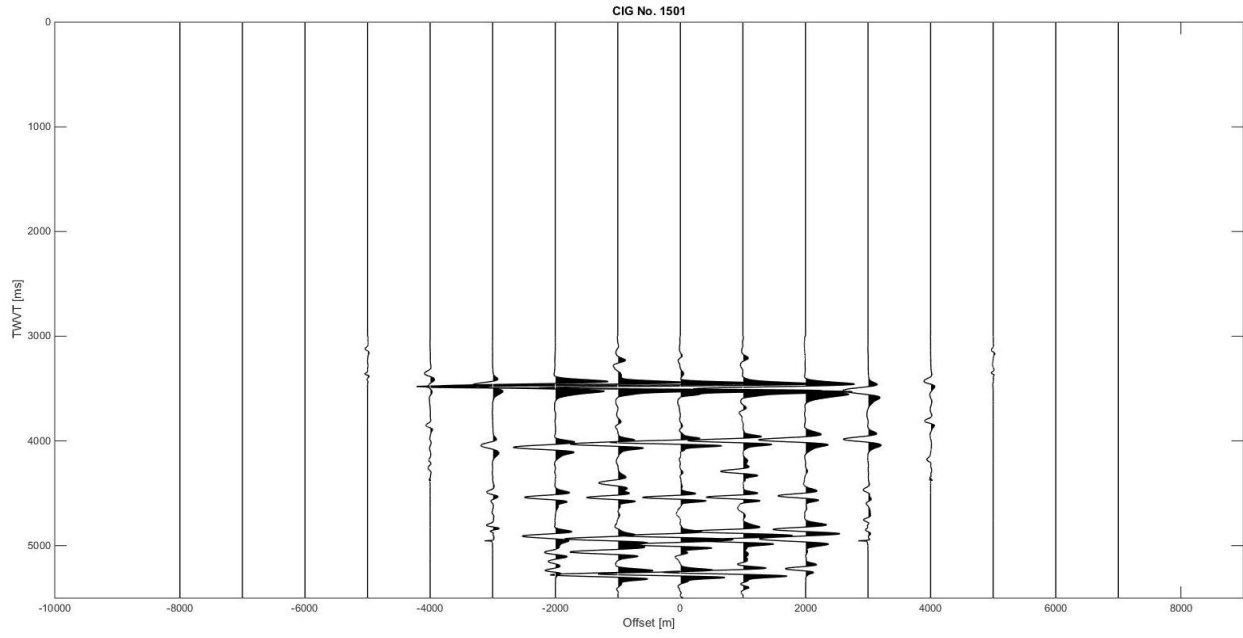


Figure 4.9: CIG No. 1501.

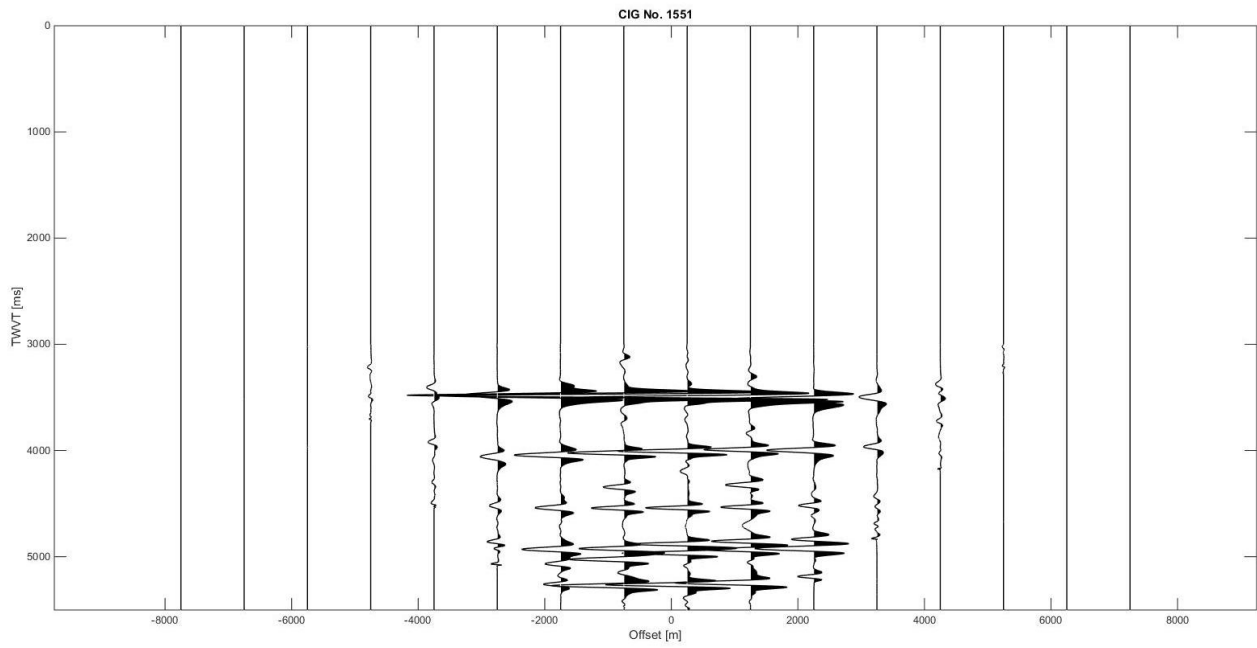


Figure 4.10: CIG No. 1551.

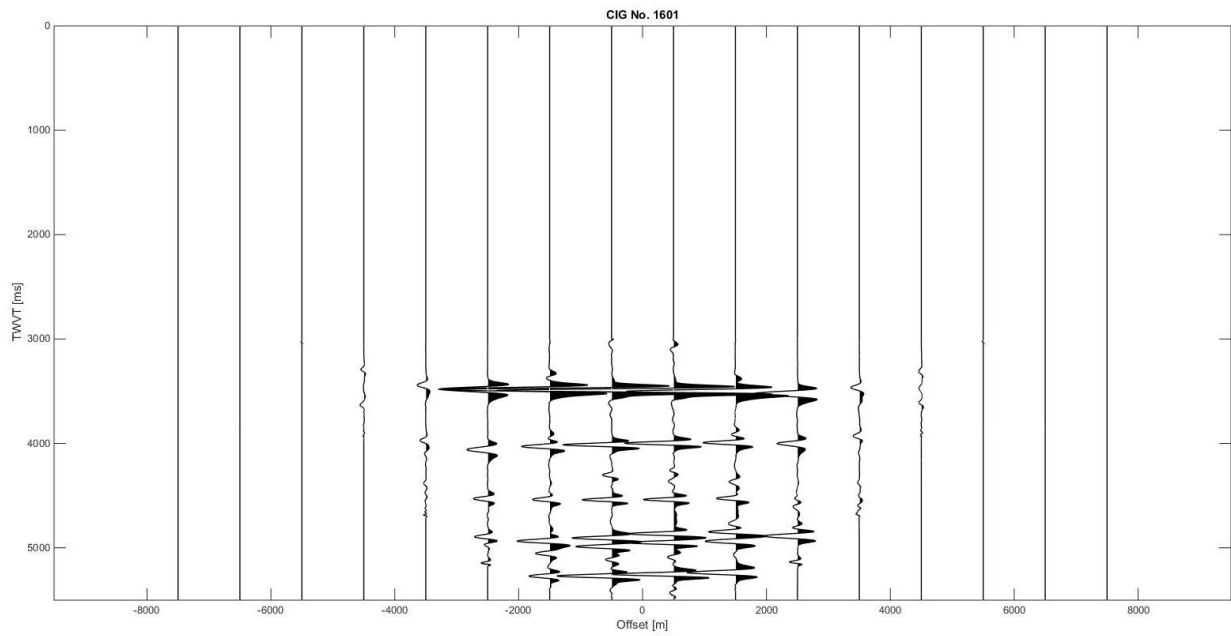


Figure 4.11: CIG No. 1601.

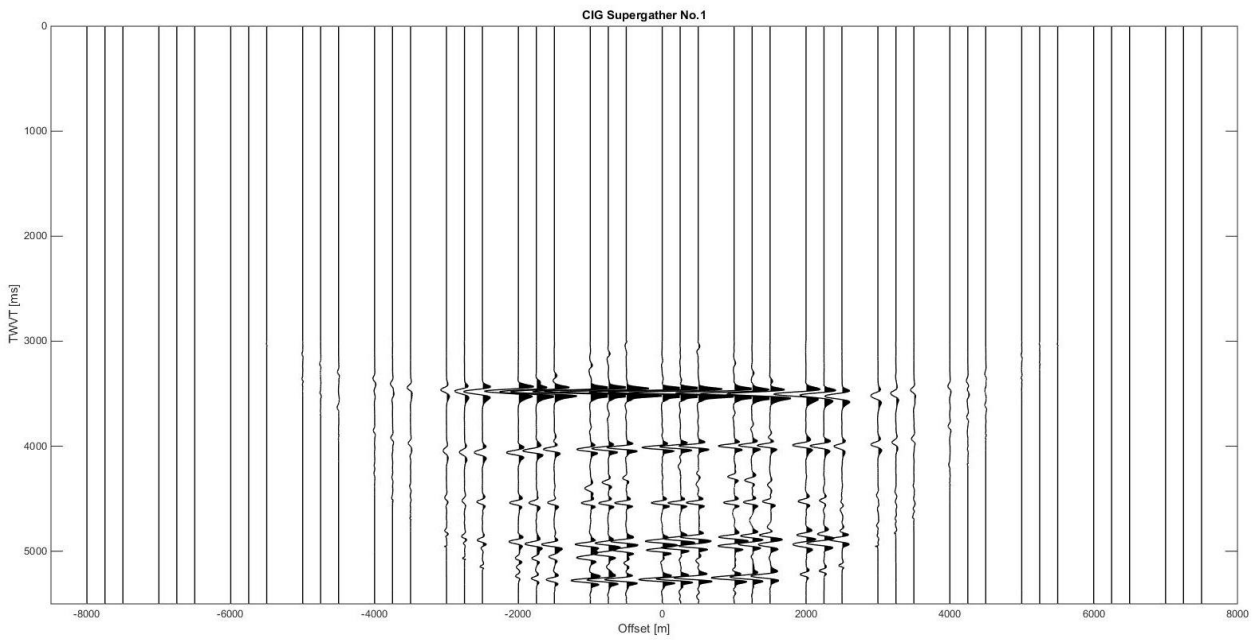


Figure 4.12: CIG Supergather No. 1.

The second CIG Supergather, shown in Figure 4.16, was created by the integration of the CIGs No. 1510, 1560 and 1610, which are displayed in Figures 4.13, 4.14 and 4.15.

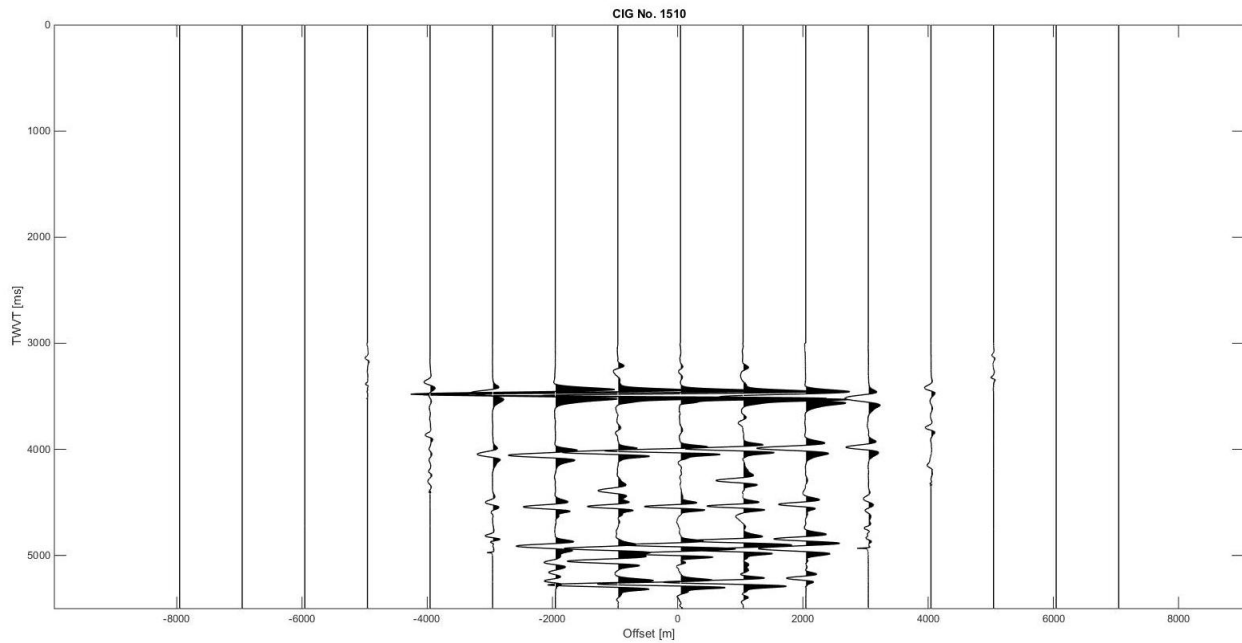


Figure 4.13: CIG No. 1510.

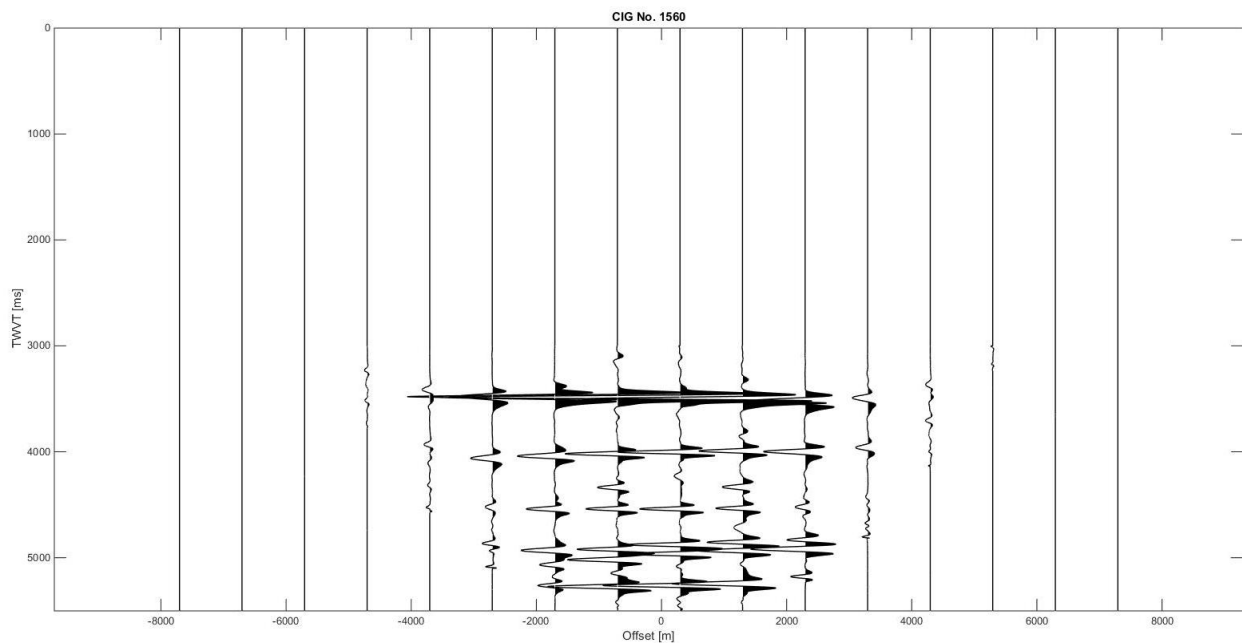


Figure 4.14: CIG No. 1560.

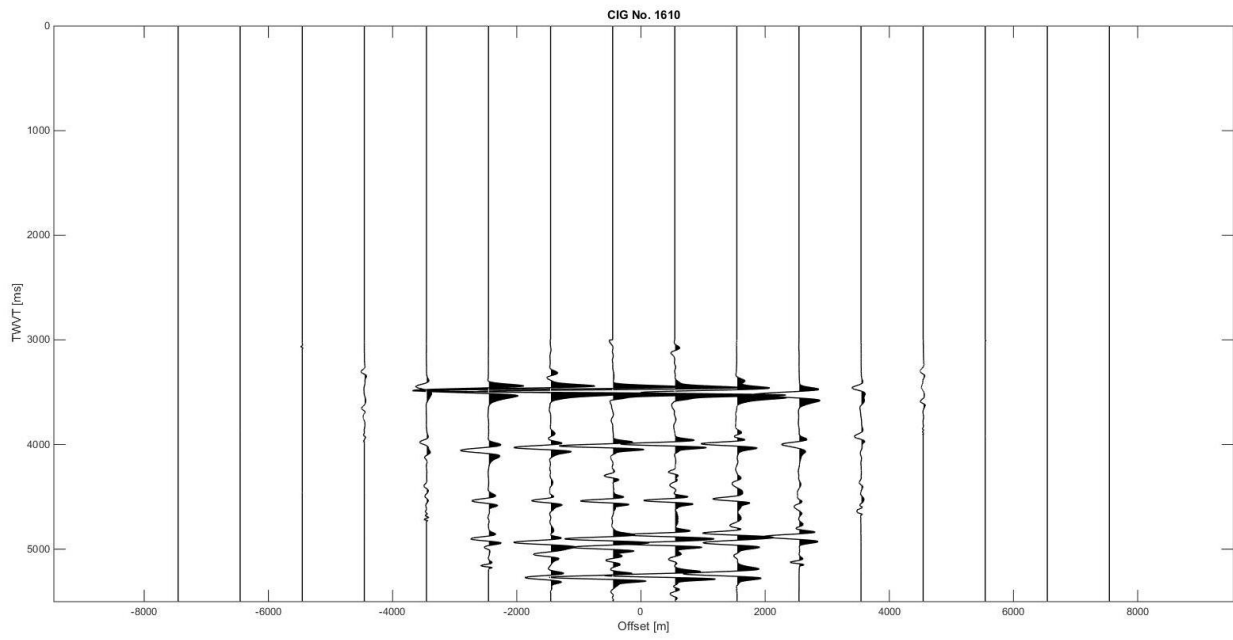


Figure 4.15: CIG No. 1610.

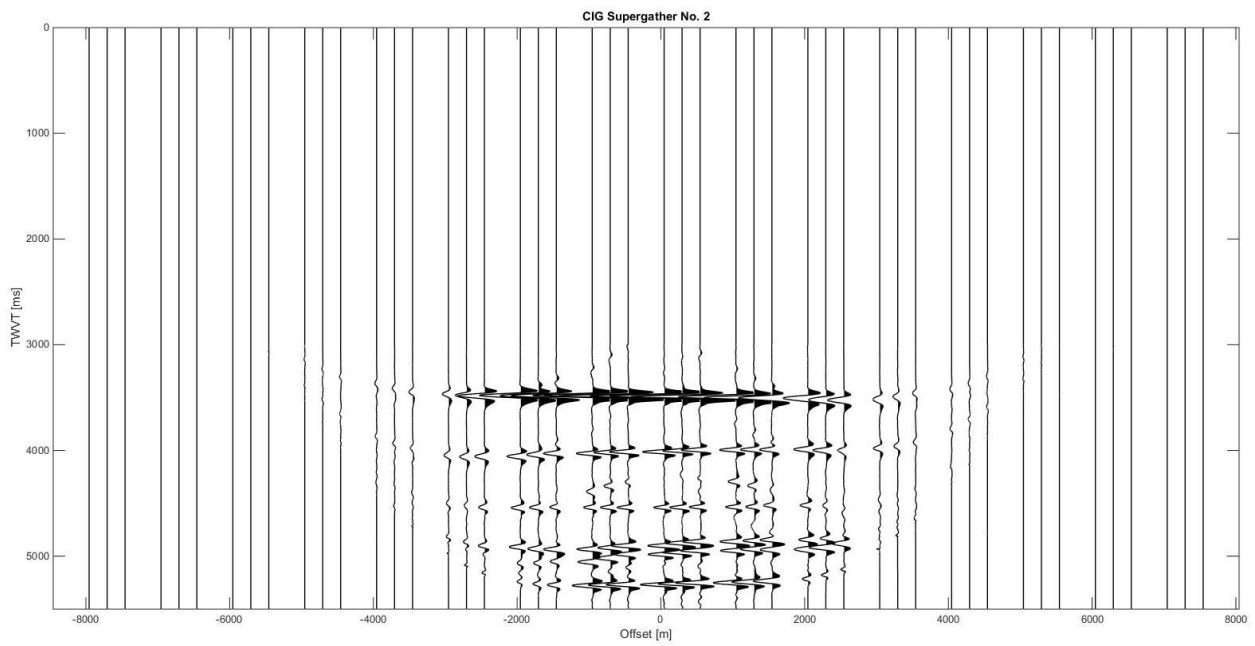


Figure 4.16: CIG Supergather No. 2.

Likewise, the third CIG Supergather, shown in Figure 4.20, was created by the integration of the CIGs No. 1570, 1620 and 1670, which are displayed in Figures 4.17, 4.18 and 4.19.

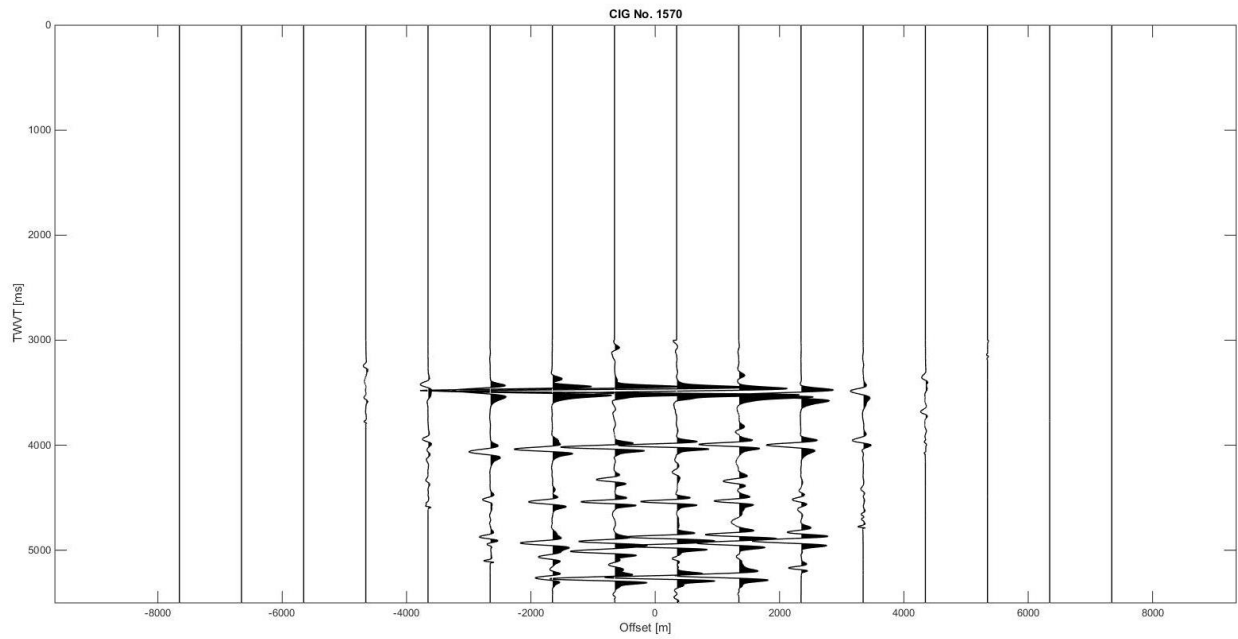


Figure 4.17: CIG No. 1570.

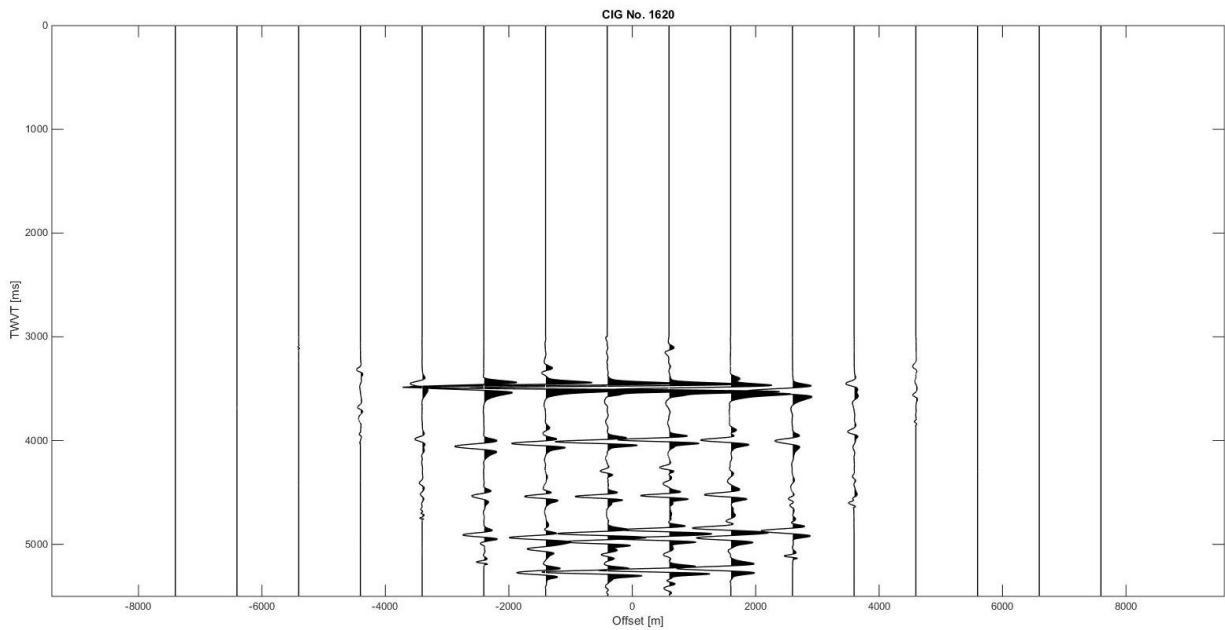


Figure 4.18: CIG No. 1620.

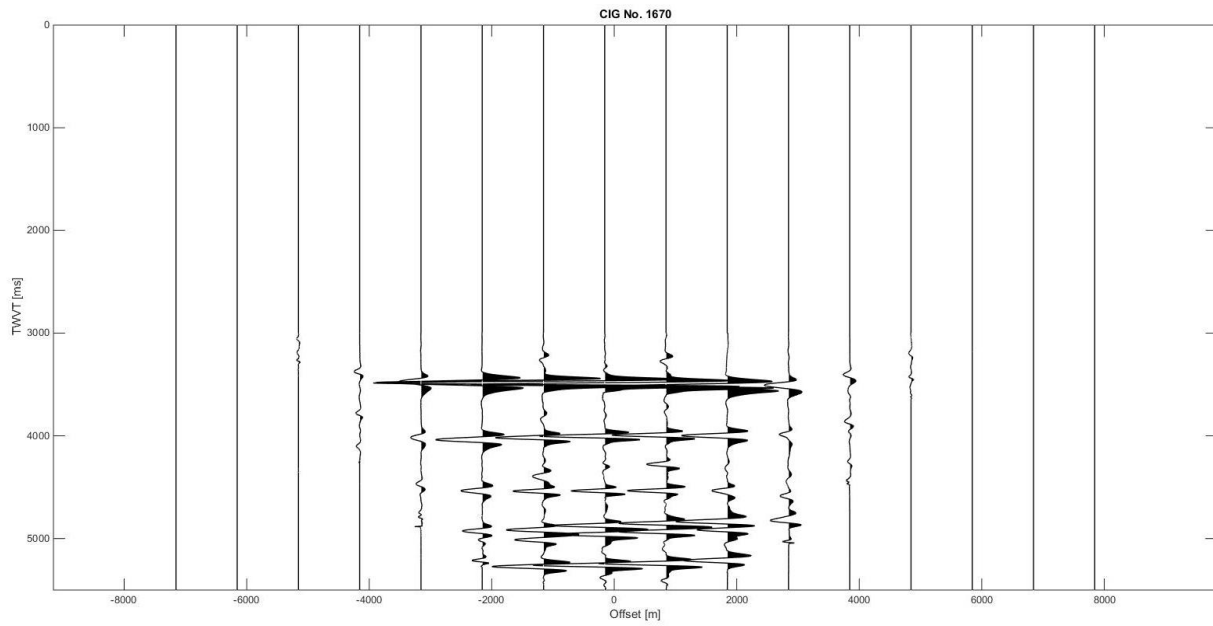


Figure 4.19: CIG No. 1670.

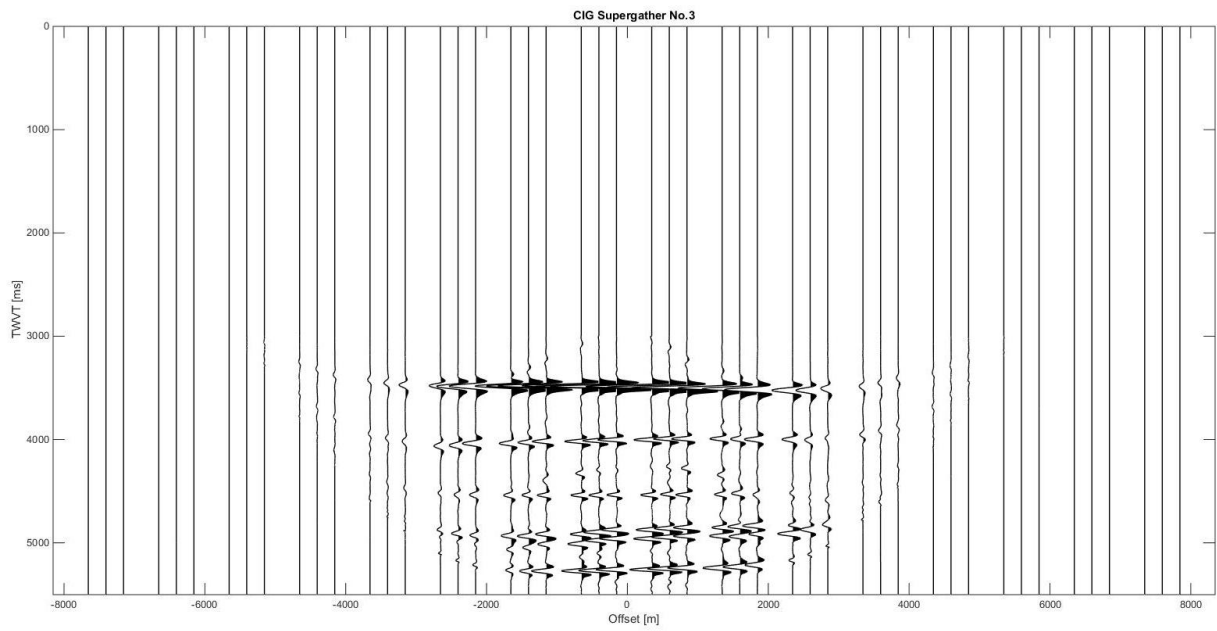


Figure 4.20: CIG Supergather No. 3.

### 4.3 Inverse NMO correction

Prestack Kirchhoff migration applies NMO correction to the data. In order to proceed to velocity analysis, the data should be inverse NMO-corrected. Inverse NMO correction was applied on CIGs No. 1501, 1551 and 1601, which were integrated as previously, in order to create the inverse NMO-corrected CIG Supergather No. 1. The CIG Supergathers No. 2 and No. 3 were inverse NMO-corrected accordingly and the results are displayed in the figures below. In Figures 4.21 to 4.32, the horizontal axis corresponds to offset and the vertical axis corresponds to the two-way traveltimes, since the data are offset-dependent.

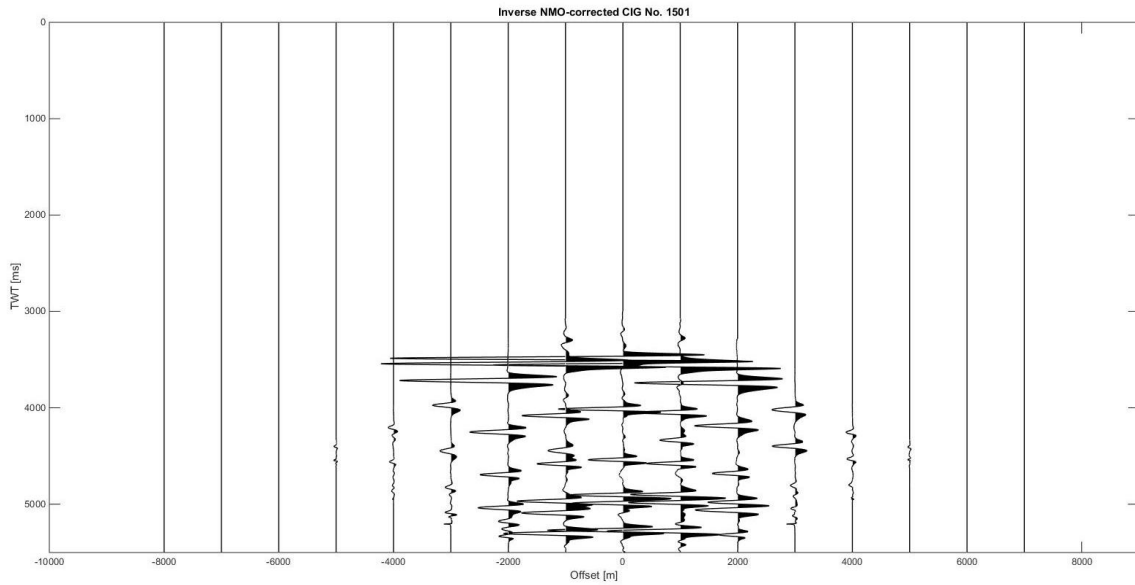


Figure 4.21: Inverse NMO-corrected CIG No. 1501.

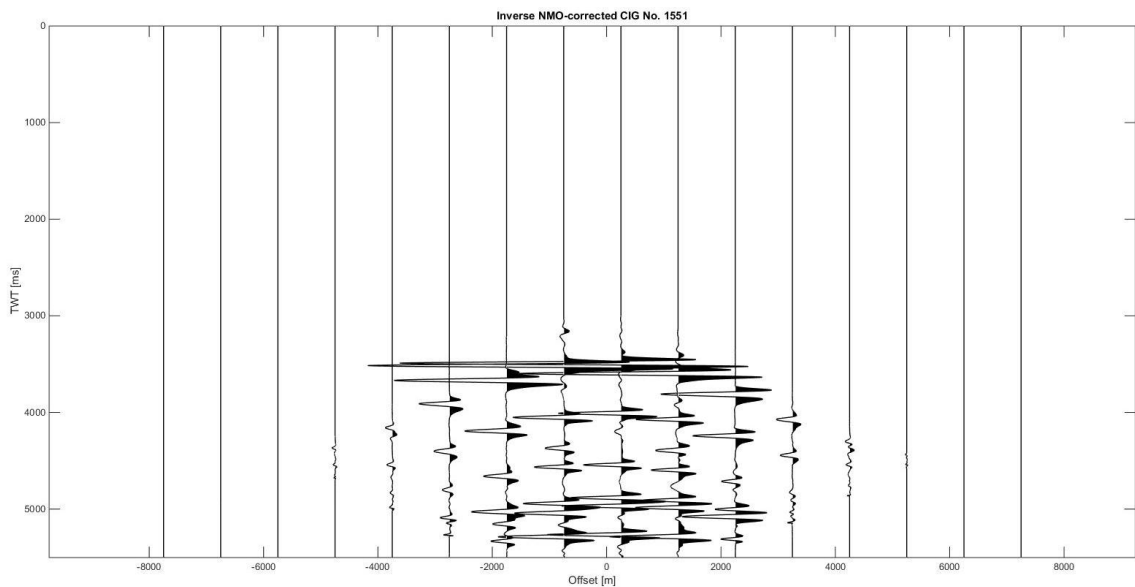


Figure 4.22: Inverse NMO-corrected CIG No. 1551.

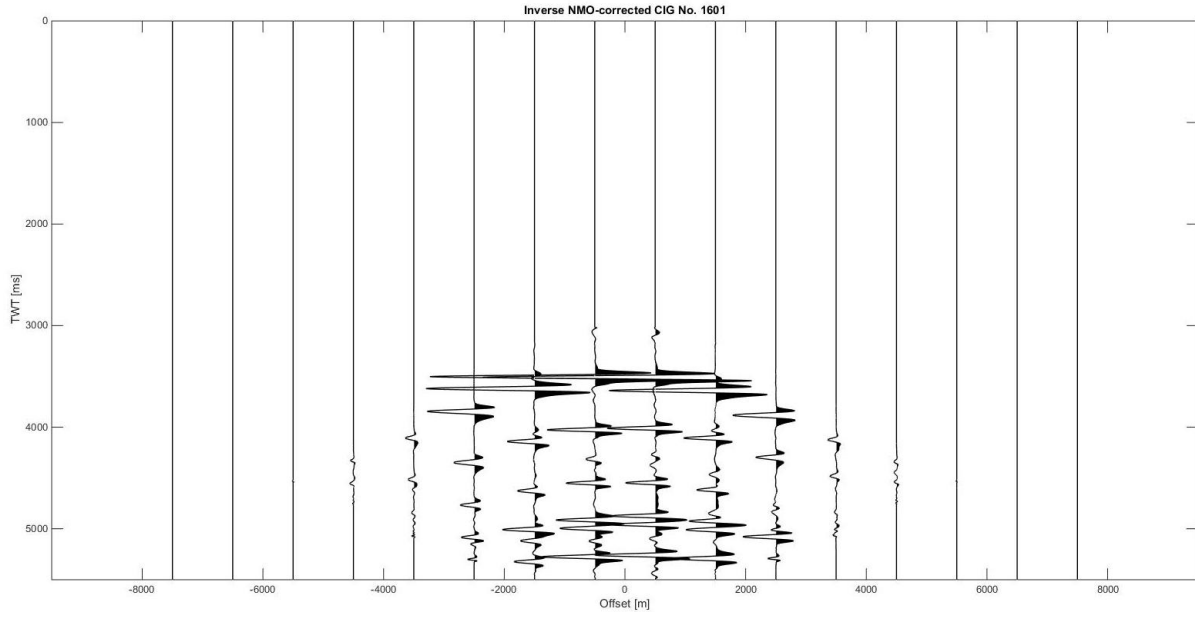


Figure 4.23: Inverse NMO-corrected CIG No. 1601.

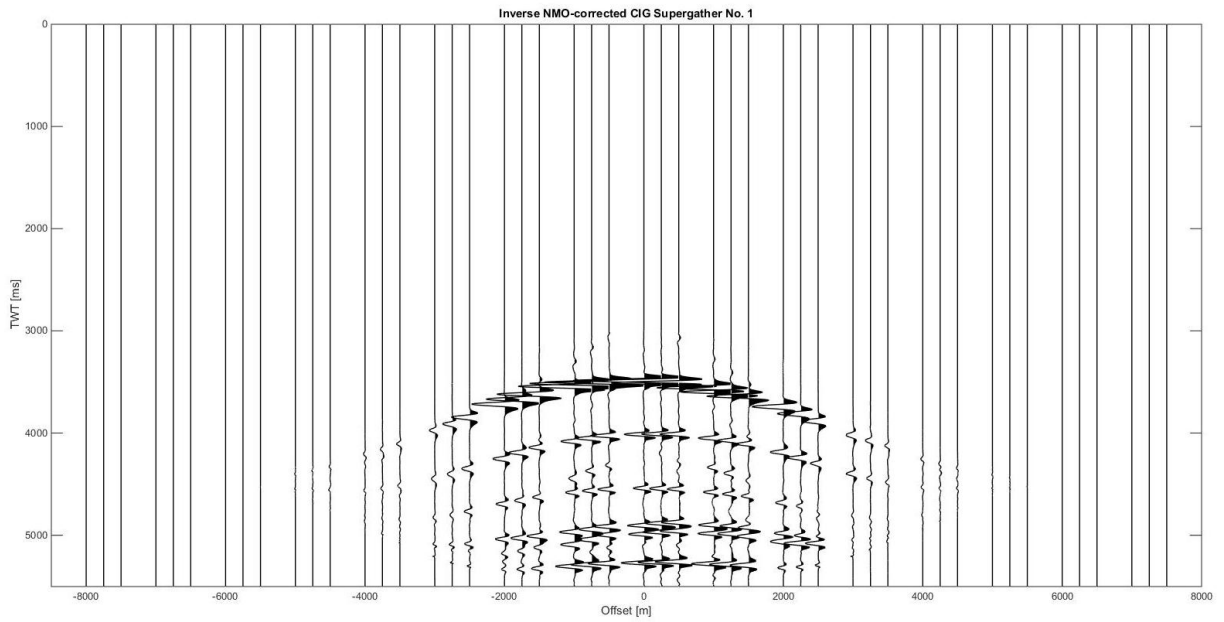


Figure 4.24: Inverse NMO-corrected CIG Supergather No. 1.

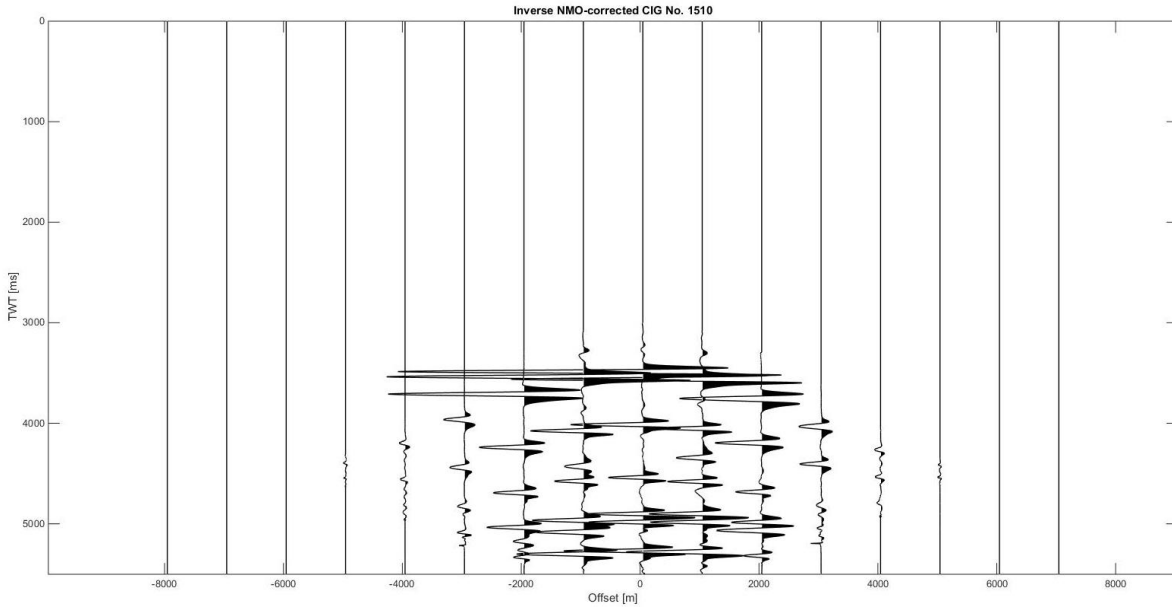


Figure 4.25: Inverse NMO-corrected CIG No. 1510.

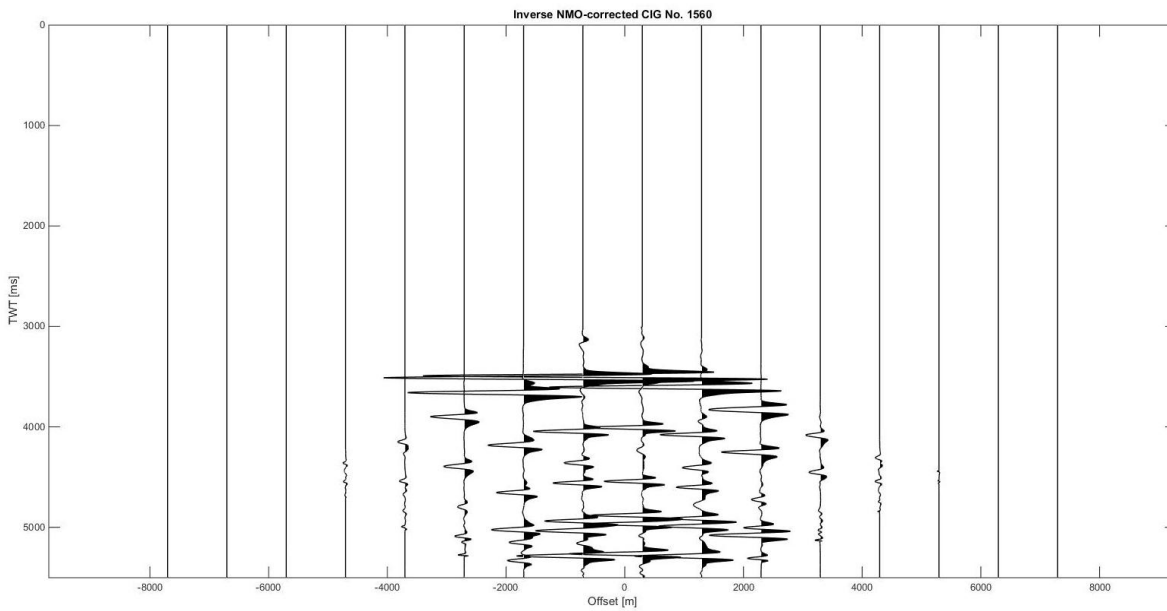


Figure 4.26: Inverse NMO-corrected CIG No. 1560.

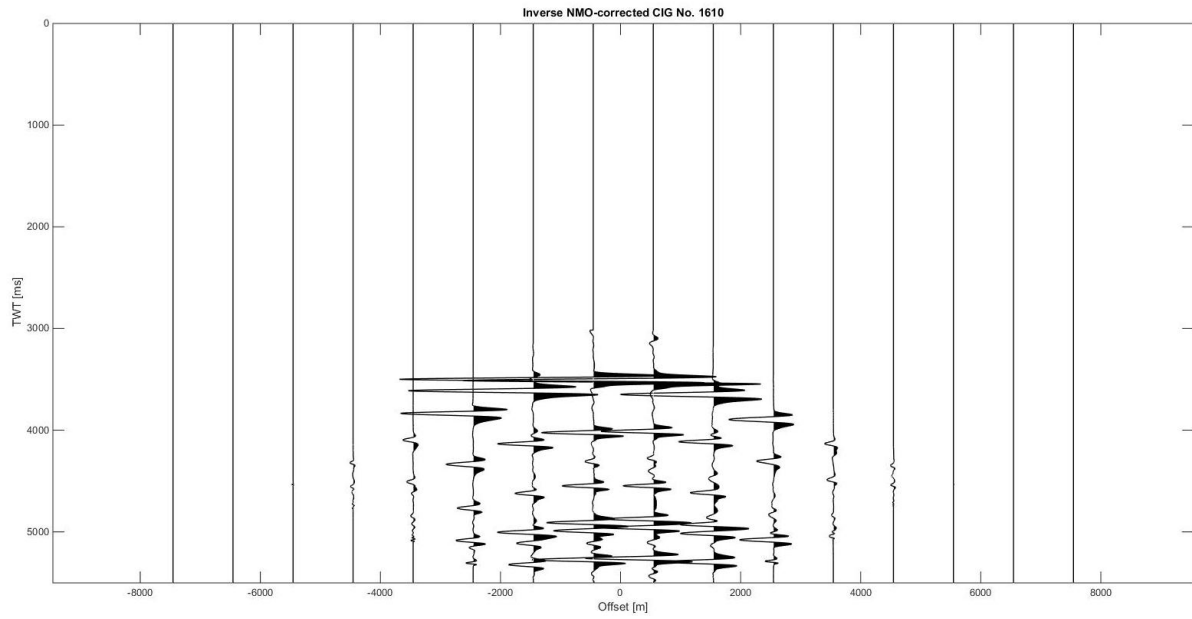


Figure 4.27: Inverse NMO-corrected CIG No. 1610.

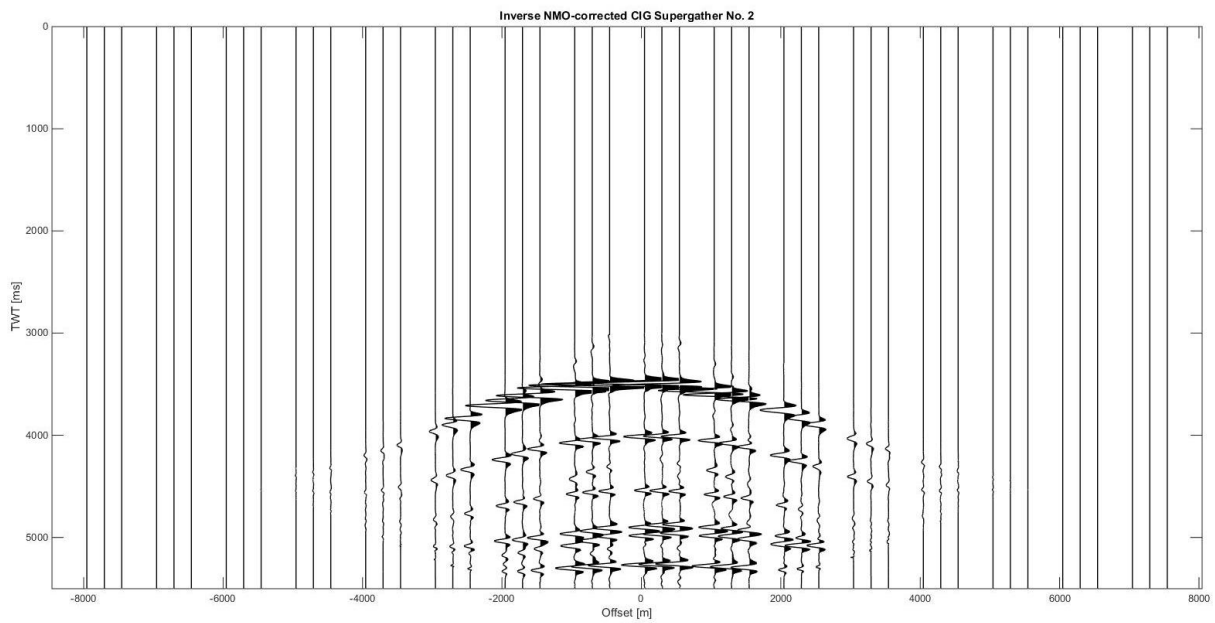


Figure 4.28: Inverse NMO-corrected CIG Supergather No. 2.

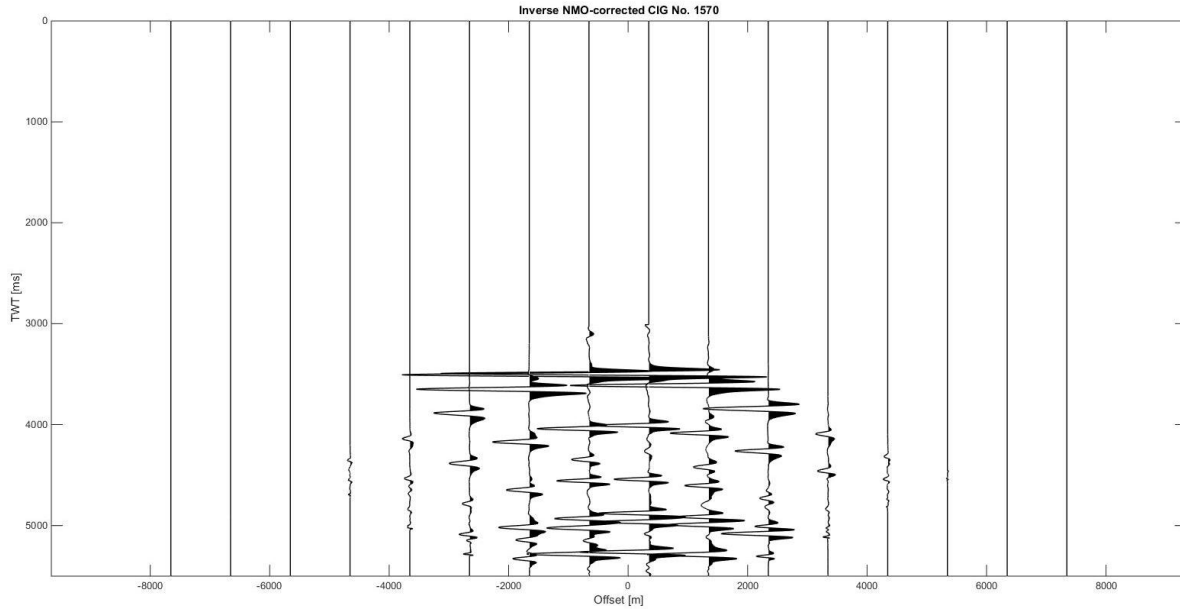


Figure 4.29: Inverse NMO-corrected CIG No. 1570.

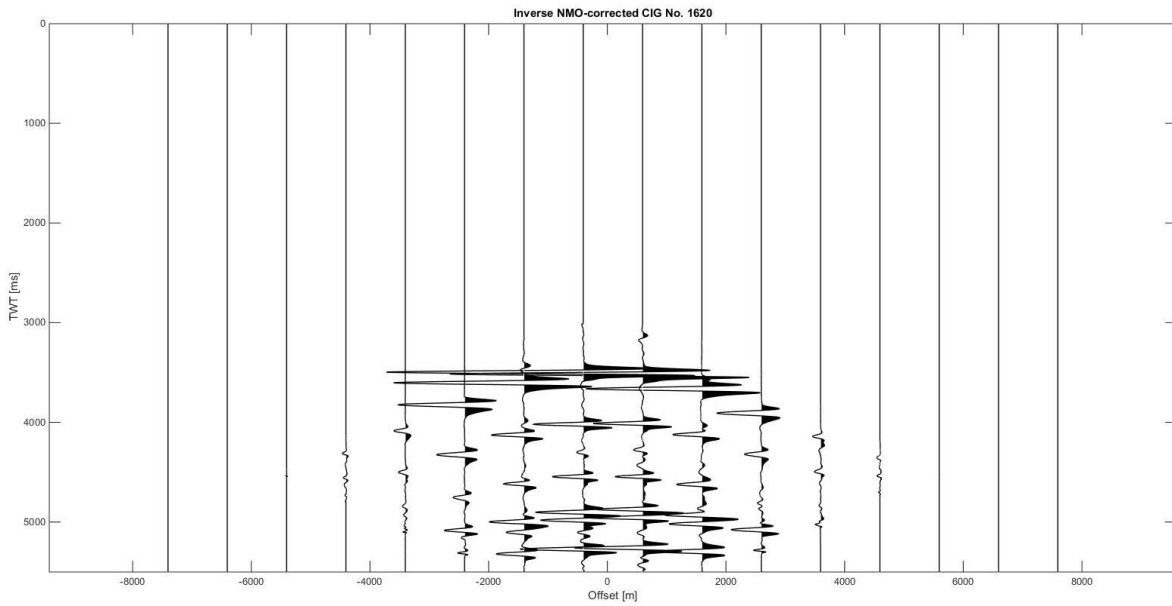


Figure 4.30: Inverse NMO-corrected CIG No. 1620.

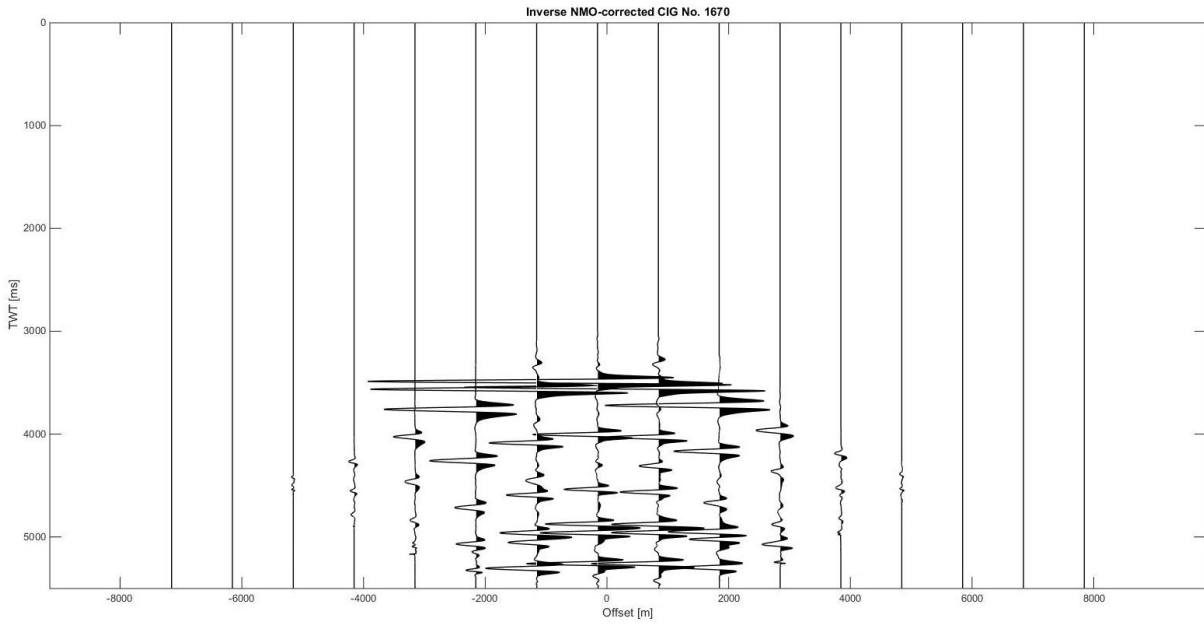


Figure 4.31: Inverse NMO-corrected CIG No. 1670.

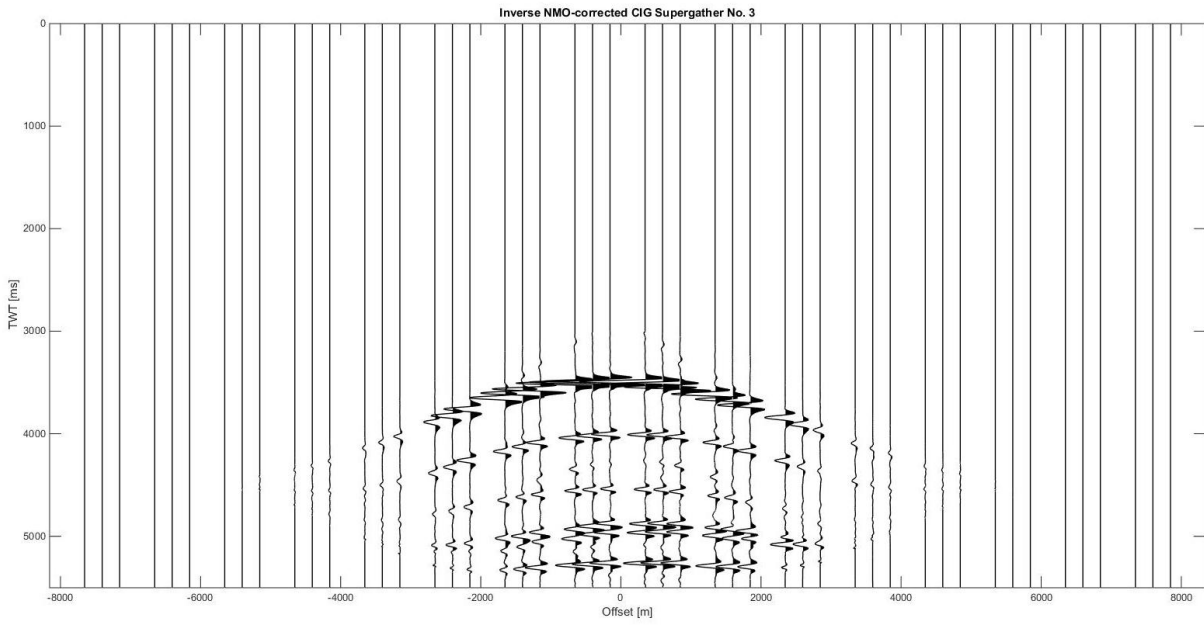


Figure 4.32: Inverse NMO-corrected CIG Supergather No. 3.

## 4.4 Velocity analysis

### 4.4.1 Picking based on MVA data

Velocity analysis was conducted for each and every inverse NMO-corrected CIG Supergather and interval velocities were calculated using the Dix equation. In the velocity analysis figures, the windows (from left to right) correspond to: 1) Semblance window with the selection picks on, 2) CIG Supergather after NMO correction using the picked velocities, 3) stacked trace displayed 5 times (in order to give a view of horizontal reflector), 4)  $V_{nmo}$  ( $V_{rms}$ ) and 5)  $V_{interval}$  versus depth.

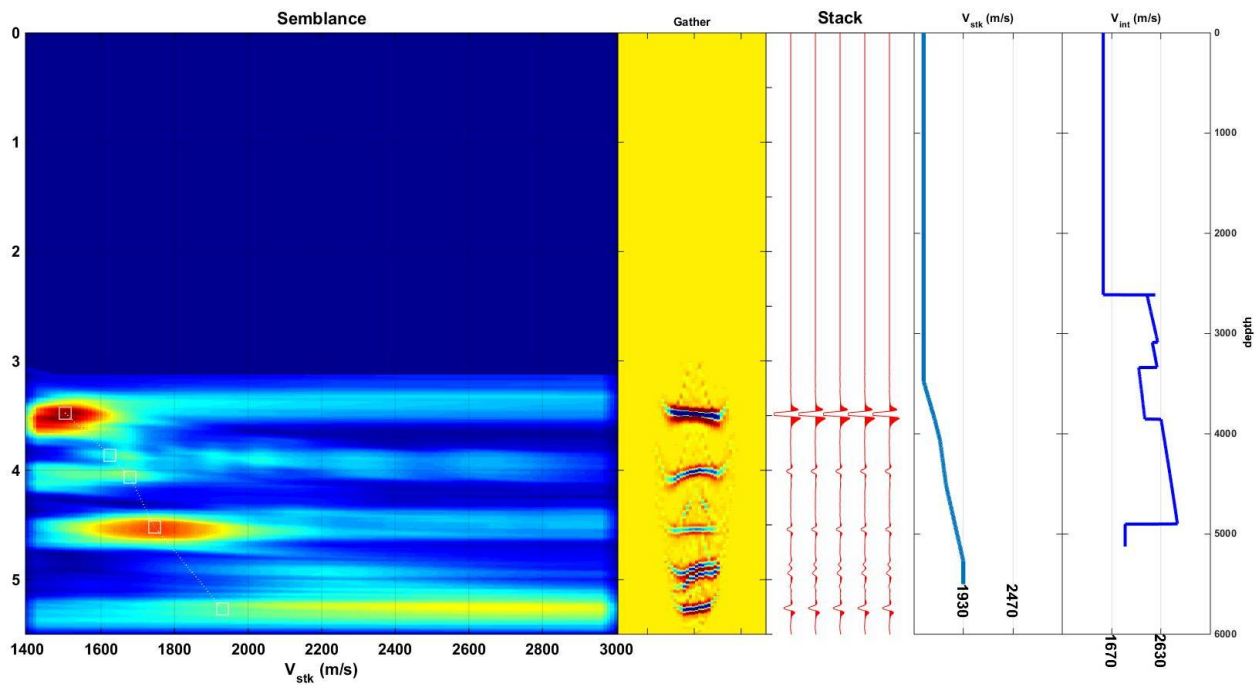


Figure 4.33: Velocity analysis of the inverse NMO-corrected CIG Supergather No. 1.

Table 4.1: Picked values of  $T(0)$  and  $V_{nmo}$  and the calculated interval velocities of the inverse NMO-corrected CIG Supergather No. 1.

Layer	1	2	3	4	5
$T(0)$ (s)	3,478	3,863	4,063	4,519	5,269
$V_{nmo}$ (m/s)	1503	1625	1679	1746	1931
$V_{int}$ (m/s)	1503	2464	2510	2257	2796

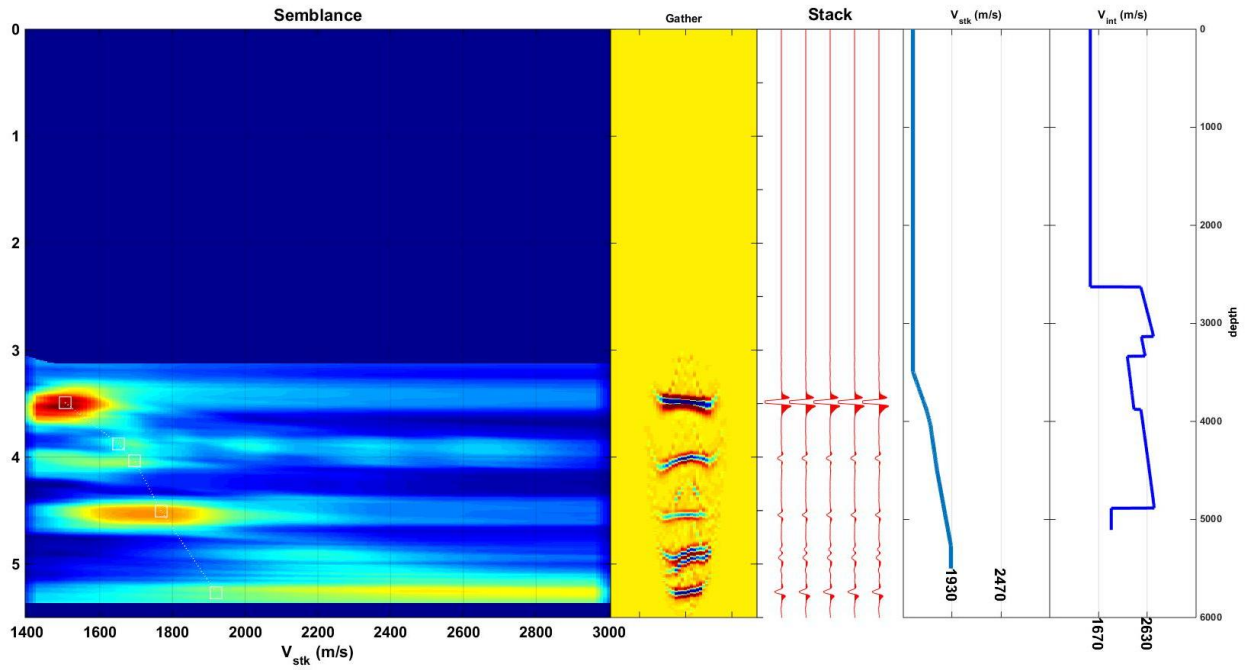


Figure 4.34: Velocity analysis of the inverse NMO-corrected CIG Supergather No. 2.

Table 4.2: Picked values of  $T(0)$  and  $V_{nmo}$  and the calculated interval velocities of the inverse NMO-corrected CIG Supergather No. 2.

Layer	1	2	3	4	5
<b>T(0) (s)</b>	3,492	3,877	4,034	4,505	5,269
<b>V<sub>nmo</sub> (m/s)</b>	1505	1652	1696	1769	1920
<b>V<sub>int</sub> (m/s)</b>	1505	2632	2553	2304	2641

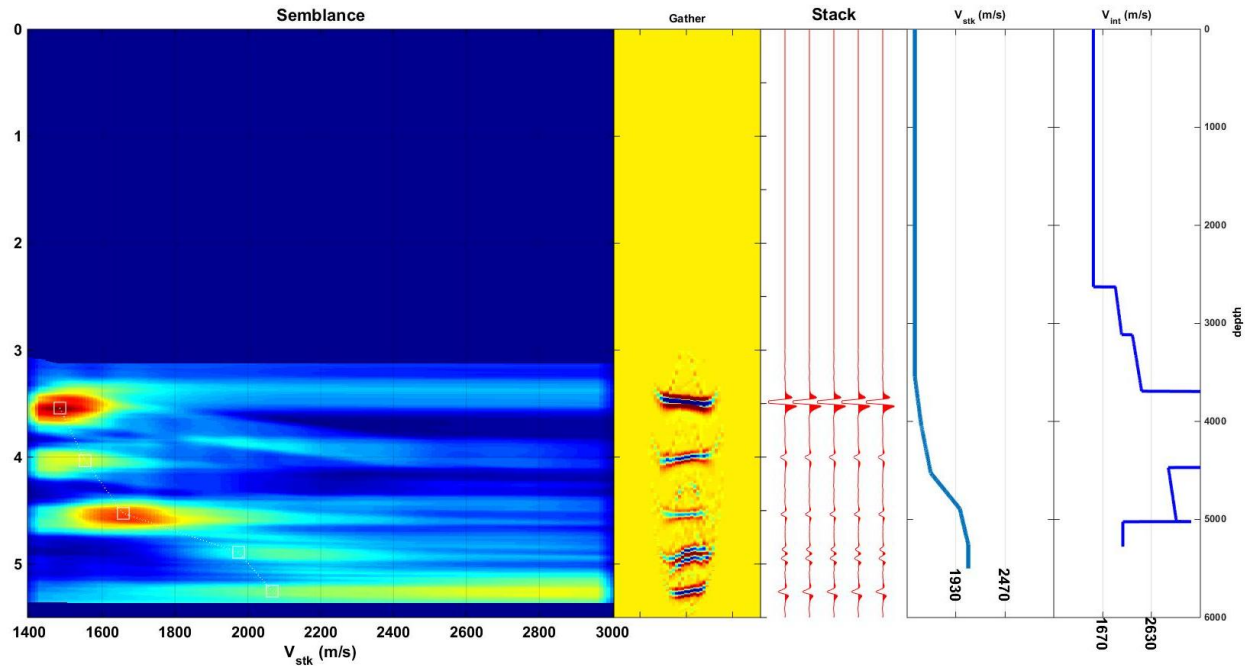


Figure 4.35: Velocity analysis of the inverse NMO-corrected CIG Supergather No. 3.

Table 4.3: Picked values of  $T(0)$  and  $V_{nmo}$  and the calculated interval velocities of the inverse NMO-corrected CIG Supergather No. 3.

Layer	1	2	3	4	5
$T(0)$ (s)	3,542	4,034	4,527	4,890	5,254
$V_{nmo}$ (m/s)	1484	1553	1658	1975	2067
$V_{int}$ (m/s)	1484	1981	2347	4267	3047

#### 4.4.2 Picking based on initial data

Furthermore, velocity analysis was conducted in the initial data that came from the previous thesis, where picking was easier. Migration velocity analysis picking was based on this picking. A Supergather, shown in Figure 4.36, was created by the integration of the initial CMP gathers No. 1501, 1551 and 1601. In Figure 4.36, the horizontal axis corresponds to offset and the vertical axis corresponds to the two-way traveltimes. Afterwards, velocity analysis with the new picks was conducted for the three inverse NMO-corrected CIG Supergathers.

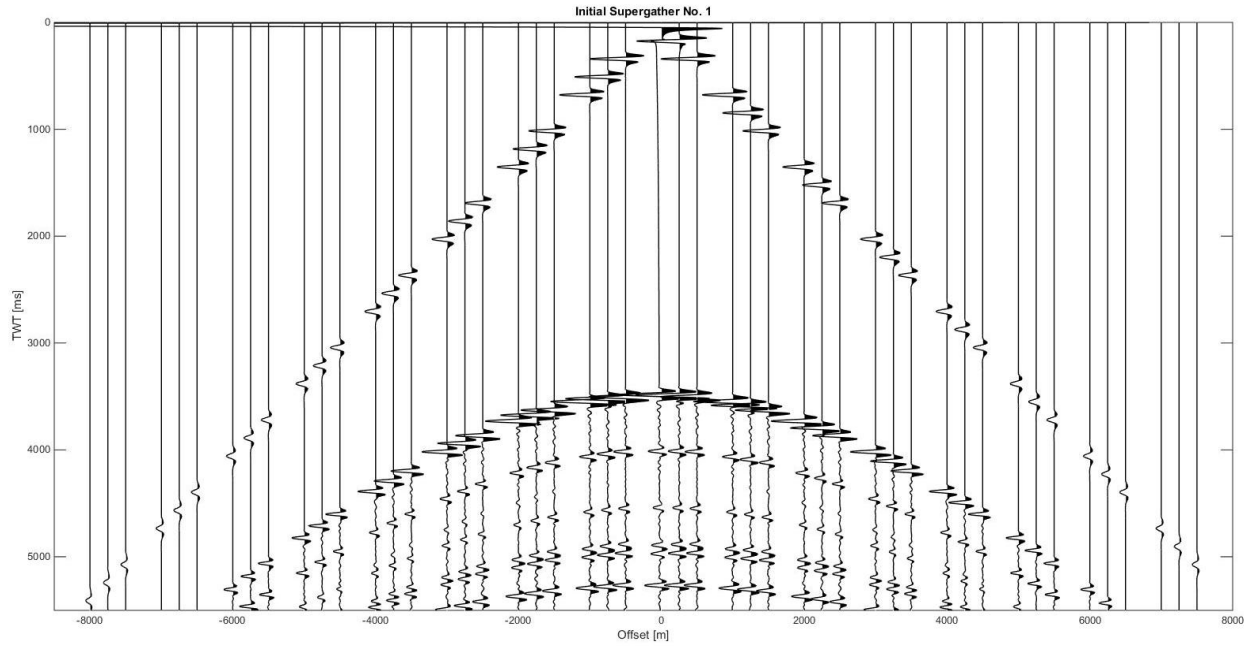


Figure 4.36: Supergather created by the initial CMP gathers No. 1501, 1551 and 1601.

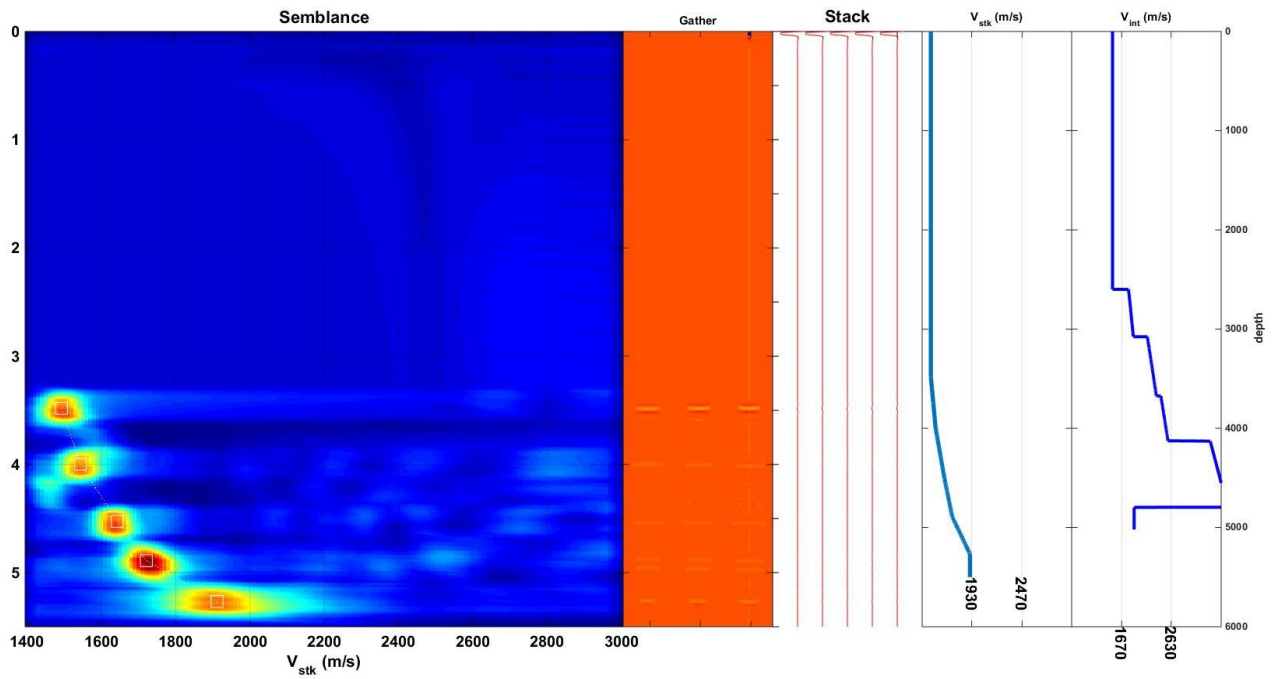


Figure 4.37: Velocity analysis of the Supergather created by the initial CMP gathers No. 1501, 1551 and 1601.

Table 4.4: Picked values of  $T(0)$  and  $V_{nmo}$  and the calculated interval velocities of the Supergather created by the initial CMP gathers No. 1501, 1551 and 1601.

Layer	1	2	3	4	5
$T(0)$ (s)	3,506	3,949	4,505	4,905	5,297
$V_{nmo}$ (m/s)	1501	1532	1639	1723	1918
$V_{int}$ (m/s)	1501	1762	2257	2480	3543

For example, the picks in Figure 4.33 are the picks based on the MVA data. The picks in Figure 4.38 are the picks of the velocity analysis of the Supergather created by the initial CMP gathers No. 1501, 1551 and 1601. Respectively, the picked values of  $T(0)$  and  $V_{nmo}$  and the calculated interval velocities of the inverse NMO-corrected CIG Supergather No. 1 are shown in Table 4.1 and the picked values of  $T(0)$  and  $V_{nmo}$  and the calculated interval velocities of the inverse NMO-corrected CIG Supergather No. 1 based on the initial data are shown in Table 4.5. The picked values of  $T(0)$  and  $V_{nmo}$  in Tables 4.5, 4.6 and 4.7 are based on the picked values of  $T(0)$  and  $V_{nmo}$  in Table 4.4.

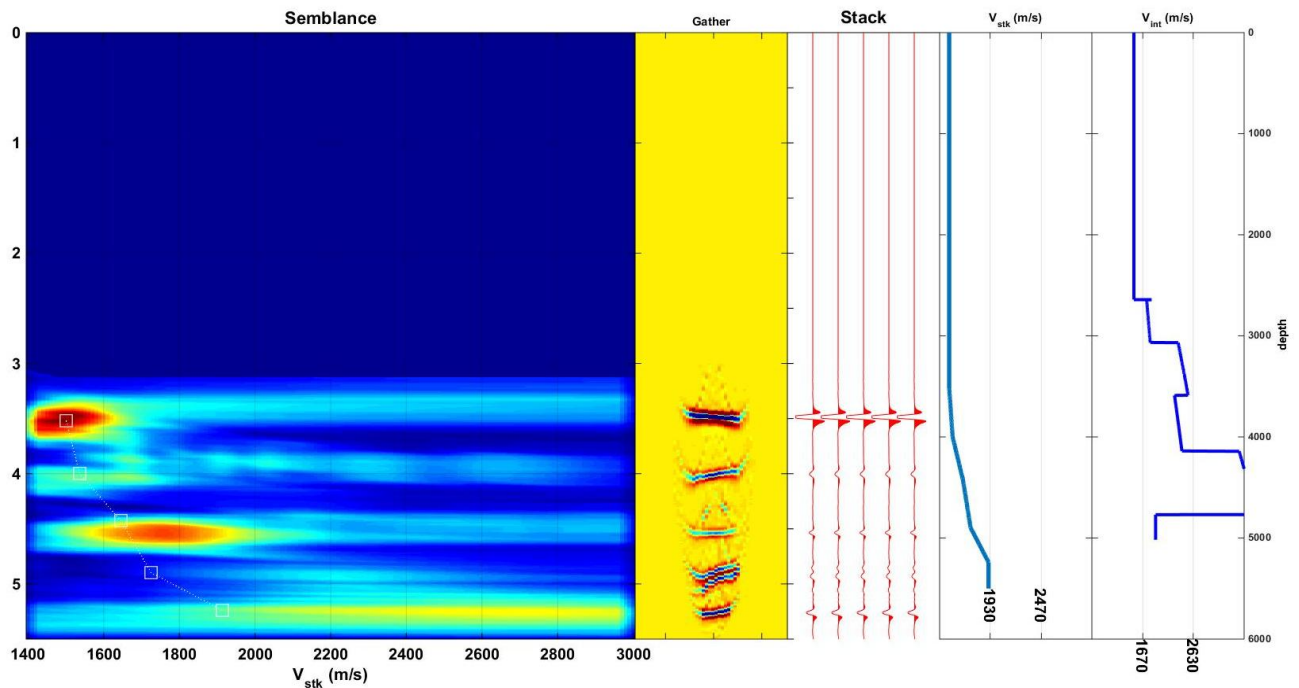


Figure 4.38: Velocity analysis of the inverse NMO-corrected CIG Supergather No. 1.

Table 4.5: Picked values of  $T(0)$  and  $V_{nmo}$  and the calculated interval velocities of the inverse NMO-corrected CIG Supergather No. 1 based on the initial data.

Layer	1	2	3	4	5
$T(0)$ (s)	3,521	3,999	4,427	4,898	5,240
$V_{nmo}$ (m/s)	1501	1537	1646	1725	1914
$V_{int}$ (m/s)	1501	1777	2439	2345	3672

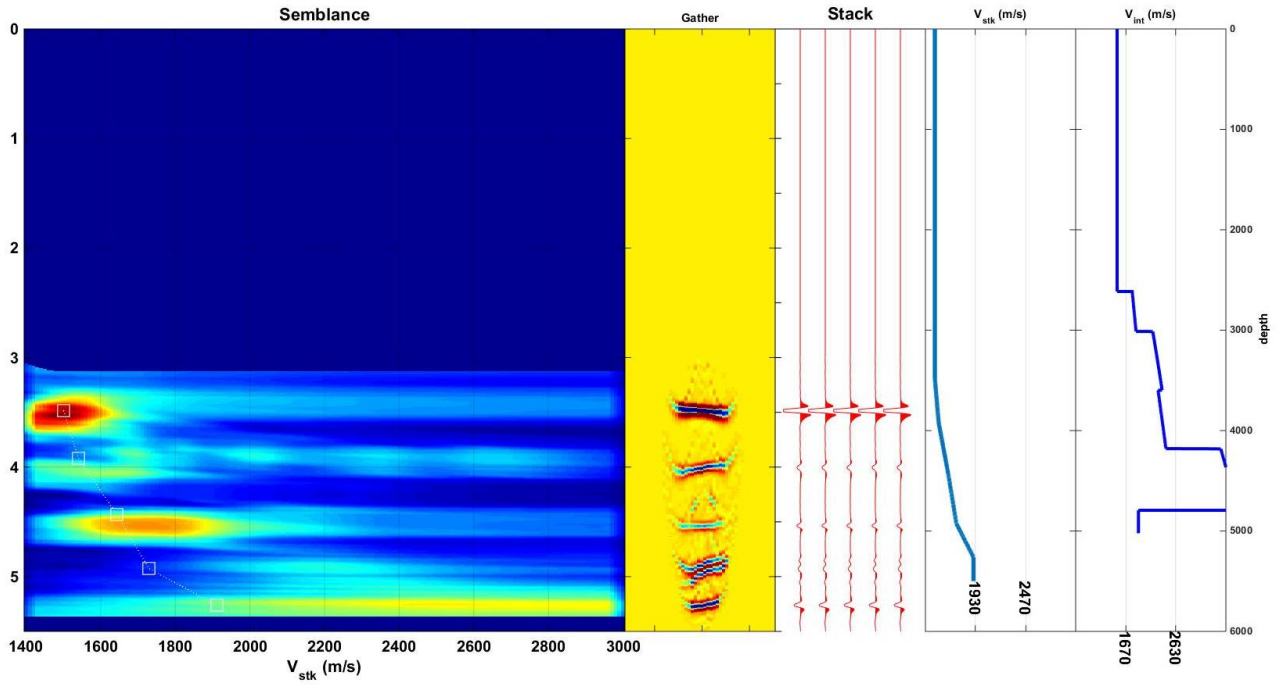


Figure 4.39: Velocity analysis of the inverse NMO-corrected CIG Supergather No. 2.

Table 4.6: Picked values of  $T(0)$  and  $V_{nmo}$  and the calculated interval velocities of the inverse NMO-corrected CIG Supergather No. 2 based on the initial data.

Layer	1	2	3	4	5
$T(0)$ (s)	3,485	3,920	4,434	4,926	5,261
$V_{nmo}$ (m/s)	1501	1541	1643	1729	1912
$V_{int}$ (m/s)	1501	1829	2280	2367	3662

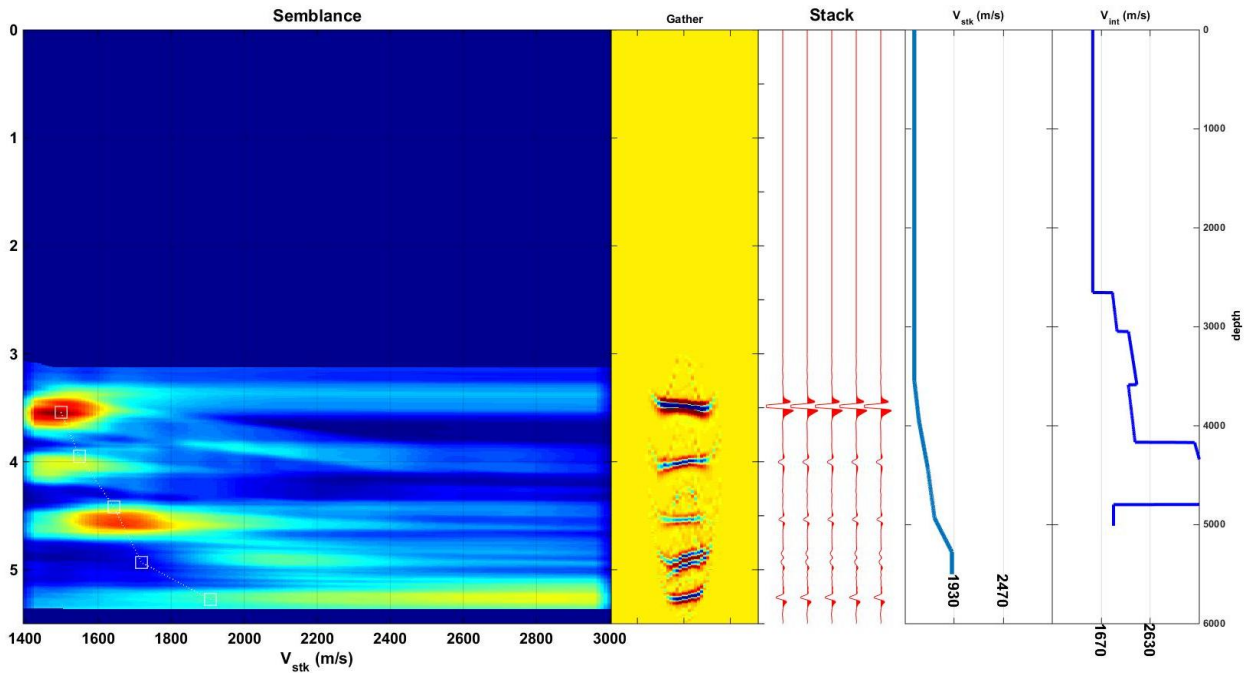


Figure 4.40: Velocity analysis of the inverse NMO-corrected CIG Supergather No. 3.

Table 4.7: Picked values of  $T(0)$  and  $V_{nmo}$  and the calculated interval velocities of the inverse NMO-corrected CIG Supergather No. 3 based on the initial data.

Layer	1	2	3	4	5
$T(0)$ (s)	3,542	3,949	4,420	4,933	5,276
$V_{nmo}$ (m/s)	1499	1549	1643	1719	1908
$V_{int}$ (m/s)	1499	1933	2286	2267	3674

### 4.4.3 Results comparison

In this chapter, the results of the two previous chapters are compared for each and every inverse NMO-corrected CIG Supergather. Tables 4.8, 4.9 and 4.10 contain the absolute differences of the the two picking methods values.

Table 4.8: Absolute differences of the picked values of  $T(0)$  and  $V_{nmo}$  and the calculated interval velocities of the inverse NMO-corrected CIG Supergather No. 1.

Layer	1	2	3	4	5
$T(0)$ (s)	0,043	0,136	0,364	0,378	0,029
$V_{nmo}$ (m/s)	2	88	34	21	17
$V_{int}$ (m/s)	2	687	71	88	875

Apparently, there is a noteworthy divergence in the picked value of  $V_{nmo}$  in the second layer. The picked value based on the MVA data is 1625 m/s and the picked value based on the initial data is 1537 m/s, which also explains the difference between the interval velocities. Moreover, differences about 0,4 s appear at the  $T(0)$  picked values in the third and fourth layer, explaining the dissimilarities presented in the interval velocities of the fifth layer.

Table 4.9: Absolute differences of the picked values of  $T(0)$  and  $V_{nmo}$  and the calculated interval velocities of the inverse NMO-corrected CIG Supergather No. 2.

<b>Layer</b>	<b>1</b>	<b>2</b>	<b>3</b>	<b>4</b>	<b>5</b>
<b>T(0) (s)</b>	0,007	0,043	0,400	0,421	0,007
<b>V<sub>nmo</sub> (m/s)</b>	4	111	52	40	8
<b>V<sub>int</sub> (m/s)</b>	4	803	273	63	1021

As previously, the second and the fifth layer seem to have noticeable differences regarding interval velocities. In the second layer, the picked  $V_{nmo}$  value based on the MVA data is 1652 m/s and the picked value based on the initial data is 1541 m/s, fact that explains the difference between the interval velocity values. Furthermore, the third and fourth layer dissimilarities of the  $T(0)$  picked values are about 0,4 s, which explains the different interval velocities in the third and the fifth layer.

Table 4.10: Absolute differences of the picked values of  $T(0)$  and  $V_{nmo}$  and the calculated interval velocities of the inverse NMO-corrected CIG Supergather No. 3.

<b>Layer</b>	<b>1</b>	<b>2</b>	<b>3</b>	<b>4</b>	<b>5</b>
<b>T(0) (s)</b>	0	0,086	0,107	0,043	0,021
<b>V<sub>nmo</sub> (m/s)</b>	15	4	15	256	159
<b>V<sub>int</sub> (m/s)</b>	15	48	61	2000	627

Evidently, notable differences appear at the fourth and the fifth layer concerning the picked  $V_{nmo}$  values, resulting to interval velocities divergence. In the fourth layer, the picked  $V_{nmo}$  value based on the MVA data is 1975 m/s, while the picked value based on the initial data is 1719 m/s. In the fifth layer, the picked  $V_{nmo}$  value based on the MVA data is 2067 m/s, while the picked value based on the initial data is 1908 m/s.

## CHAPTER 5: CONCLUSIONS AND RECOMMENDATIONS

The first stage of the process was the creation of an initial velocity model of RMS velocities resulting from the interval velocities utilized for the synthetic data creation. Secondly, prestack Kirchhoff migration was applied on every common shot gather for 16 sources from zero to 5,5 s. It should be mentioned that the number of sources is limited, so it is recommended to increase fold. Also, the migrated section was created in order to examine Kirchhoff migration, which depicts the reflectors, but creates some residues at the dipping reflectors after 6000 m and 4 s. Therefore, the examination of other prestack migration methods is recommended in order to operate at areas with dipping reflectors.

Afterwards, the offset-domain common image gathers were created. It should be noted that the CIG interval was 2,5 m, the total number of CIGs is 3170 and the fold was relatively low and variant. Also, angle-domain common image gathers could be used instead. Moreover, inverse NMO correction was applied on the CIGs, which delays the reflected waves arrival. For large offsets, move-out is possible to be large and as a consequence, reflections at distant traces are not visible. Move-out at distant traces could be visible if the two-way traveltime was not reduced at 5,5 s and this might be the source of the velocity analysis complications.

Furthermore, three inverse NMO-corrected CIG Supergathers were created by the integration of neighboring inverse NMO-corrected CIGs. In order to sum neighboring CIGs, it is assumed that every CIG in a CIG Supergather belongs in the same area, where there are no depth variations. CIG Supergathers contribute to increasing the number of traces for the velocity analysis, but the required analysis was not achieved because of the large spacing of the CIGs. The velocity analysis seems to perform better for the first reflector at 3,5 s and the third at 4,5 s because they are flat in contrast to the rest. For the CIG Supergathers created, the reflectors should be flat at the location of the involved common image points. It is recommended to reduce the distance between the CIGs used for the creation of the three CIG Supergathers, which could be achieved by increasing the fold of the initial data. Hence, the process could be successful utilizing two CIG Supergathers.

---

## REFERENCES

1. Alsadi, H.N. (2017). *Seismic Hydrocarbon Exploration*, Springer International Publishing, Switzerland.
2. Araya-Polo, M., S. Farris, and M. Florez, (2019). Deep learning-driven velocity model building workflow, *The Leading Edge* 38: 872a1-872a9.
3. Biondi, B.L. (2006). *3D Seismic Imaging*, Investigations in Geophysics Series No. 14, Society of Exploration Geophysicists, Tulsa, Oklahoma, U.S.A..
4. Bolt, B.A. (1982). *Inside the Earth: Evidence from Earthquakes*, W.H. Freeman, San Francisco, U.S.A..
5. Deregowski, S.M. (1990). Common-offset migrations and velocity analysis: *First Break*, 8, 225-234.
6. Jones, I.F., (2003). Data Visualisation and Interpretation: A review of 3D PreSDM model building techniques, *First Break* 21, pp. 45-58.
7. Jones, I.F., (2010). *An Introduction to: Velocity Model Building*, EAGE Publications bv, Netherlands.
8. Kearey, P., M. Brooks, I. Hill (2002). *An Introduction to Geophysical Exploration Third Edition*, Blackwell Publishing.
9. Koren, Z. and I.Ravve (2006). Constrained Dix inversion, *Geophysics*, vol. 71, No. 6, R113–R130.
10. Liu, Z. and Bleistein, N. (1995). Migration velocity analysis: Theory and an iterative algorithm: *Geophysics*, 60, 142-153.
11. Nolen-Hoeksema, R. (2014). A beginner's guide to seismic reflections, *Oilfield Review* 26, pp. 55-56.
12. Nowroozi, A. A. (1989). Generalized form of the Dix equation for the calculation of interval velocities and layer thicknesses, *GEOPHYSICS* 54: 659-661.
13. Reynolds, J.M. (2011). *An Introduction to Applied and Environmental Geophysics Second Edition*, A John Wiley & Sons, Ltd., Publication.
14. Sheriff, R.E. (2002). *Encyclopedic Dictionary of Applied Geophysics*, Society of Exploration Geophysicists Tulsa, Oklahoma, U.S.A..
15. Veeken, P.C.H. and B. van Moerkerken (2013). *Seismic Stratigraphy and Depositional Facies Models*, EAGE Publications bv, Netherlands.
16. Wu, W.J. (2001). The advantage and significance of prestack migration, Geo-X Systems Ltd. 500, 440 – 2<sup>nd</sup> Avenue S.W. Calgary, Alberta, Canada T2P 5E9.
17. Yilmaz, Ö. (1987). *Seismic data processing*, Investigations in Geophysics, Society of Exploration Geophysicists.
18. Yilmaz, Ö. (2001). *Seismic data analysis*, Investigations in Geophysics, Society of Exploration Geophysicists.
19. Zhao, H. (2020). Improvements in seismic imaging and migration-velocity model building, Series of dissertations submitted to the Faculty of Mathematics and Natural Sciences, University of Oslo No. 2218.

20. Χρηστίδη, Β.Λ. (2019). Σχεδιασμός πειράματος σεισμικής ανάκλασης για την απεικόνιση του υπεδάφους σε περιβάλλον βαθιάς θάλασσας νότια της Κρήτης, Διπλωματική εργασία, Πολυτεχνείο Κρήτης, Τμήμα Μηχανικών Ορυκτών Πόρων, Χανιά.

Sites

1. [https://archive.epa.gov/esd/archive-geophysics/web/html/marine\\_seismic\\_methods.html](https://archive.epa.gov/esd/archive-geophysics/web/html/marine_seismic_methods.html)
2. <https://crewes.org/ResearchLinks/>
3. <https://wiki.seg.org/wiki/Acquisition>

## ANNEX

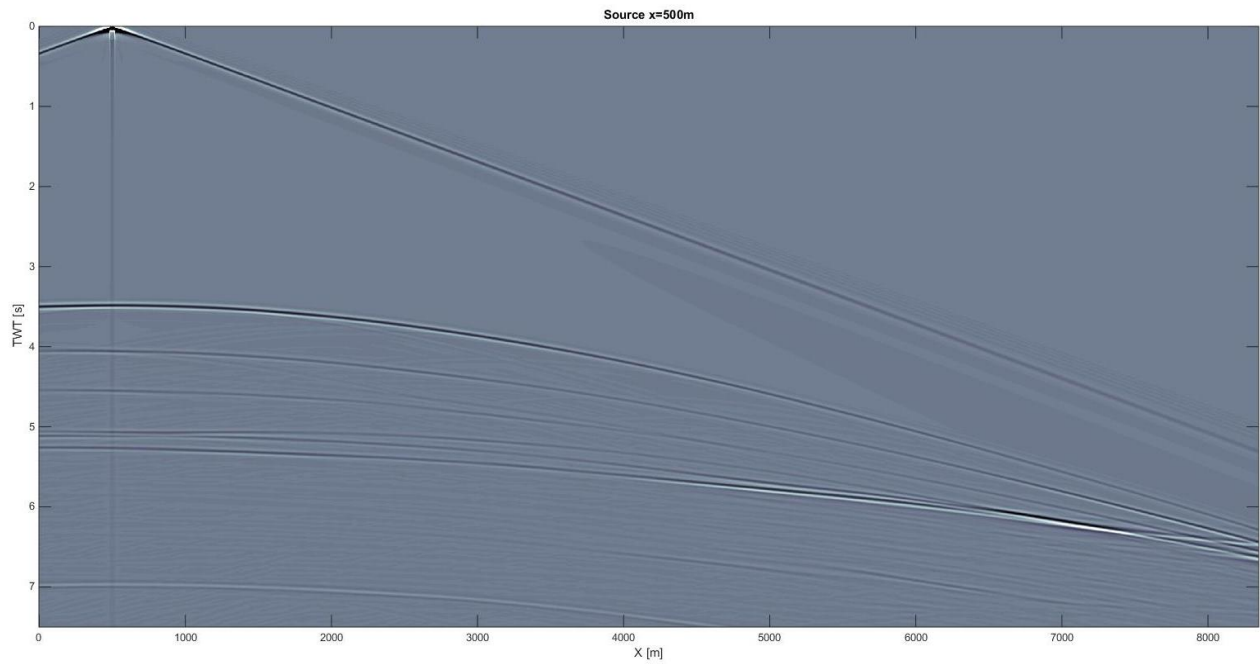


Figure 1: Common shot gather. The source is in the position 500 m.

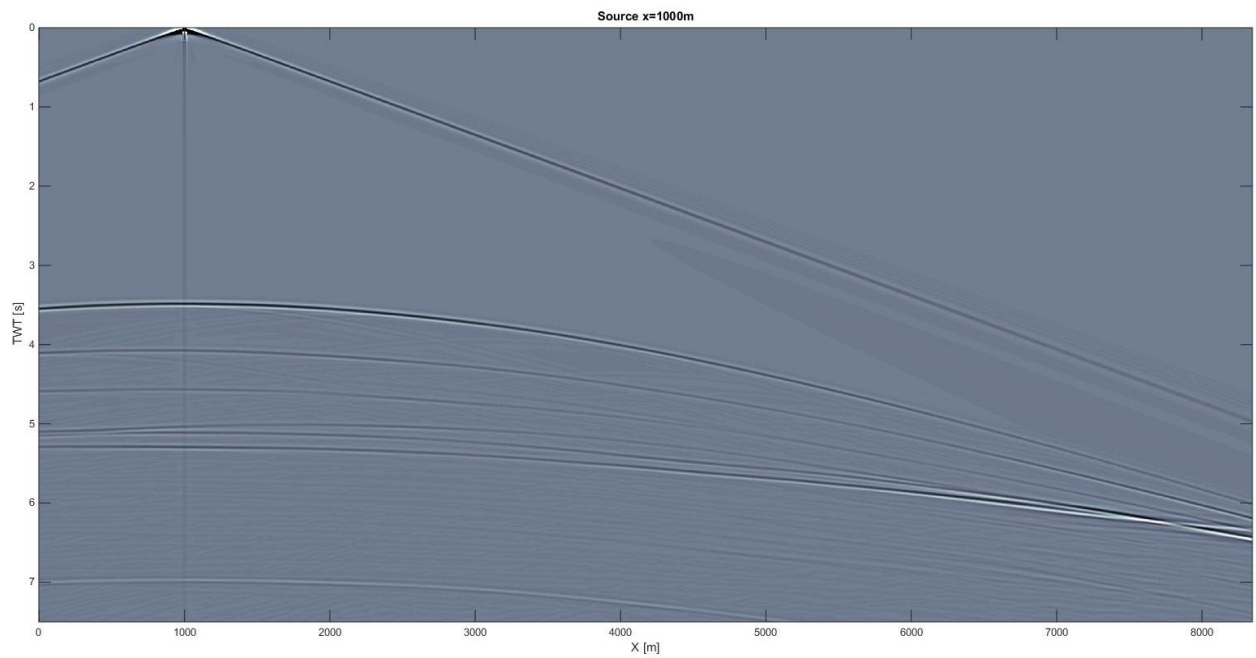


Figure 2: Common shot gather. The source is in the position 1000 m.

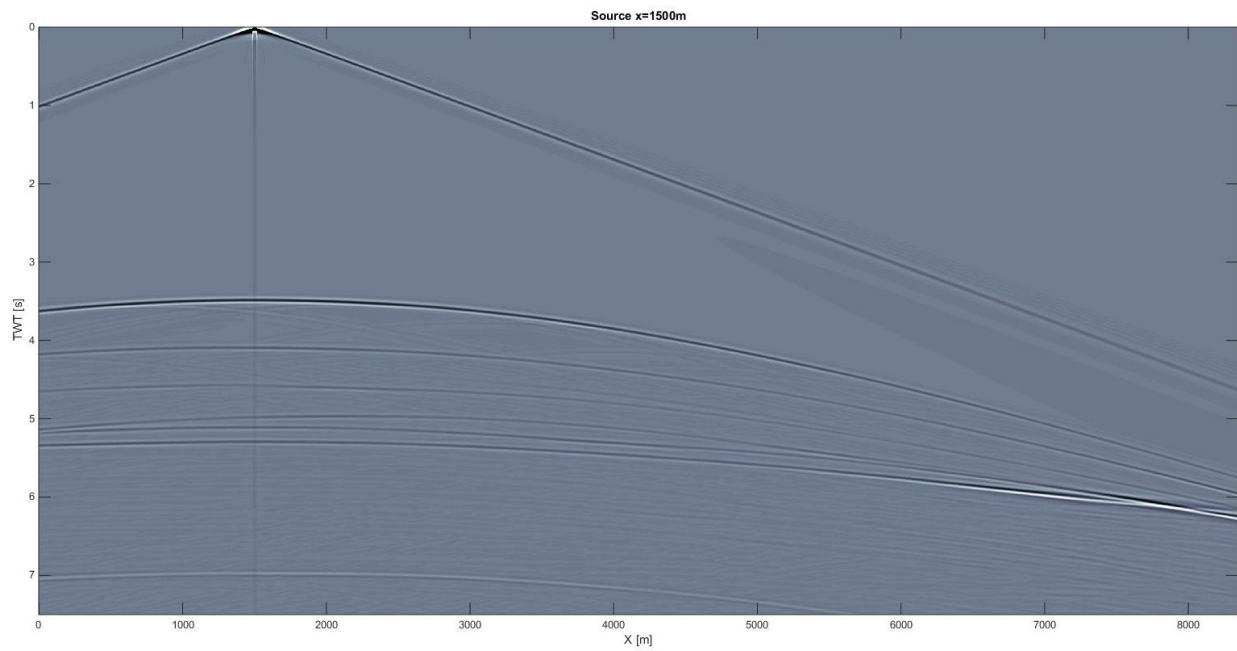


Figure 3: Common shot gather. The source is in the position 1500 m.

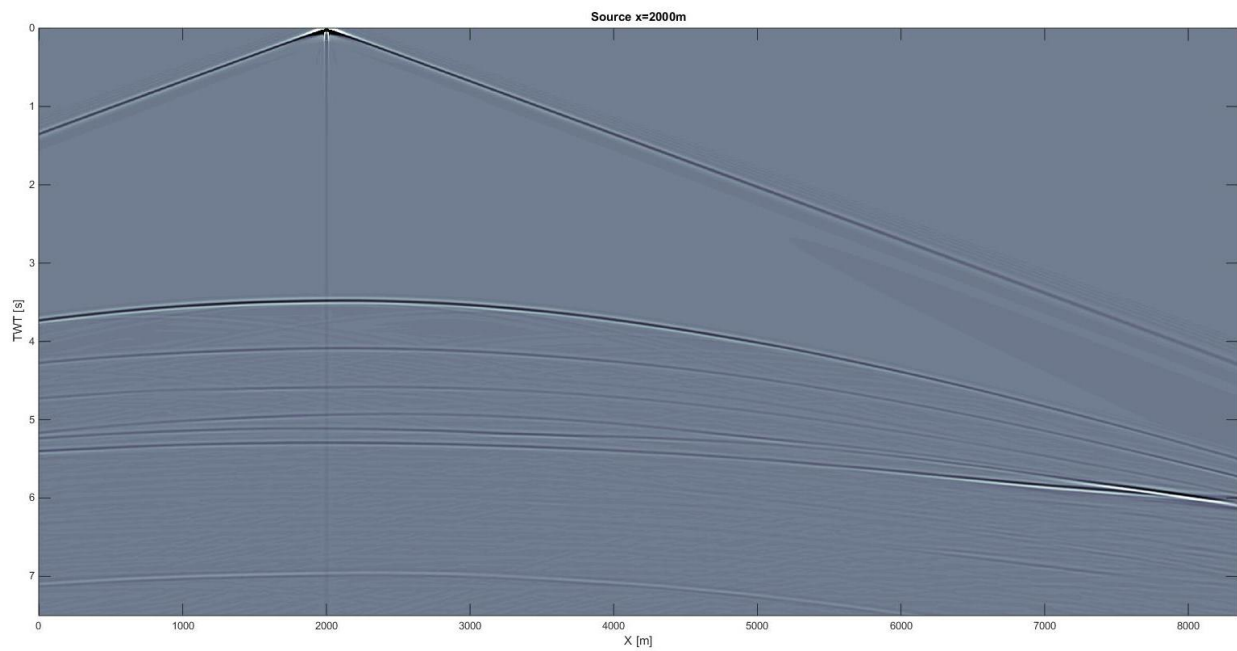


Figure 4: Common shot gather. The source is in the position 2000 m.

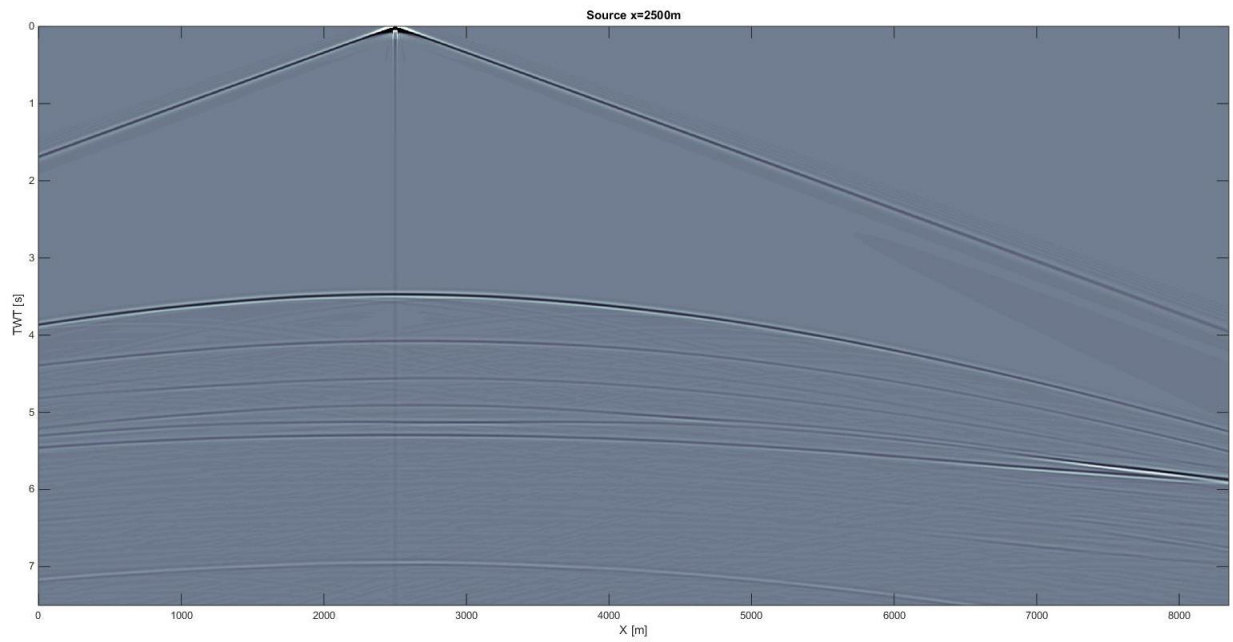


Figure 5: Common shot gather. The source is in the position 2500 m.

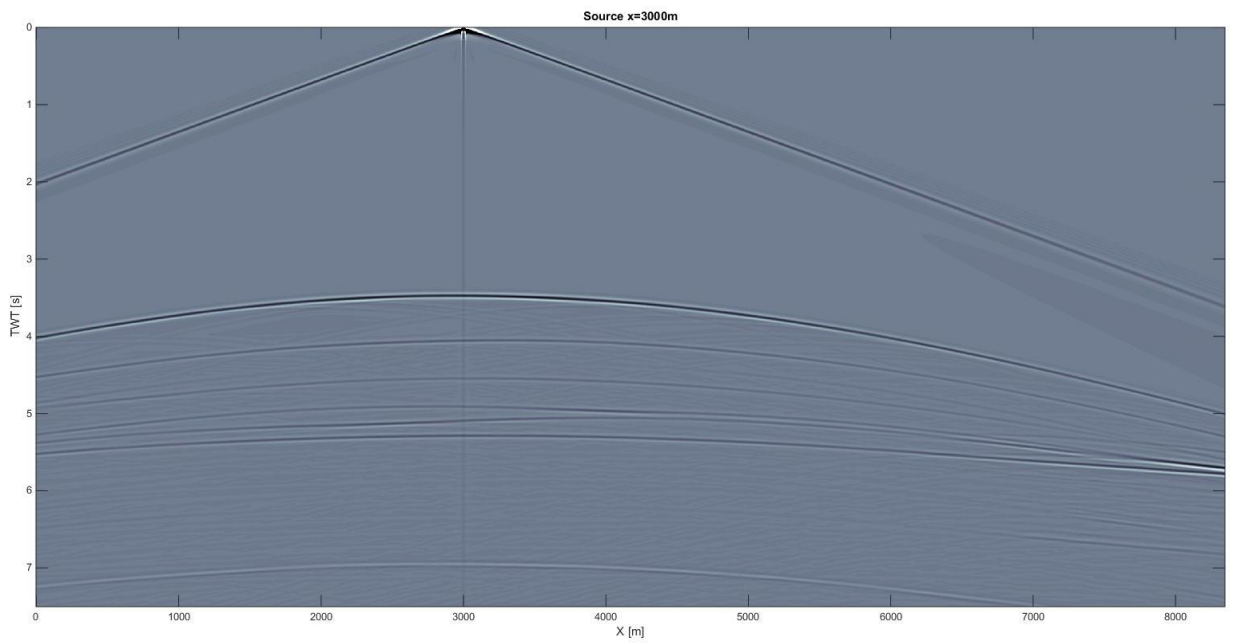


Figure 6: Common shot gather. The source is in the position 3000 m.

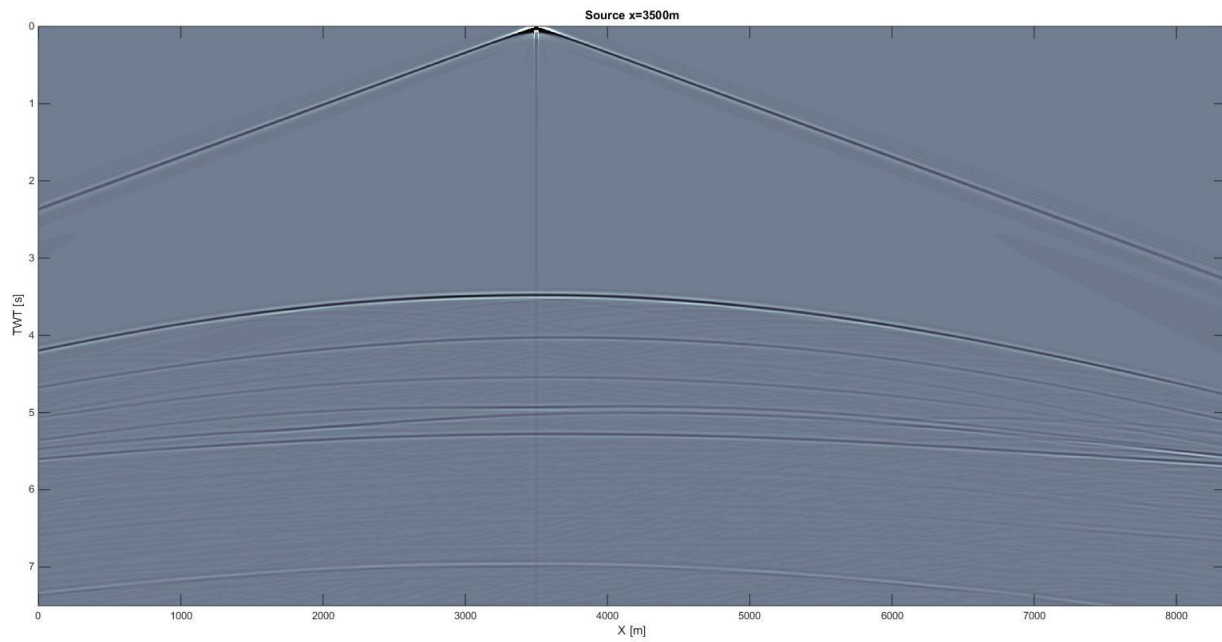


Figure 7: Common shot gather. The source is in the position 3500 m.

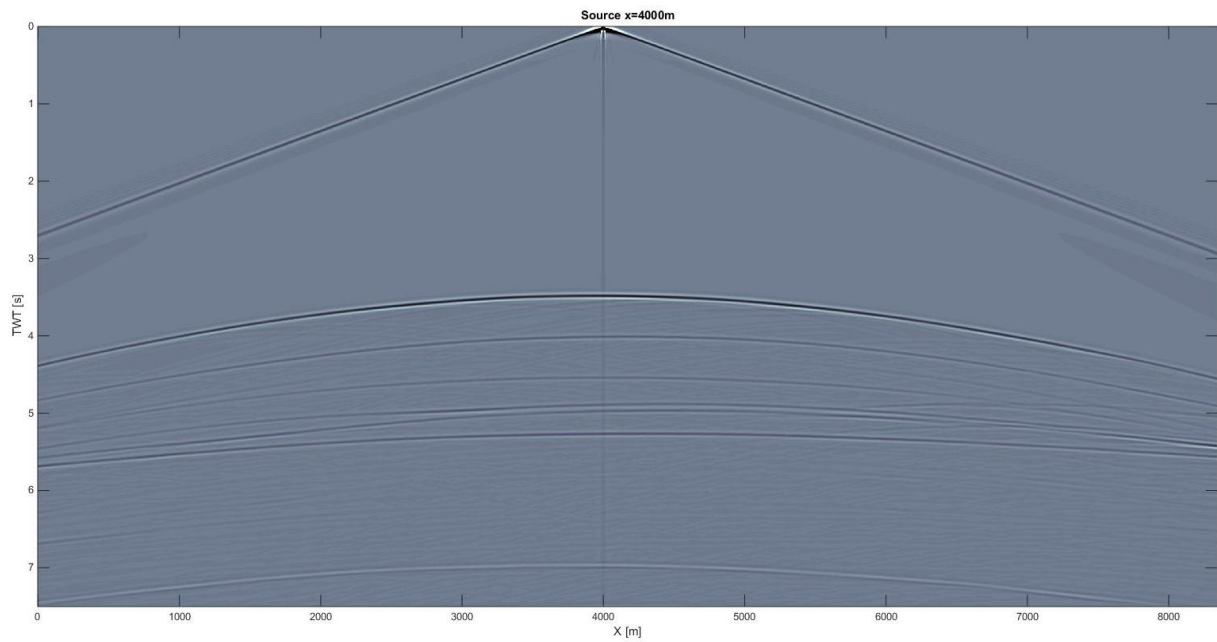


Figure 8: Common shot gather. The source is in the position 4000 m.

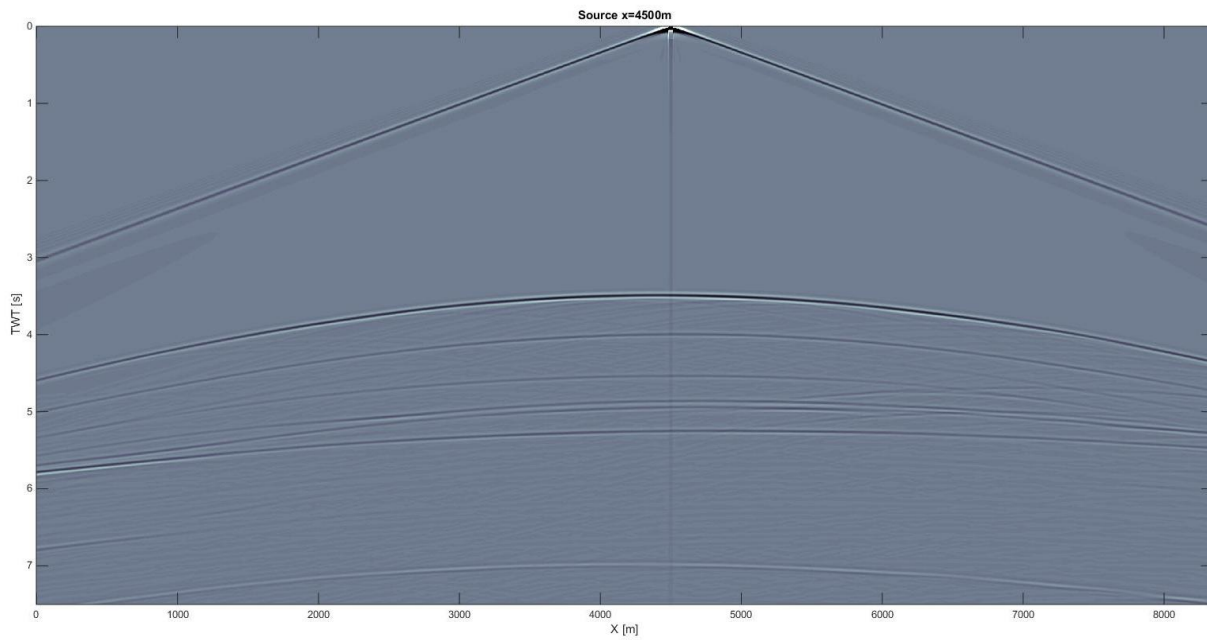


Figure 9: Common shot gather. The source is in the position 4500 m.

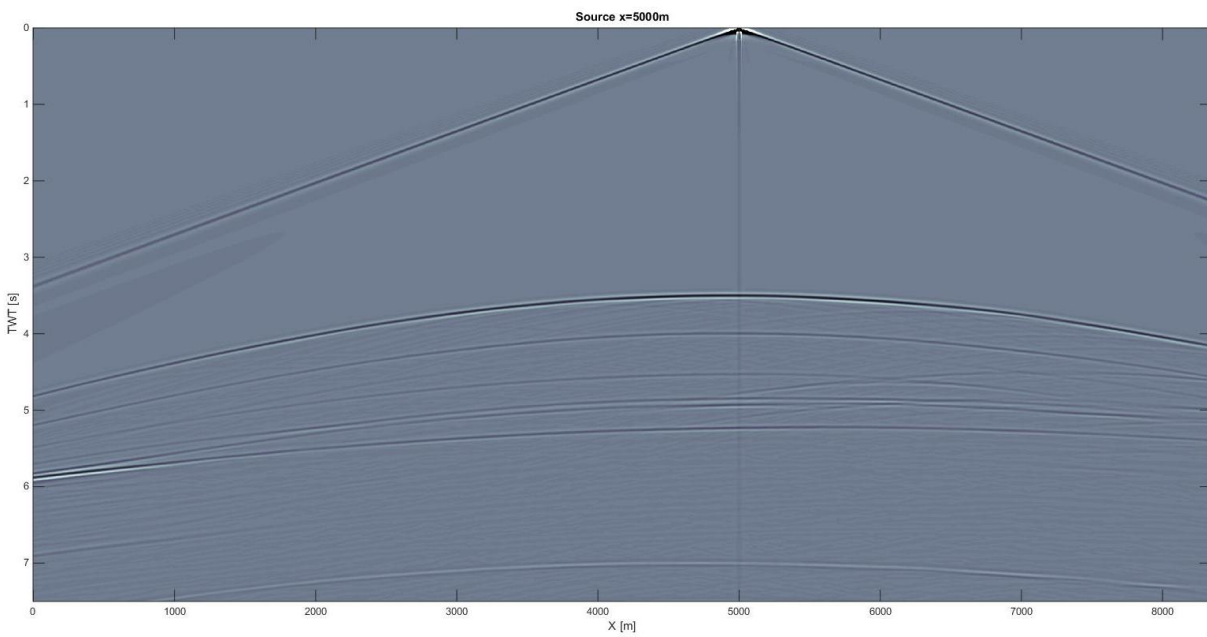


Figure 10: Common shot gather. The source is in the position 5000 m.

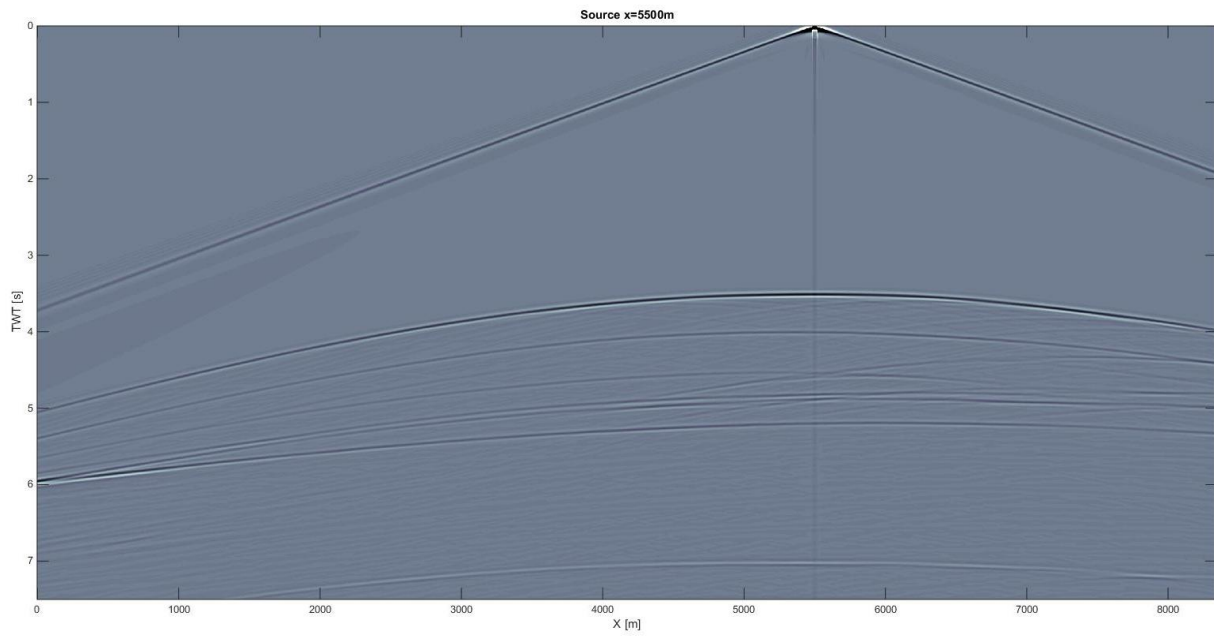


Figure 11: Common shot gather. The source is in the position 5500 m.

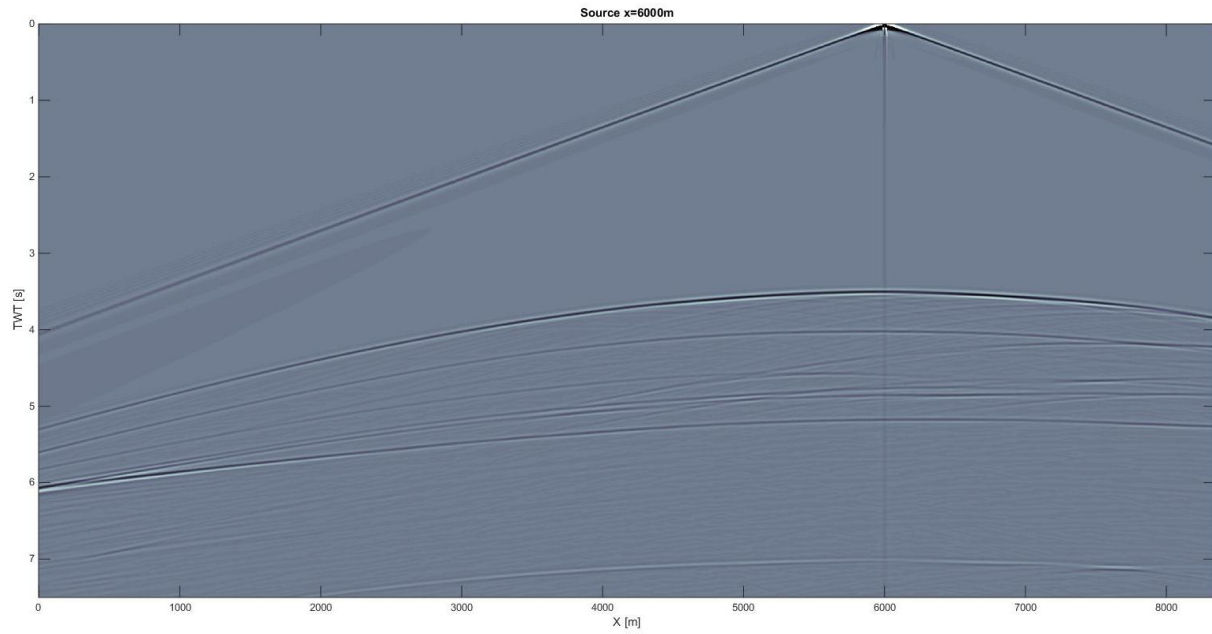


Figure 12: Common shot gather. The source is in the position 6000 m.

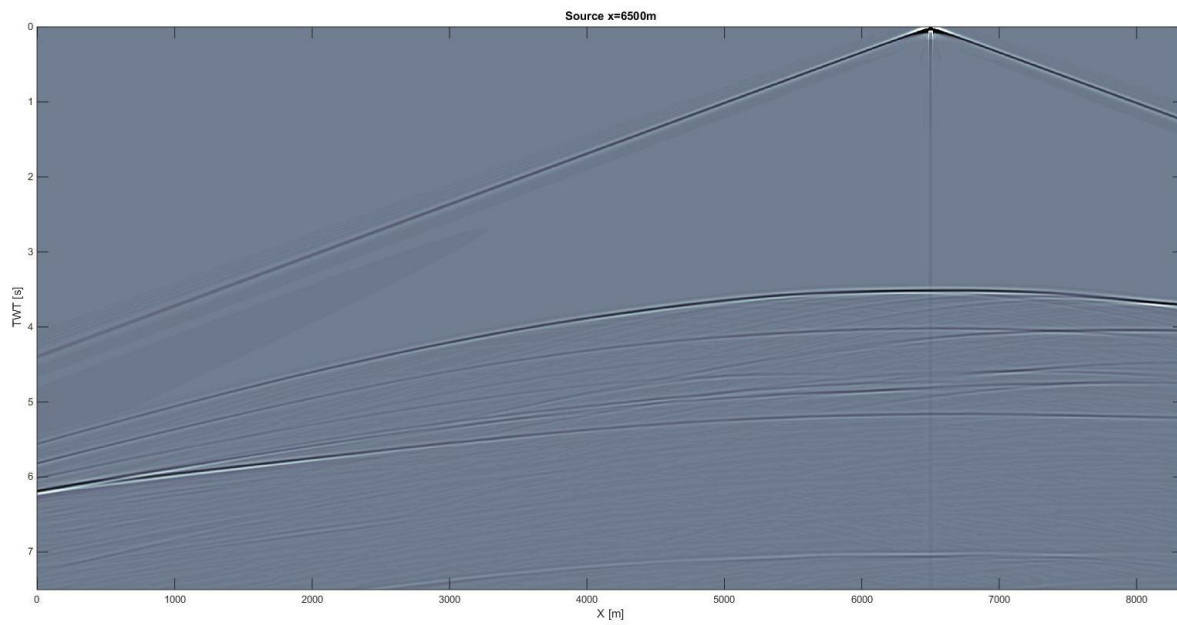


Figure 13: Common shot gather. The source is in the position 6500 m.

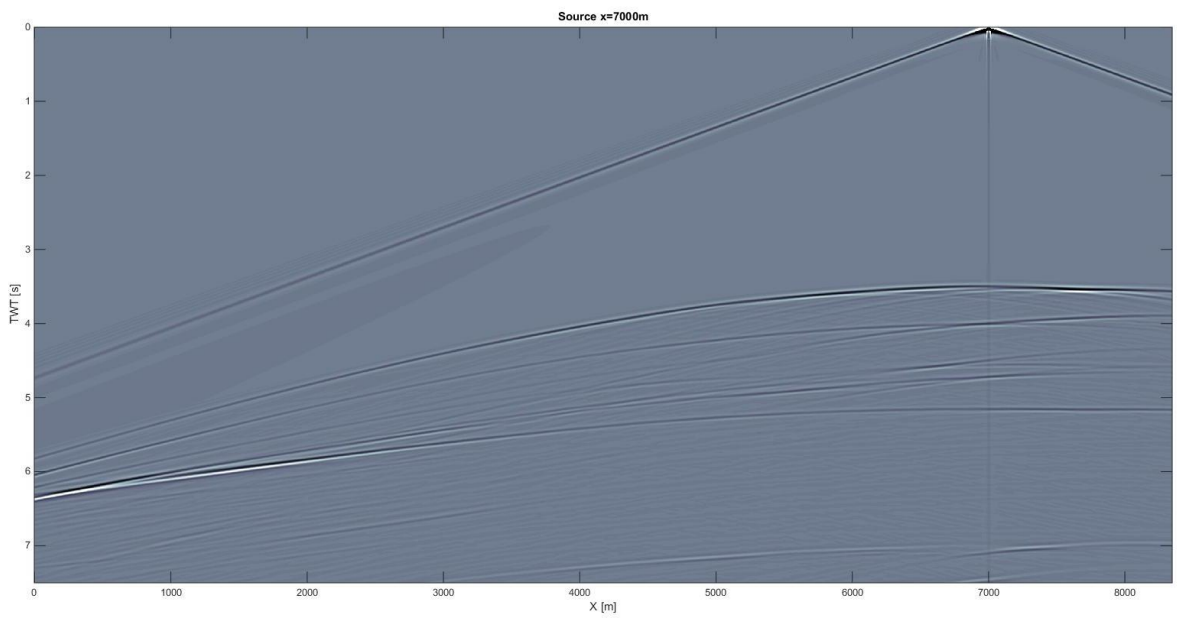


Figure 14: Common shot gather. The source is in the position 7000 m.

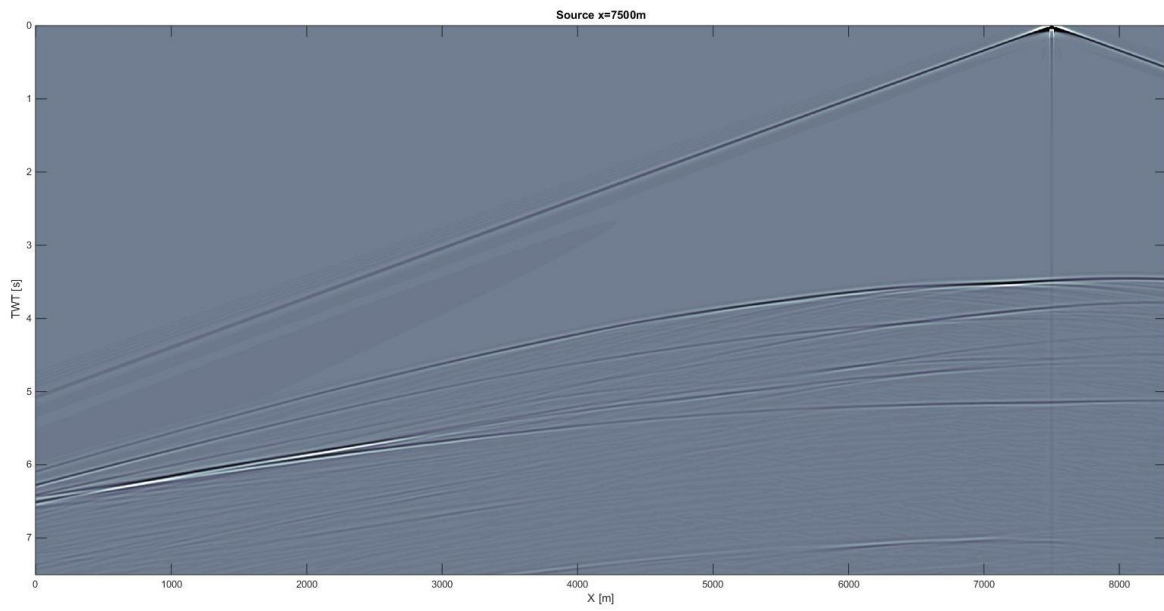


Figure 15: Common shot gather. The source is in the position 7500 m.

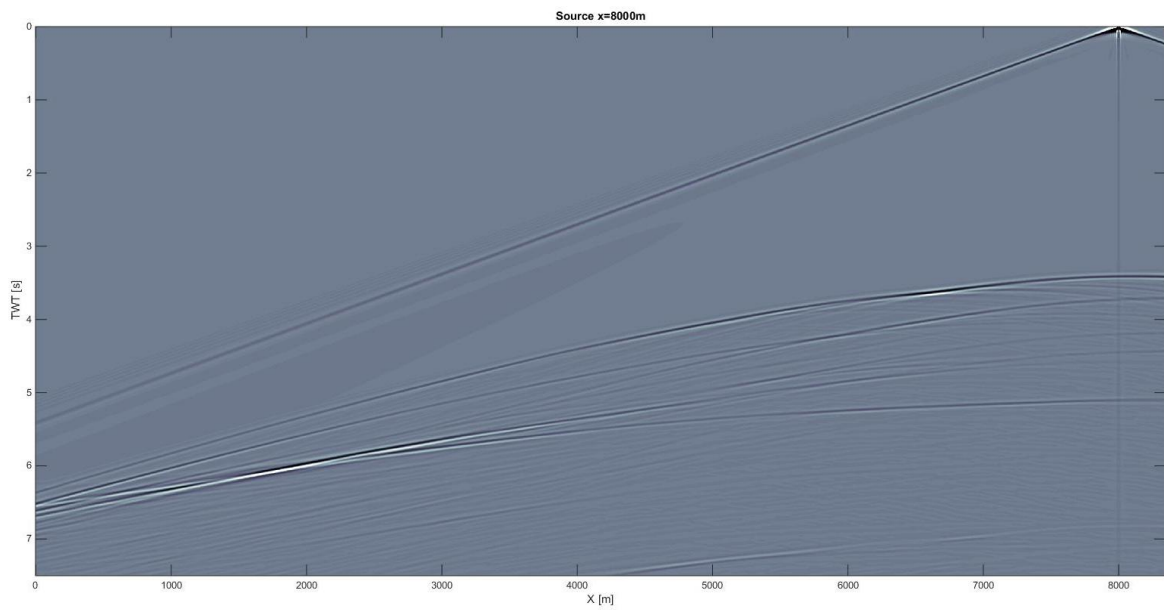


Figure 16: Common shot gather. The source is in the position 8000 m.

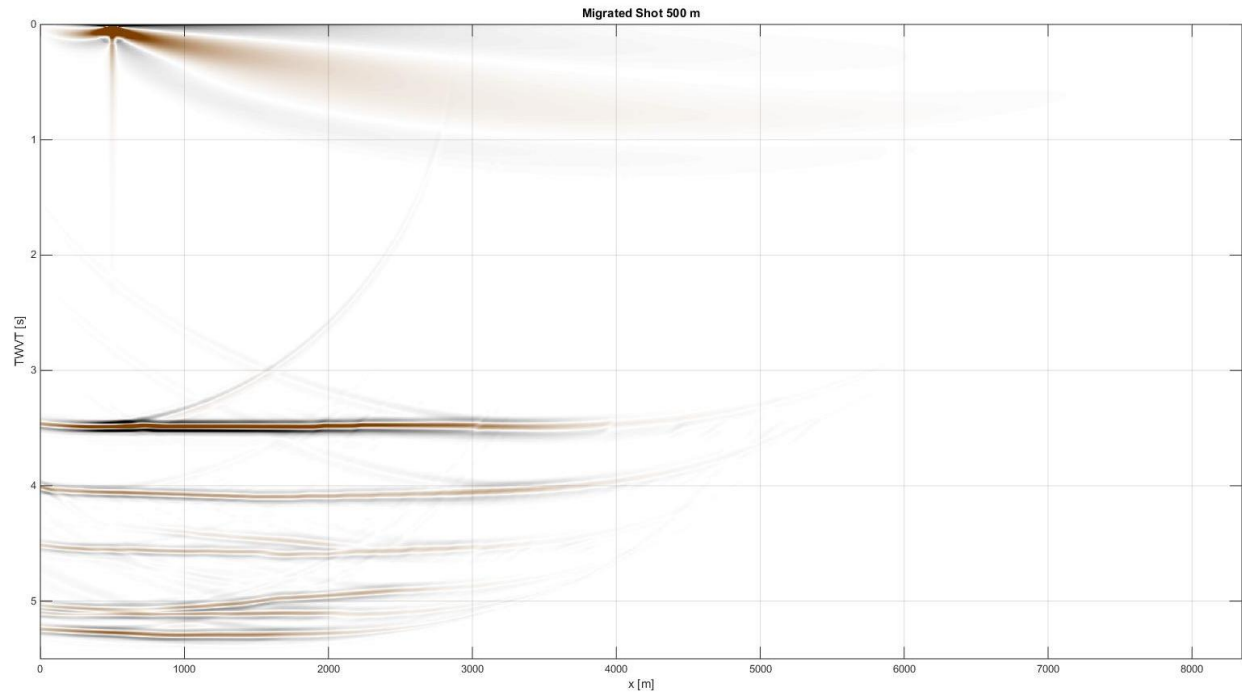


Figure 17: Migrated common shot gather. The source is in the position 500 m.

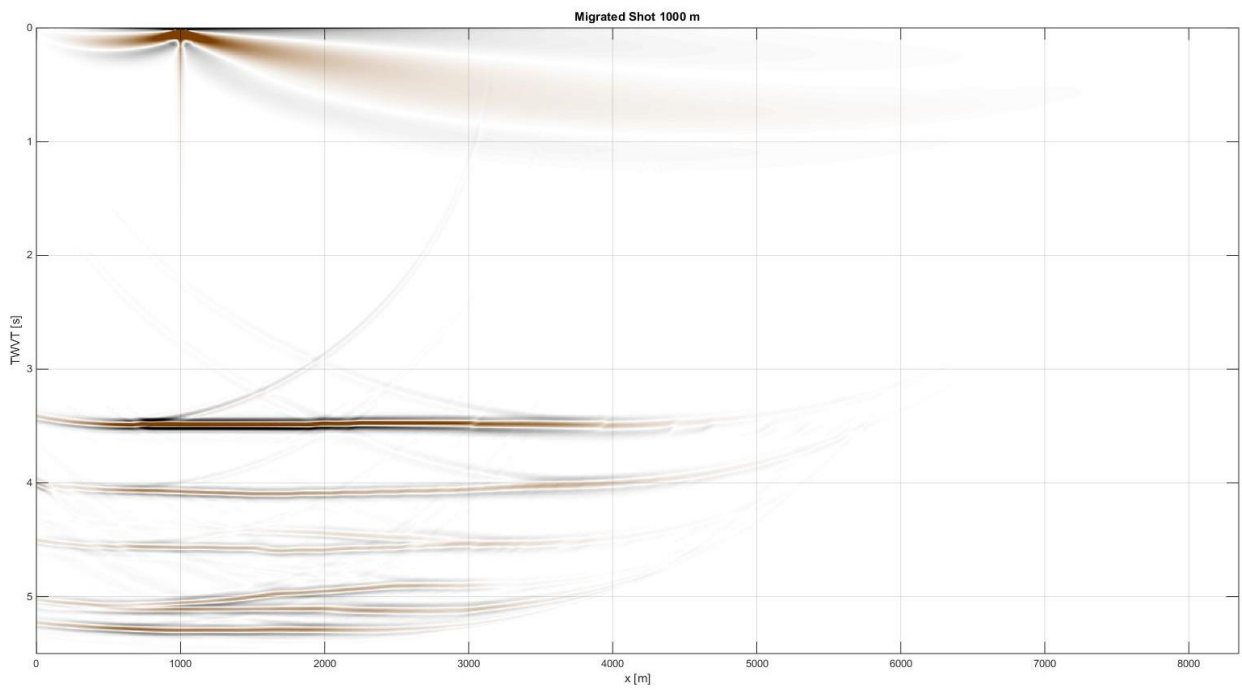


Figure 18: Migrated common shot gather. The source is in the position 1000 m.

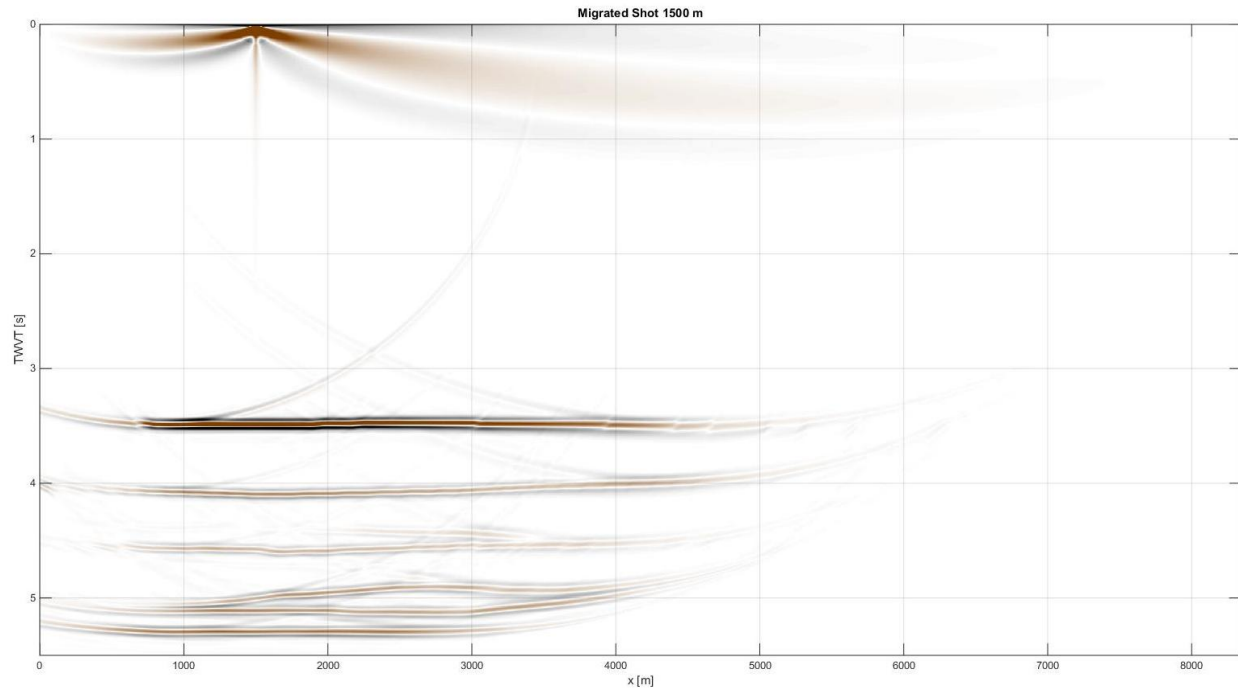


Figure 19: Migrated common shot gather. The source is in the position 1500 m.

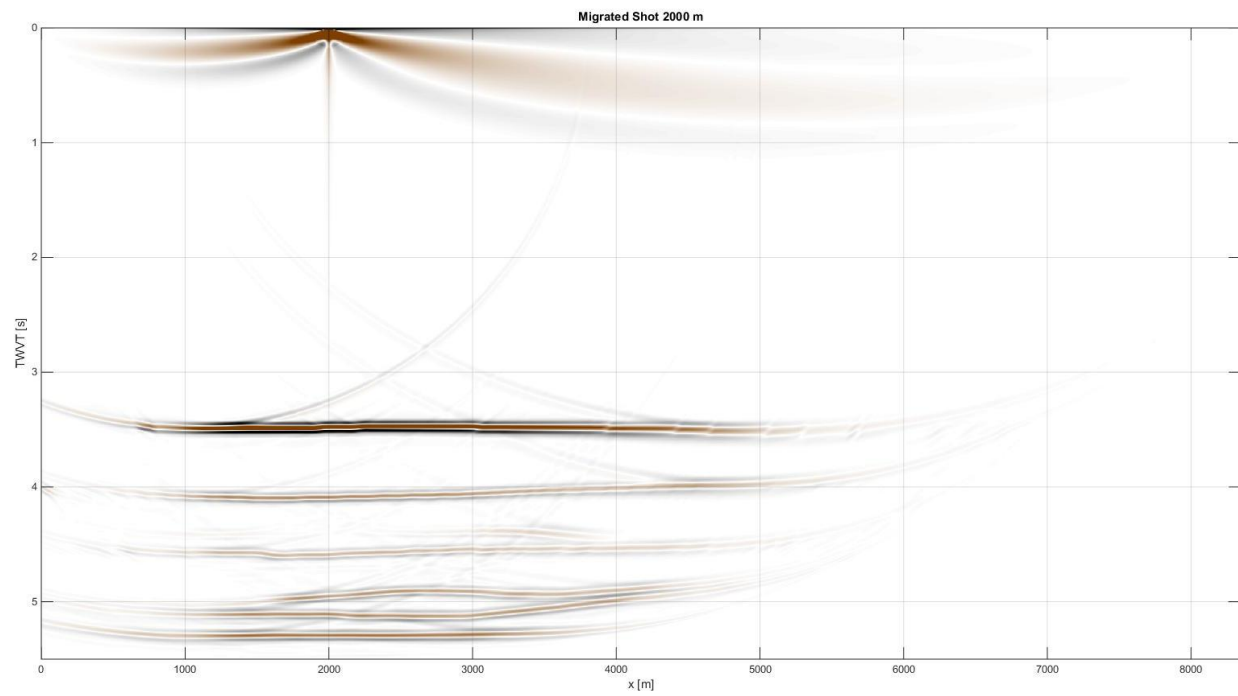


Figure 20: Migrated common shot gather. The source is in the position 2000 m.

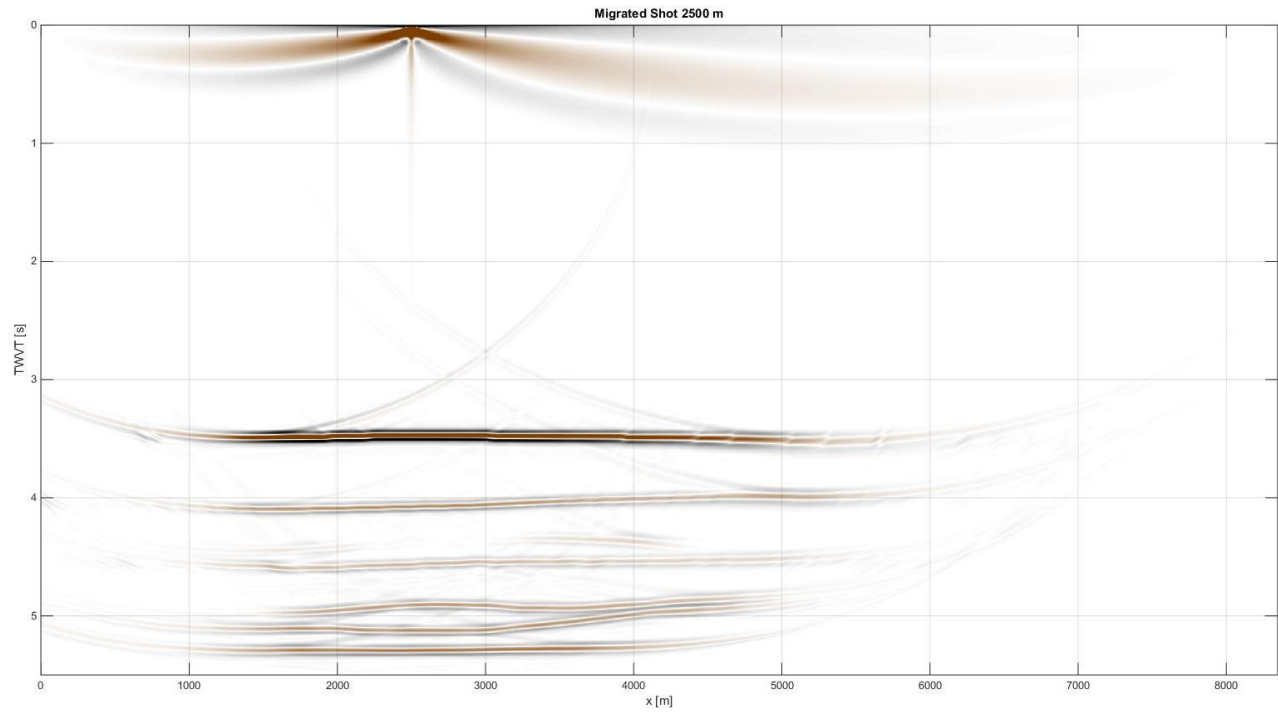


Figure 21: Migrated common shot gather. The source is in the position 2500 m.

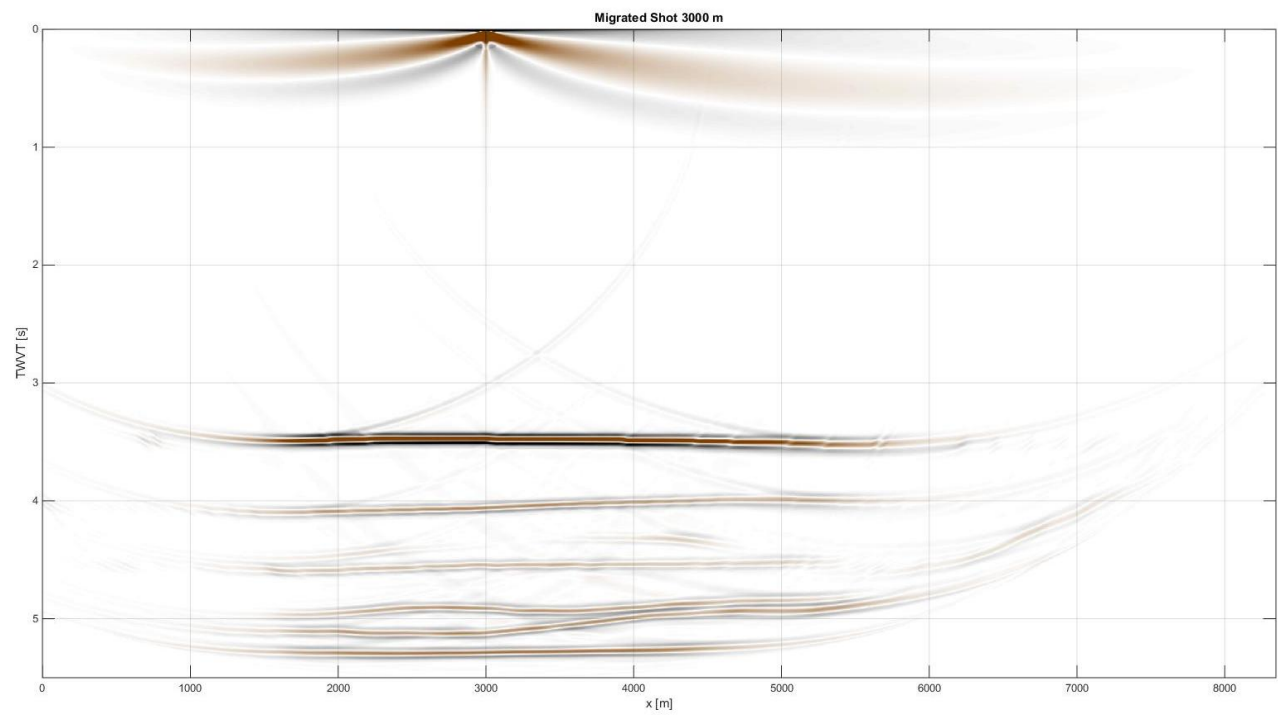


Figure 22: Migrated common shot gather. The source is in the position 3000 m.

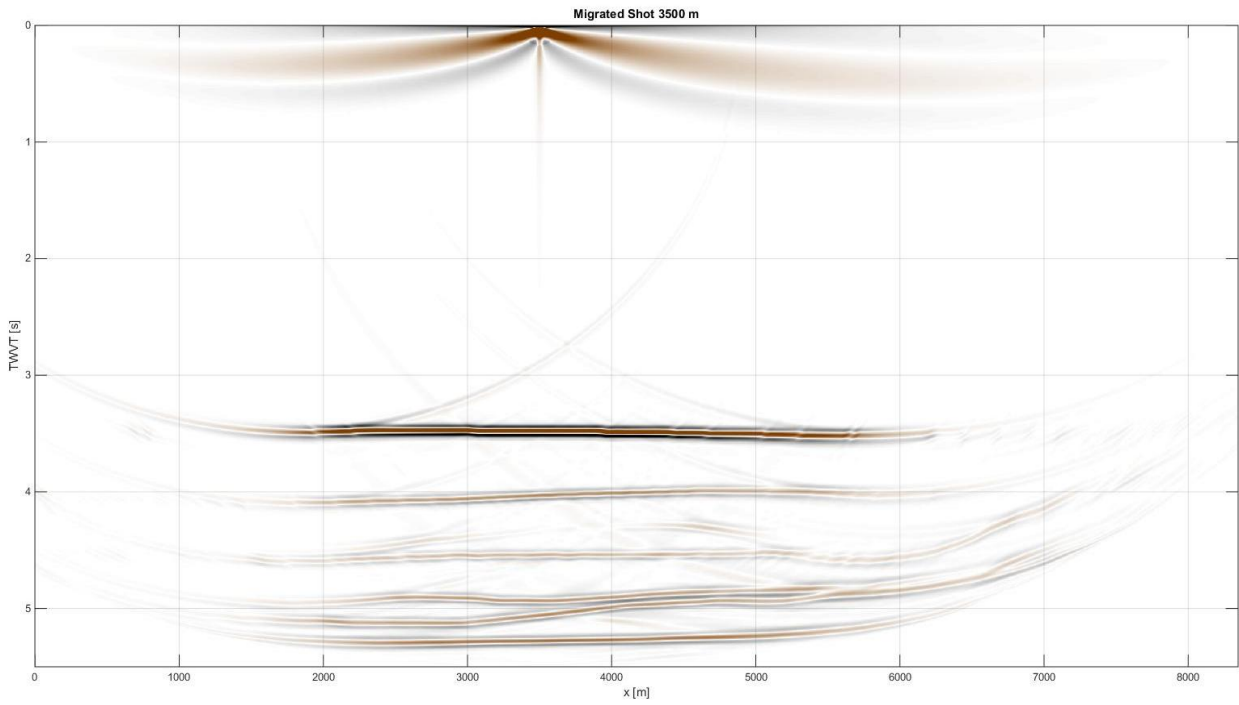


Figure 23: Migrated common shot gather. The source is in the position 3500 m.

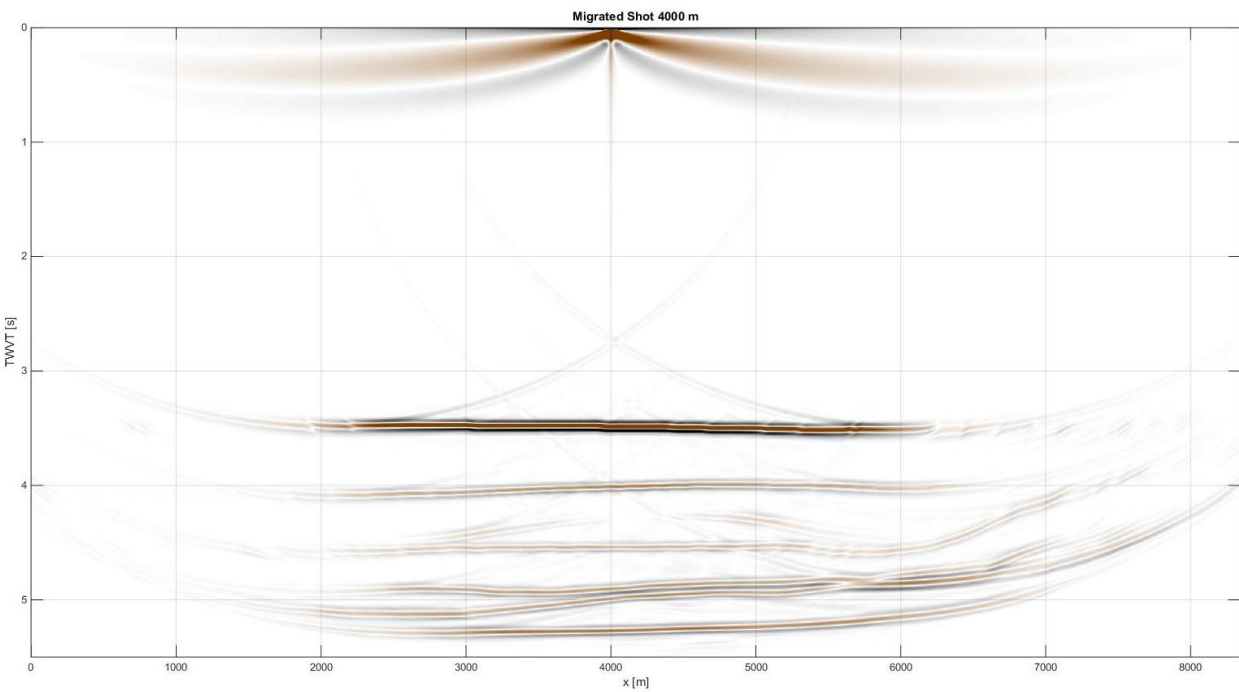


Figure 24: Migrated common shot gather. The source is in the position 4000 m.

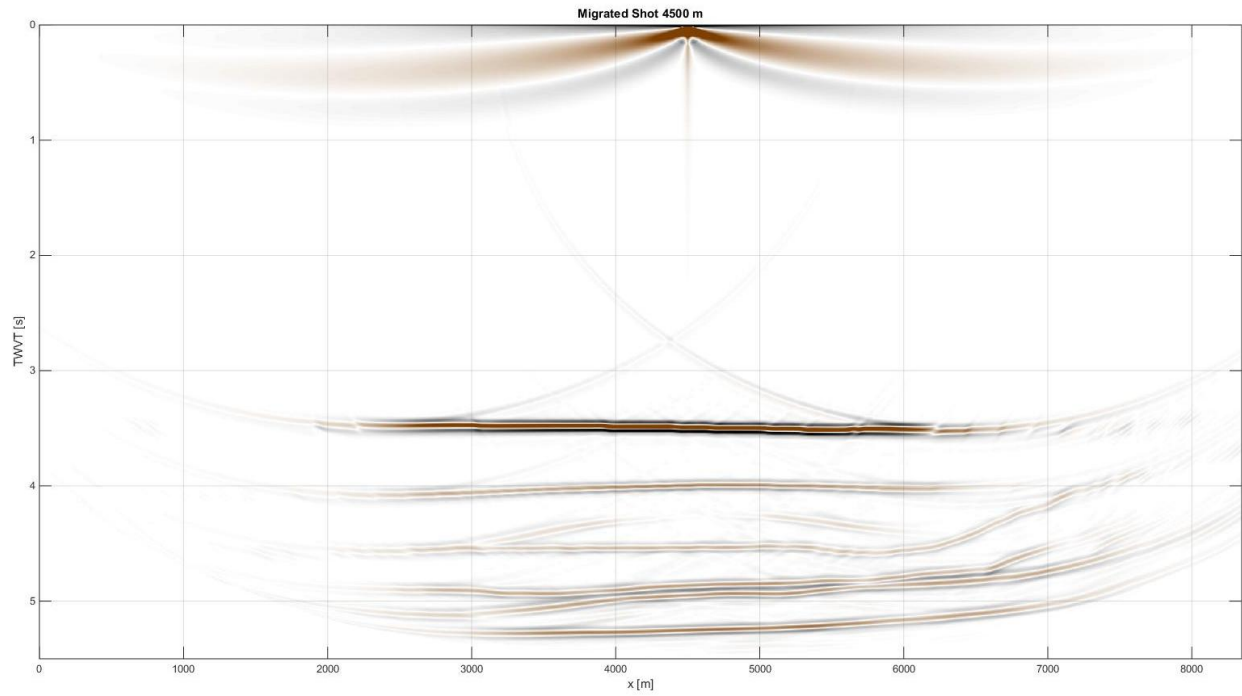


Figure 25: Migrated common shot gather. The source is in the position 4500 m.

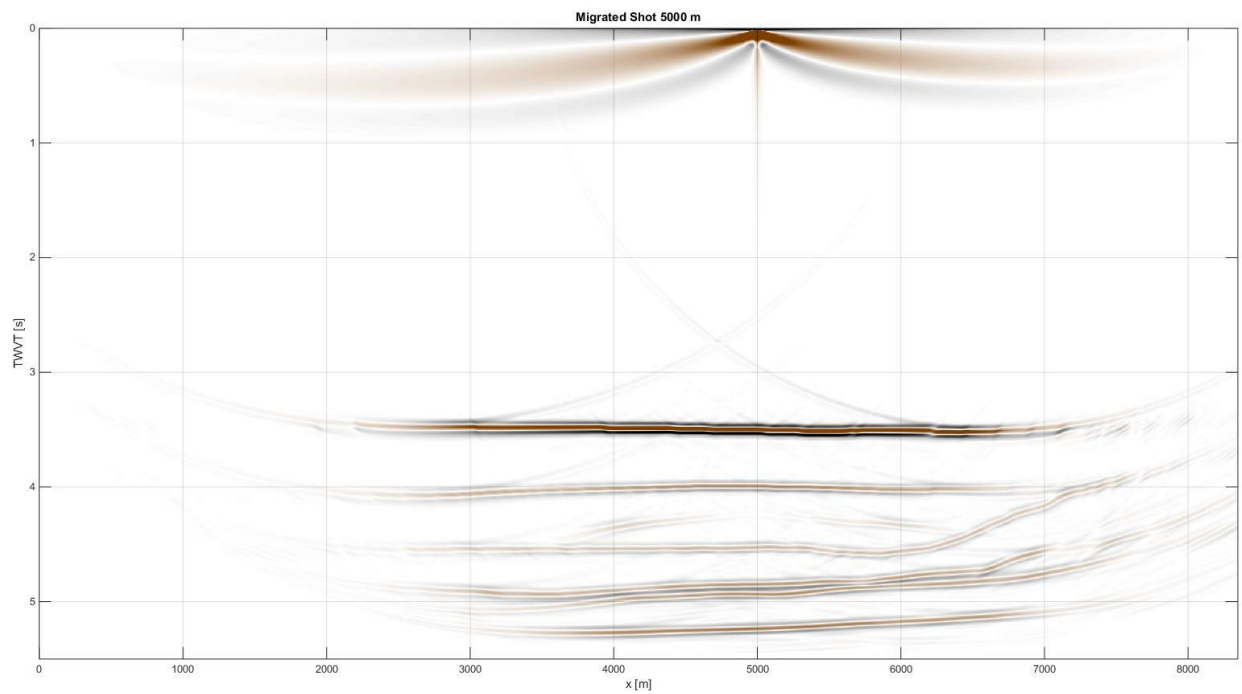


Figure 26: Migrated common shot gather. The source is in the position 5000 m.

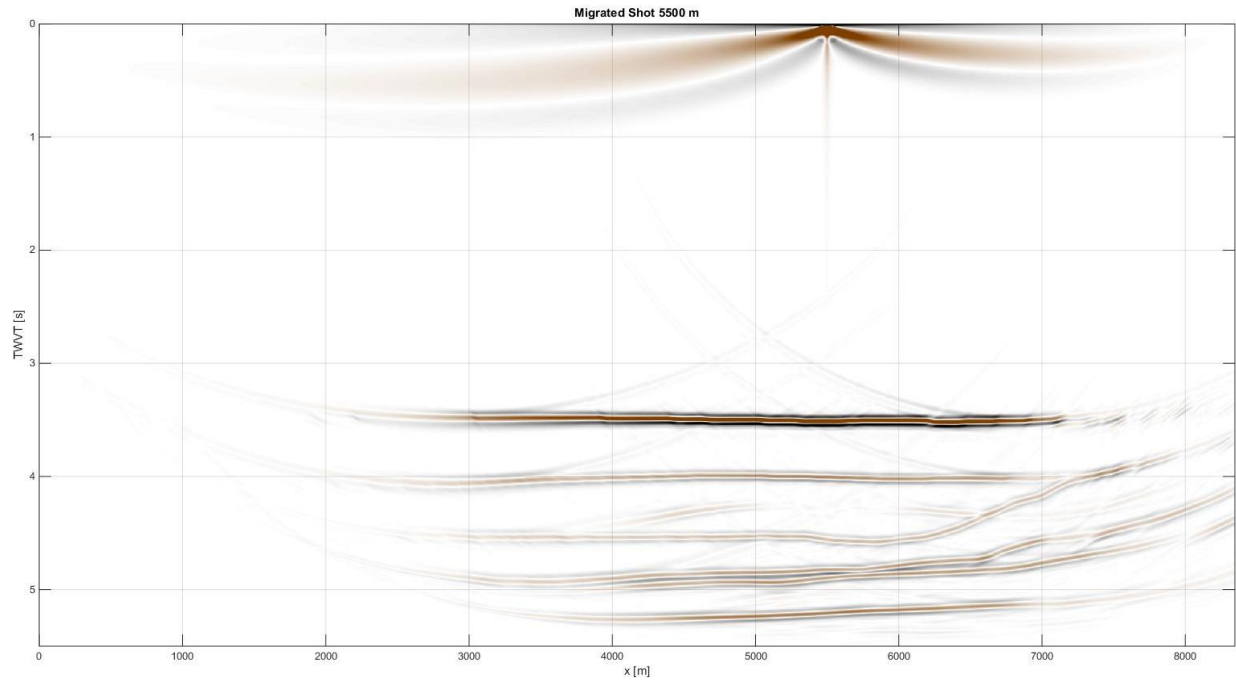


Figure 27: Migrated common shot gather. The source is in the position 5500 m.

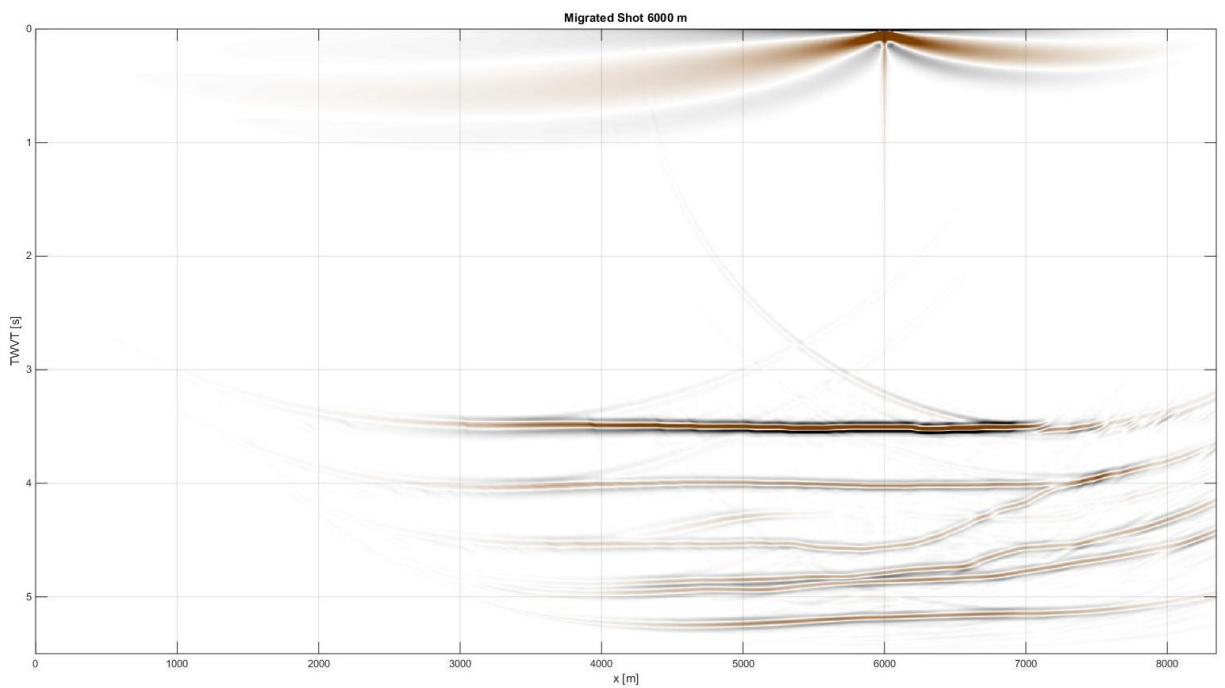


Figure 28: Migrated common shot gather. The source is in the position 6000 m.

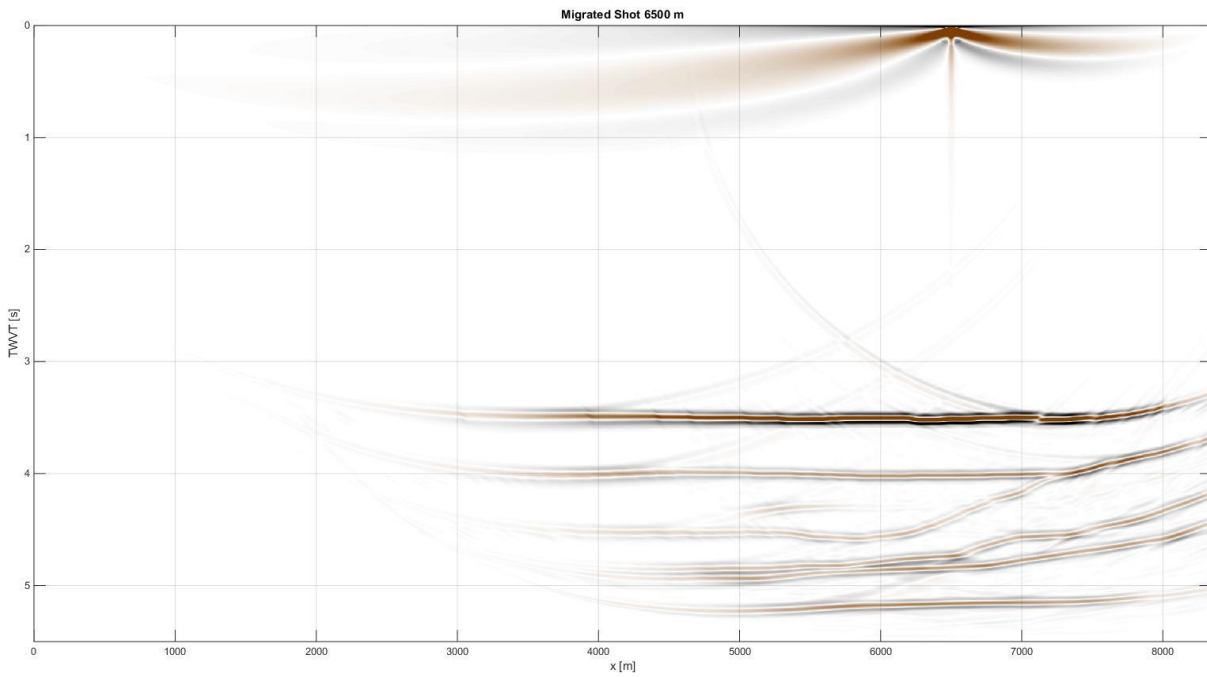


Figure 29: Migrated common shot gather. The source is in the position 6500 m.

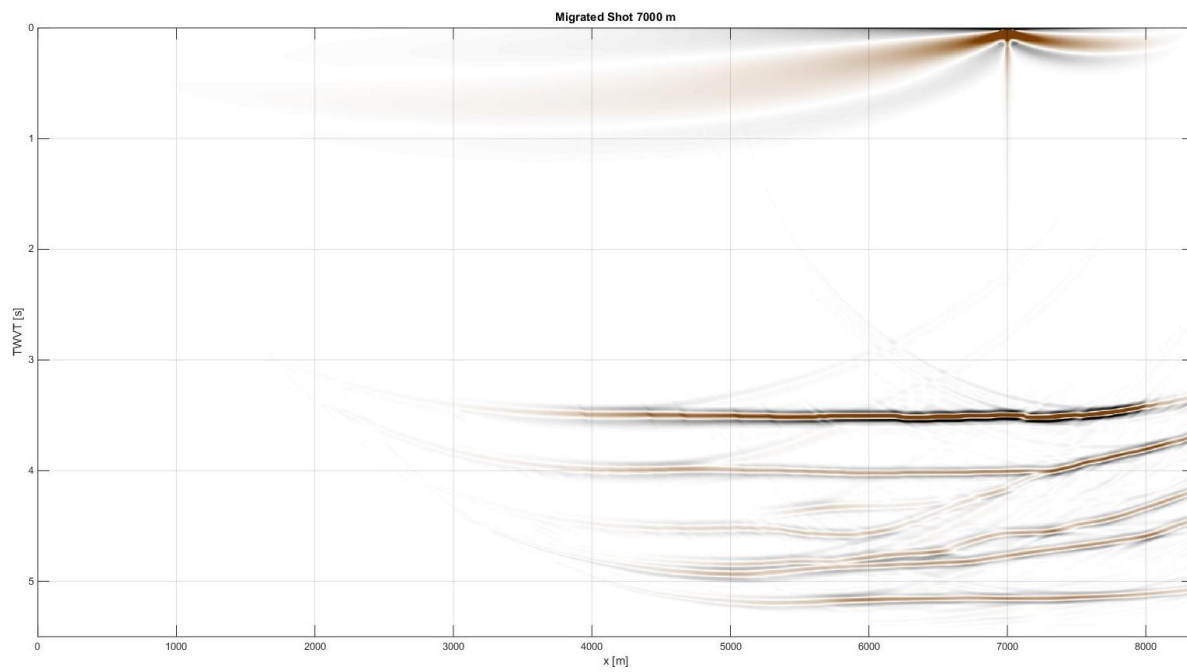


Figure 30: Migrated common shot gather. The source is in the position 7000 m.

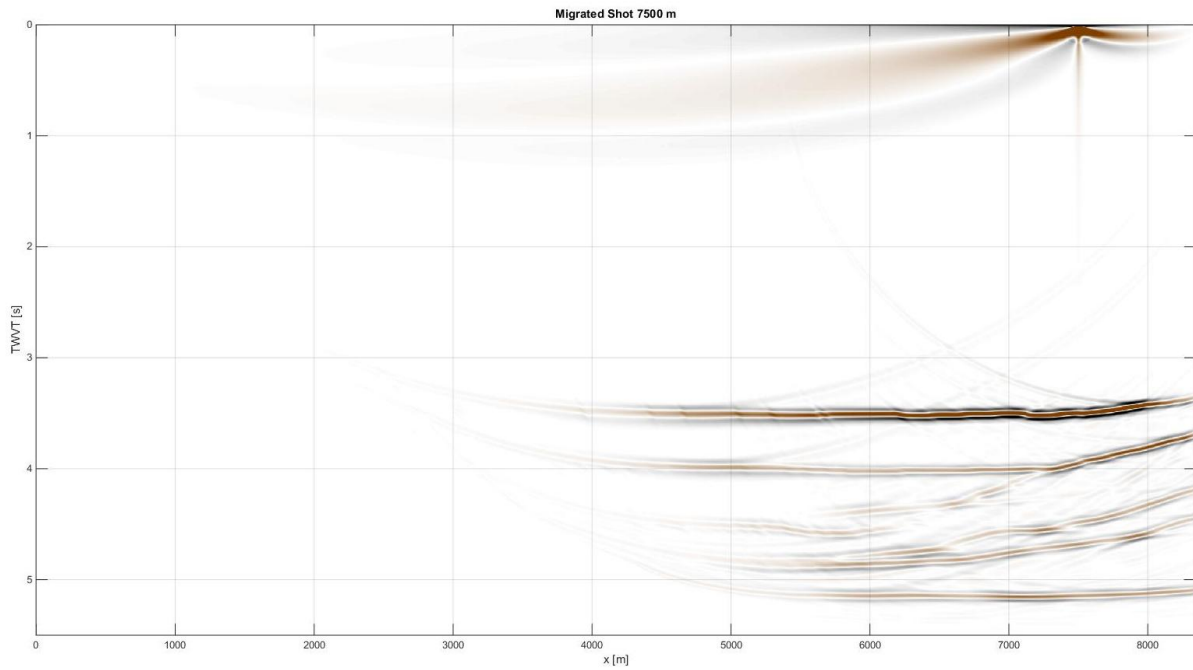


Figure 31: Migrated common shot gather. The source is in the position 7500 m.

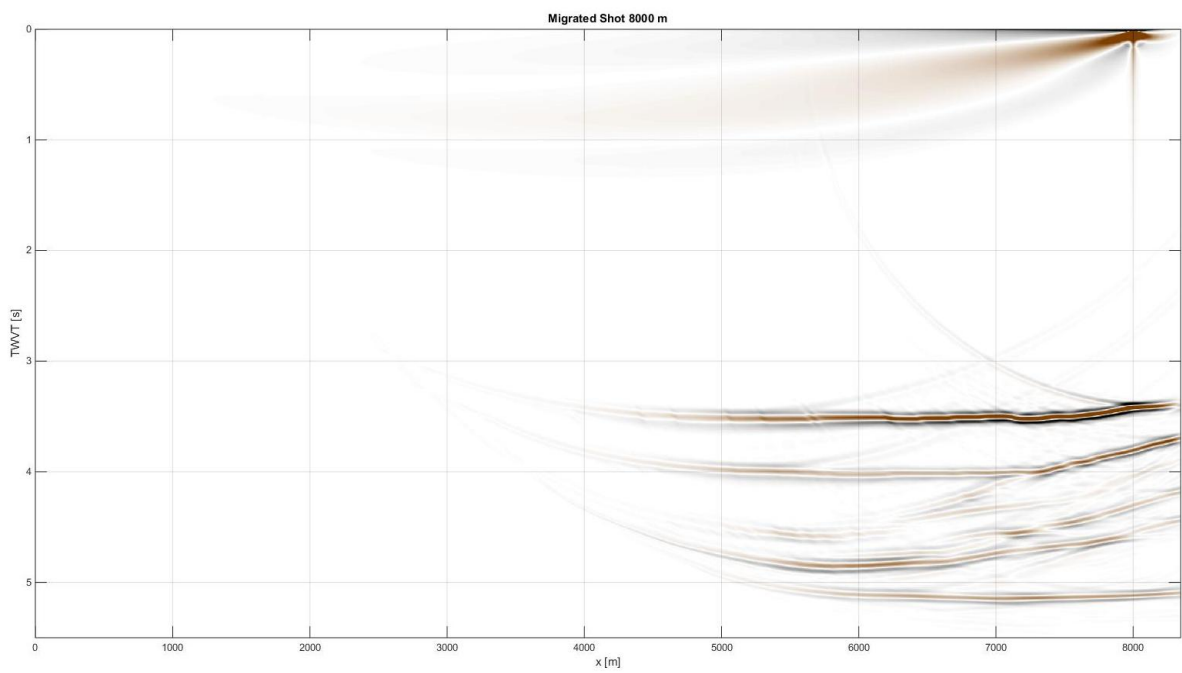


Figure 32: Migrated common shot gather. The source is in the position 8000 m.

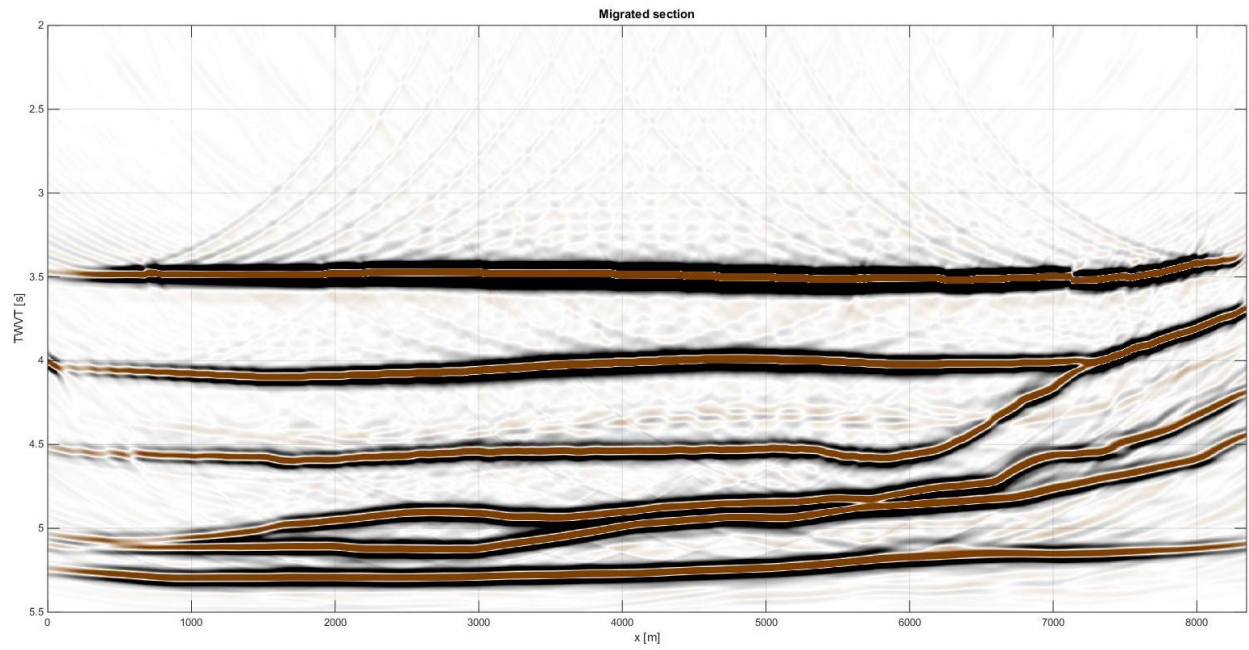


Figure 33: Migrated section.